Identification of Motor Neuron Pool Marker Genes and Analysis of their Roles in Motor Circuit Assembly

Inauguraldissertation

zur

Erlangung der Würde eines Doktors der Philosophie

vorgelegt der

Philosophisch-Naturwissenschaftlichen Fakultät

der Universität Basel

von

Simon Dalla Torre di Sanguinetto

aus Solothurn, Schweiz

Basel, 2011

Genehmigt von der Philosophisch-Naturwissenschaftlichen Fakultät

auf Antrag von

Prof. Dr. Silvia Arber
(Dissertationsleitung)

Prof. Dr. Pico Caroni
(Korreferat)

Basel, den 17. Feb. 2009

Prof. E. Parlow
(Dekan)

TABLE OF CONTENTS

Summary

In order to produce behavioral output, nervous systems critically depend on the establishment of selectively connected intricate neuronal networks. The overwhelming number and complexity of intersecting neuronal pathways complicates efforts to improve our understanding of the brain. Experiments are therefore ideally performed in well-defined neuronal networks, such as the monosynaptic stretch reflex circuits in the spinal cord (SC). The establishment of this sensory-motor feedback loop relies on the formation of highly selective synaptic contacts between group Ia proprioceptive afferents, spinal motor neurons (MNs) and their target muscles in limbs. The high degree of connective specificity exhibited by this circuit paralleled with its relative simplicity combine to a set of favorable features for experimental neurobiological research directed at the elucidation of neuronal circuit formation.

The goal of my PhD thesis was to investigate the molecular mechanisms controlling the diversification of MNs into discrete subpopulations, referred to as MN pools, which establish precise axonal trajectories to individual muscles and specific sensory connectivity patterns. Since synaptic specificity is largely controlled by genetic programs, we acquired gene expression profiles of four individual cervical motor neuron (MN) pools, supplying Cutaneous Maximus, Triceps, Pectoralis Minor and Pectoralis Major muscles, using a combination of retrograde labeling, Laser Capture Microdissection and Affymetrix gene chip technology.

Comparison of the obtained expression profiles allowed the identification of genes expressed specifically in single MN pools. Our analysis was particularly focused on the interplay between transcription factors and their cognate repertoire of cell surface molecules. MN pool expression of many such genes could be validated by *in situ* hybridization. We also performed a second genome-wide screen in order to determine

whether identified CM marker genes were regulated by the ETS transcription factor Pea3 known for its key role in the specification of the CM MN pool.

Based on the results of our screening experiments we chose the G-protein coupled prokineticin receptor 2 (Pkr2) and the extracellular matrix protein developmental endothelial regulated locus 1 (Del1), both of which are expressed in CM MNs and positively regulated by Pea3, for further analysis. In addition, we report on the upregulation of the transcription factor Pou3f1 (Scip) in CM MNs of *Pea3* mutant mice.

I addressed the functionality of Pkr2 in MNs by means of a genetic null mutant engineered in our laboratory. Based on its roles in other neuronal systems and because Pkr2 expression is dependent on Pea3, our experiments primarily explored its function with respect to potential contributions to motor circuit formation defects detected in *Pea3* mutant mice. Our analysis did however not reveal any abnormalities in cell migration, sensory-motor connectivity or muscle innervation patterns or a role in axon pathfinding in DRG sensory neurons, in subpopulations of which Pkr2 is expressed as well.

As an extracellular matrix protein involved in chemotactic signaling events, the second downstream target of Pea3, Del1, also disposed of all necessary characteristics to play an essential role in neuronal circuit assembly. For this reason, the functionality of Del1 was addressed analogously to Pkr2. Although the function of Del1 in the CM MNs remains uncertain to date our experimental results are not indicative of an important role in axon pathfinding or neuronal migration.

Scip was the only gene validated as negatively regulated by Pea3 in CM MNs. We were speculating that in *Pea3* mutants the transcriptional identity conferred by Scip could endow CM MNs with molecular features normally inherent to forearm projecting

MN pools that express Scip in wild-type. This scenario is of interest insofar as in *Pea3* mutant mice, CM motor neurons change the status and the specificity of their sensory-motor connectivity. In the future, the role of Scip could be addressed by experiments using ectopic expression and *Scip* loss of function mice.

In summary, I identified and functionally characterized genes expressed in distinct MN pool with the potential to contribute to the process of motor circuit assembly. To our knowledge this is the first time the expression profiles of MNs were resolved at single MN pool resolution and our findings have thus provided an entry point to a deeper understanding of the molecular events that govern the specification of MNs and the establishment of motor circuits. Future research should be directed at the functional elucidation of additional molecular factors identified by our approach and could also contribute to an increased understanding of the developmental processes underlying neuronal network formation in the brain.

1 General Introduction

1.1 Neuronal circuit formation

The human brain consists of 100 billion individual neurons forming an estimated 60 trillion synaptic contacts. The result is a highly complex neuronal network capable of receiving, filtering and computing unconceivable amounts of simultaneous sensory inputs, of orienting ourselves in space, of seemingly effortlessly coordinating the movements of our bodies in space and of automatically forming millions of incidental memories of our perceptions in the outside world. At the same time our brain is the source of our minds and emotions and capable of planning most intricate future actions. More than anything else our brain defines who we are.

To improve our understanding of cognition was and still is one of the most challenging tasks of science. In the beginnings, neuroscientific research was aimed at the elucidation of the anatomical aspects of neuronal wiring, which sets the framework and defines the biological potential of any species' nervous system. Much progress has been made in the description of anatomical connectivity since more than hundred years ago Nobel laureate Santiago Ramón y Cajal first described in great detail morphological characteristics of neurons and their structural arrangements in layers using Golgi stainings (Figure 1). While the basic function of any neuron can be reduced to the spatial propagation of information through electrical signals, individual neurons are at the same time highly specialized to best fulfill divergent functions. This functional diversification is reflected in a great variety of neuronal morphologies in different brain structures, layers within a brain structure and even between neighboring neurons of the same layer but divergent synaptic connectivity. Over the last century it has become clear that the basis for the anatomical architecture and connectivity of the central nervous system (CNS) is established during embryonic development, when

neurons are born, progressively differentiate into distinct subtypes, migrate towards their terminal targets and establish synaptic connectivity. Identifying the molecular and transcriptional determinants that control these early events in neuronal subtype specification and circuit formation will thus be of great importance in order to decipher and understand mature brain function.

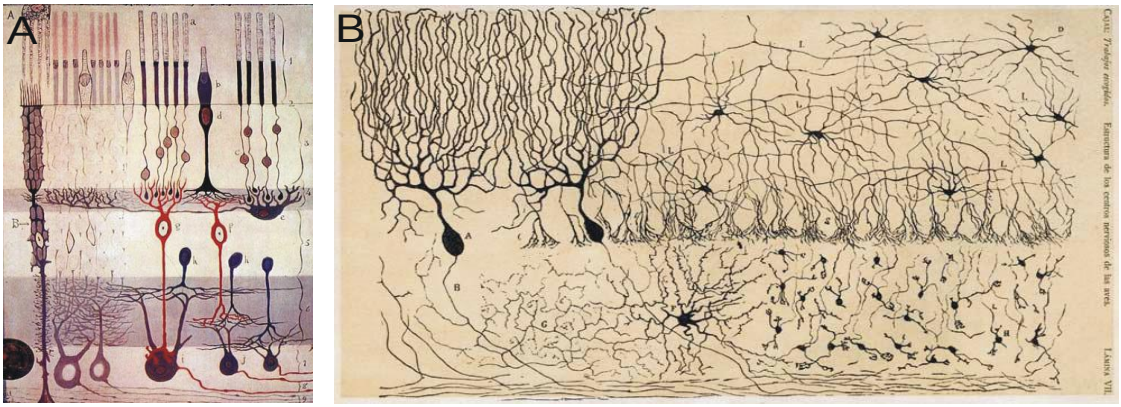

Figure 1: Neuronal diversity and structural organization of the brain by Ramón y Cajal

These drawing are based on Cajal's observations of Golgi stained tissue sections using a light microscope. **A:** Structural organization of the mammalian retina showing the different types of photoreceptors on the top, amacrine cells in the middle layers and retinal ganglion cell projecting to higher brain centers on the bottom. Adapted from “Structure of the Mammalian Retina" Madrid, 1900. **B:** Architecture of the chick tectum illustrating the variety of neural cell types and their organization in distinct layers. Adapted from "Estructura de los centros nerviosos de las aves", Madrid, 1905.

Ever since these early revelations by Cajal at the beginning of the 20th century, continuous technological advances have led to the development of invaluable electrophysiological and genetic tools enabling us to describe and classify neurons according to more sophisticated criteria. We can address more complex questions such as how spatial and temporal gene and protein expression profiles of emerging neuronal subpopulations interrelate to create functional biological outputs. However, despite accumulating data adding to our appreciation of also the molecular mechanisms at play, the tremendous complexity of the mammalian brain still constitutes a major obstacle in modern neuroscience.

In order to tackle this difficulty, it has proven fruitful to address certain neurobiological questions using model organisms with less complex nervous systems such as

arthropods or nematodes. For instance the nervous system of *C.elegans* has been deciphered at single neuron resolution: 302 neurons and 56 glial cells have been characterized and ordered into 118 distinct neuron classes (Hobert, 2005). Despite some astoundingly conserved functional mechanisms in body patterning, evolutionary strategies coordinating communication within more complex neuronal systems must have emerged at later time points of evolution and there are therefore problems which can only be studied in higher organisms. Moreover, the development of biotechnological methods, such as the possibility to also engineer genetically modified mice, contributed to the rise of mammalian model systems. Today, the value and applicability of mechanistic insights derived from studies with rodents to the understanding of our own nervous system are beyond doubt highly appreciated, although complexity of the system remains an issue. For these reasons neurobiologists seek to use simple neuronal circuits, which exemplify molecular mechanisms and processes with more universal applicability.

In the mammalian CNS, the monosynaptic stretch reflex circuit of the SC is in many ways ideally suited for the investigation of neuronal circuit formation: MNs projecting to limb muscles receive selective monosynaptic input from Ia proprioceptive sensory afferents innervating the same or synergistic muscles (Eccles et al., 1957; Chen et al., 2003). The foremost advantages of the monosynaptic stretch reflex circuit lies therefore in its relative simplicity (as in principle only two neuronal populations, connect and interact with each other), its ease of accessibility for manipulation, the possibility to perform specific circuit tracing as well as its readily recordable biological output (muscle contraction, withdrawal reflexes and locomotion). The combination of these characteristics make the monosynaptic reflex circuit an ideal model for the study of as diverse interdependent processes such as axonal pathfinding (Arber et al., 2000; Kania

and Jessell, 2003; Marquardt et al., 2005), specificity in synaptogenesis (Mendelson and Frank, 1991; Wenner and Frank, 1995; Vrieseling and Arber, 2006), cell migration (Livet et al., 2002; Price et al., 2002), dendritic patterning (Vrieseling and Arber, 2006) and the establishment of neuromuscular connectivity (Hippenmeyer et al., 2007; Garcia and Jessell, 2008). Moreover, spinal reflex circuits have been the focus of numerous studies in the past which led to the establishment of valuable experimental techniques, notably electrophysiological recordings from spinal neurons, retrograde labeling of isolated motor units (Romanes, 1951) or the induction and manipulation of alternating locomotor-like activity in ex-vivo preparations (Butt et al., 2002).

The wealth of data form previous work has provided important insights into the molecular mechanisms that direct neuronal specification and circuit formation in the SC (Eccles et al., 1957; Chen et al., 2003; Ladle et al., 2007) and paved the way for the application of more sophisticated analysis. Ideally, biological concepts emerging from our work on spinal circuitry could provide an entry point into the functional analysis of more complex brain division and through this eventually contribute a piece of the puzzle to the understanding of the human CNS in general.

1.2 Components of proprioceptive reflex circuits

For a species to navigate coordinately in space, sensory feedbacks from the moving limb are essential. The information about limb position is acquired by proprioceptive receptors residing in limb muscles and joints and allows an animal to undertake constant adaptations to the environment and quickly compensate for unexpected postural disturbances. Logically, the term proprioception is composed of the Latin term proprius, meaning "one's own" and perception. Thus proprioception is the bodily sense that perceives the relative position of our limbs in space and is employed during movement to provide feedback about the progression of and deviations from the

intended motion, making coordinated muscle-activity possible. The adjustment of stepping by means of proprioceptive sensory feedback is based on information about muscle length, stretch, contraction and joint angles and occurs via central reflex pathways to MNs, either directly or by acting on central pattern generator networks controlling gait.

It should be noted, that proprioception constitutes only one of four major classes of somatosensory modalities conveyed through dorsal root ganglia (DRG) which are found aligned adjacent the rostrocaudal axis of the SC. The three other sensory modalities comprise (1) discriminative touch, mediated by subcutaneous mechanoreceptors, (2) nociception, mediated by thermal-mechanical receptors and (3) temperature sense, mediated by thermal receptors. Historically, the subclassification of proprioceptive sensory fibers from muscles is based on axon diameters. Table 1 summarizes the different types of proprioceptive afferents and the location of their receptor terminals in the periphery.

Type	Receptor	Axon	Sensitive to
Ia	Primary spindle endings	12-20 μm myelinated	Muscle length and rate of change in lenght
Ib	Golgi tendon organs	12-20 μm myelinated	Muscle tension
II	Secondary spindle endings	6-12 μm myelinated	Muscle length (little rate sensitivity)
II	Non-spindle endings	6-12 μm myelinated	Deep pressure

Adapted from Principles of Neural Science, 4/e, Ch. 21, p. 414

Table 1: Major classes of proprioceptive afferents

The monosynaptic reflex circuit is exceptional among all reflex modalities, insofar as the involved Ia proprioceptive fibers are the only peripheral sensory afferents that make direct, monosynaptic, connections to MNs (Figure 2). Typically, the monosynaptic stretch reflex circuit is activated by sudden unanticipated stretch of a skeletal muscle such as occur in tripping. Rapid stretch is perceived by Ia proprioceptive afferents inside muscle spindles, activation of which contributes to quickly regain balance by

inducing the necessary corrections in limb position. The peripheral terminals of Ia proprioceptive afferents innervate specialized encapsulated receptor structures referred to as intrafusal muscle fibers which are embedded in parallel with extrafusal muscle fibers responsible for actual muscle contraction. Electrical activity in Ia proprioceptive afferents positively correlates with the rate at which a muscle changes its length and its thus especially sensitive to sudden stretches of the muscle. Electrical impulses of Ia proprioceptive afferents are propagated through their cell bodies in the DRG, enter the SC via dorsal root and activate MNs located in the grey matter of the ventral horn. Selective activation of these MNs will counteract the detected involuntary stretch by stimulating muscle fibers which contract and thus shorten the muscle back to its intended length.

Besides Ia afferents terminals, intrafusal muscle fibers are also contacted by type II sensory terminals, which primarily convey information about the length of the muscle rather than its speed of change. In addition, the CNS disposes of means to adjust the sensitivity of intrafusal muscle through activation of γ-MNs that form efferent neuromuscular terminals on intrafusal muscle fibers. γ-MNs can be employed to increase the dynamic sensitivity of Ia nerve endings (Boyd, 1986; Jami, 1992).

Ib type sensory neurons innervating Golgi tendon organs which are located at the junction between muscle fibers and tendon. Whereas muscle spindles are most sensitive to changes in muscle length, Golgi tendon organs are tuned to detect alterations in muscle tension and their firing rate is in good correlation with the general contractile state of the muscle (Figure 2) (Jami, 1992). Their functionality implies comparably high activity during locomotion, but they are not required to maintain rhythmic left right alternation during walking.

In contrast, noxious stimuli to the skin elicit limb withdrawal reflexes which are detected by nociceptive sensory neurons. These sensory feedbacks are exclusively conveyed via polysynaptic pathways to MNs, meaning the signal is relayed through at least one additional local interneuron, sometimes referred to as reflex encoders (Schouenborg et al., 1995; Schouenborg, 2008). Among other functions, nociceptive feedback circuits are employed to coordinate and time movement involving simultaneous activation of multiple muscles that result in more complex movements, such as required for the withdrawal of an entire limb from a noxious source.

1.2.1 The sensory component of the reflex circuit

The major subclasses of proprioceptive sensory afferents not only differ with respect to their peripheral targets but they also display differences in their synaptic targets in the SC.

Monosynaptic connections between Ia afferents and MNs are highly specific and are only established between motor neuron pools innervating the same (homonymous) from which Ia afferents arise or functionally related (synergistic) muscles. In order to facilitate the biological output of the system, antagonistic muscles, excitation of which would counteract the intended limb movement, are inhibited via so called Ia inhibitory interneuron. Unraveling the molecular mechanisms which govern the regulation of proprioceptive sensory-motor specificity is still a major challenge of today's neurbiological research as it requires profound understanding of the developmental processes specifying the identity of both, Ia proprioceptive afferents and their cognate group of MNs. Identification of the transcriptional programs engaged in the diversification of MN pools has received considerable attention in recent years and important insights about a number of molecular mechanisms at play have been achieved (see review below).

Differentiation of DRG neurons is controlled in progenitor cells by sequential activities of the two basic helix-loop-helix transcription factors neurogenin1 and neurogenin2, and their combined loss results in a complete absence of DRG neurons (Ma et al., 1999). While in *Ngn2* mutant mice, the generation of sensory neurons is delayed but not abolished, *Ngn1* mutant mice exhibit a marked decrease in the number of cutaneous DRG sensory neurons (Ma et al., 1999). More recently, the family of Runt transcription factors has been shown to be implicated in the specification of distinct submodalities of sensory neurons. Generally, expression of Runx1 is restricted to the neurotrophic factor receptor TrkA and Runx3 in the TrkC population (Inoue et al., 2002; Levanon et al., 2002) and their activities control expression of an array of cell surface molecules including thermal receptors, ion channels and G-protein coupled receptors, as well as the positions of central terminations (Chen et al., 2006b; Kramer et al., 2006). Similarly, differential expression of TrkA, TrkB and TrkC have been shown to play essential roles in the initiation of the early diversification processes (Bibel and Barde, 2000; Huang and Reichardt, 2003) and can be used in combination with other molecular markers, such as Runx transcription factors or peptidergic neurotransmitters, to distinguish sensory neurons of different modalities in DRG. However, we can only speculated about how TrkC/Runx3 expressing Ia proprioceptive afferents diversify into distinct subclasses in order to meet the specificity requirements of their peripheral and central targets (Price et al., 2002).

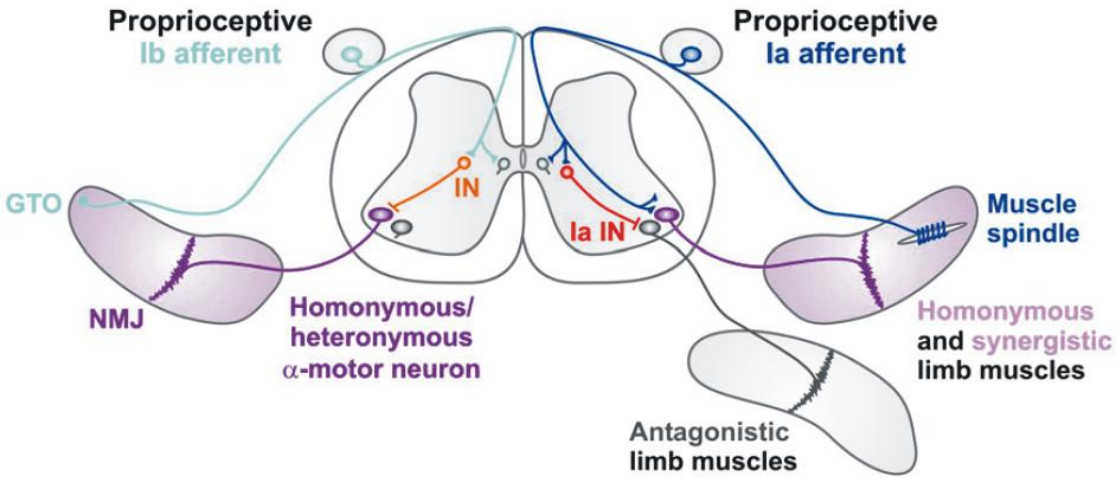

Figure 2: Spinal reflex circuitry of proprioceptive sensory neurons

Central and peripheral projections of group Ia (right: blue) and Ib (left: light green) proprioceptive sensory neurons. **Left:** Group Ib proprioceptive sensory neurons innervate Golgi tendon organs located at the junction between muscle fibers and tendons of skeletal limb muscles. Group Ib afferents extend through the DRG into the intermediate SC where they form synapses with interneurons (IN: orange), some of which make direct contact with α–MNs (blue and turquoise) in the ventral horn. **Right:** Group Ia proprioceptive sensory neurons peripherally innervate muscle spindles and centrally form direct monosynaptic connections to homonymous and synergistic MN pools (blue and turquoise). MNs projecting to antagonistic muscles (turquoise) are innervated in polysynaptic fashion via Ia inhibitory interneurons (Ia IN: red).

While MNs and Ia inhibitory interneurons are essential components of the monosynaptic stretch reflex circuit, they are by no means the only synaptic partners of Ia proprioceptive afferents in the SC. Additional termination zones exist in defined regions of the central grey matter and the dorsal horn, from where somatosensory information is relayed into local, ascending and descending neural pathways. Yet, because of the increasing complexity of higher order connectivity and the lack of molecular markers for many subpopulations of interneurons, little is understood about the organization of higher order sensory connectivity.

In contrast to Ia terminals, group Ib proprioceptive afferents only form polysynaptic connections with MNs (Figure 2). Their firing pattern is strongly correlated with the state of muscle contraction (its tension) and consequently direct synaptic connections on MNs are not functionally meaningful (Jami, 1992). Instead, excitatory signals from Golgi tendon organs are first integrated by networks of local interneurons and/or higher brain centers before they are fed back to spinal MNs. The information provided by

group Ib proprioceptive afferents can for instance be used to adjust the firing rates of MNs such that an intended contractile state is maintained despite growing muscle fiber fatigue.

1.2.2 The motor unit and muscle action

The specialized type of synapse connecting motor axons with muscle fibers is referred to as neuromuscular junction (NMJ) and insofar unique as it constitute the only direct contact point between neurons of the CNS and non-neuronal cells in the body. For this reason, MNs truly represent the ultimate behavioral output system of the CNS.

With the exception of the first two developmental weeks, when synaptic pruning takes place (Sanes and Lichtman, 1999), every muscle fiber is stimulated by only a single MN. However, depending on the functionality of a muscles, a single motor axon can ramify and contact between 100 and 1000 individual muscle fibers (Kandel et al., 2000). The group of muscle fibers contacted by a single MN is called muscle unit and together with the associated MN the ensemble is referred to as a motor unit (Liddell and Sherrington, 1925). Motor units size can in principle be regarded as a measure of dexterity for the movement of a given muscle insofar as the smaller it is, the more fine-tuned and precise is also the control of movements for this muscle.

In the SC, MNs distinguish themselves from interneurons by their large soma size. Although, morphologically dendritic patterns can vary significantly between MN pools supplying muscles with distinct behavioral functionalities (Vrieseling and Arber, 2006), most synaptic connections are probably formed in the ventral horn and central grey matter. However, MN dendrites can also expand into the white matter and, medially, across the midline into the contralateral hemisphere of the SC. The distribution of boutons on spinal motor dendrites has been studied in primates and is surprisingly uniform. Roughly half of the membrane of the MN soma and equally much its proximal

and distal most dendrites are covered by presynaptic boutons (Starr and Wolpaw, 1994). In cat, a single MN can receive an estimated 100'000 synaptic boutons from roughly 10'000 – 20'000 presynaptic neurons (Kernell, 2006). In this context it should be considered, that the large size of MN somas also reflects the spatial requirement of the cytoplasmatic protein synthesis and trafficking machinery necessary to supply the enormous surface of dendritic and axonal membrane (Shepherd, 2004).

Besides direct monosynaptic inputs from the sensory system, which account only for 1-2% of the total input to MNs in cat (Burke and Glenn, 1996), spinal motor neurons receive important inputs from local interneurons, some of which are part of central pattern generator networks controlling gait (Kiehn, 2006). In addition MNs can be directly contacted by descending fibers from higher brain centers, including a number of nuclei in the brain stem and corticospinal projection neurons (Terashima, 1995).

In the SC, two major types of MNs are distinguished. First, α-MNs (in the present study usually simply "MNs") innervate extrafusal muscle fibers and are responsible for the exertion of contractile force. Second, γ-MNs exclusively innervate intrafusal muscle fibers located in muscle spindle stretch receptors and regulated the sensitivity of the two types of muscle spindle afferents, group Ia and group II both innervating muscle spindles.

α-MNs are generally bigger than γ-MNs and exhibit faster speeds in action potential (AP) propagation (Andrew and Part, 1972; Shepherd, 2004). Moreover, unlike γ-MNs, almost all α-MN receive monosynaptic group Ia proprioceptive afferents. Although, α- and γ-MNs have been characterized physiologically, virtually nothing is known about the molecular programs that direct their differentiation. For a given MN pool however, the one-to-one connectivity of γ-MNs and their peripheral targets allows at least an estimation of their numbers by counting stretch receptor spindles in the muscle.

γ-MNs are further subdivided into static and dynamic subtypes. While static γ-MNs regulated the sensitivity of changes in muscle length, dynamic type γ-MNs are responsible for the modulation of sensitivity to rates of change in muscle length (Shepherd, 2004).

Similarly, limb muscles are innervated by two fundamentally different types of motor units which have been categorized by morphological and mechanical properties of the muscle fibers they innervate. Slow twitch (S) motor units are opposed to fast twitch motor units (F), whereas the latter is further subdivided in fast fatigable (FF) and fatigue resistant (RF) subpopulations (Shepherd, 2004). S and F motor units are primarily distinguished on the basis of the relation between the maximal contractile force and the duration of the muscle twitch they elicit. F type units cause a quick and strong unitary response while the contraction of S type muscle units last longer but exert less contractile force per unit time. Centrally, these motor units also exhibit a number of anatomical and physiological differences in terms of their interactions with proprioceptive feedback loops (Powers and Binder, 2001). Collectively, the existence of these different α-motor unit modalities allows the motor system to adjust the contractile state of individual muscles in a more sophisticated manner and most subtle modulations of voluntary movement or body posture become possible. However, despite the lack of knowledge about the molecular processes specifying the differentiation of these distinct types of motor units within a single MN pool, the present study is not designed to address them, but has set its focus on molecular differences between the ensembles of MNs belonging to different MN pools

2 Transcriptional Mechanisms Controlling Motor Neuron Diversity and Connectivity

Current Opinion in Neurobiology 2008 Feb;18(1):36-43;
Dalla Torre di Sanguinetto SA, Dasen JS, Arber S
Mechanisms Controlling Motor Neuron Diversity and Connectivity

The control of movement relies on the precision with which motor circuits are assembled during development. Spinal MNs provide the trigger to signal the appropriate sequence of muscle contractions and initiate movement. This task is accommodated by the diversification of MNs into discrete subpopulations, each of which acquires precise axonal trajectories and central connectivity patterns. An upstream Hox factor-based regulatory network in MNs defines their competence to deploy downstream programs including the expression of Nkx and ETS transcription factors. These interactive transcriptional programs coordinate MN differentiation and connectivity, defining a sophisticated roadmap of motor circuit assembly in the spinal cord. Similar principles using modular interaction of transcriptional programs to control neuronal diversification and circuit connectivity are likely to act in other CNS circuits.

2.1 Introduction

The assembly of neurons into precisely interconnected neural circuits is crucial for nervous system function and depends on the specification of defined neuronal subpopulations during development. Motor circuits are responsible for the control of movement, an animal behavior that is the final output of most nervous system activity. Initiation and execution of body movement are controlled at many levels, but all information is ultimately channeled towards MNs in the spinal cord, the activation of which triggers contraction of muscles in the periphery. MNs therefore provide the exclusive action link between the nervous system and motor output. To cope with this challenging task, MN subpopulations acquire unique identities during development

allowing them to receive specific connections centrally and relay this information to defined muscles peripherally.

Spinal progenitor cell differentiation is initiated by inductive signaling interactions operating through transcriptional programs (Jessell, 2000). As a consequence of dorso-ventral signaling, MNs acquire a unique transcriptional profile (e.g. expression of the homeodomain proteins Hb9 and Isl2) distinguishing them from spinal interneuron populations shortly after leaving the cell cycle (Arber et al., 1999; Thaler et al., 1999; Jessell, 2000; Thaler et al., 2004). Recent work has begun to shed light on how distinct transcriptional networks act at postmitotic stages of MN differentiation to diversify MNs, the topic representing the main focus of this review. In particular, we will address how different sequential and parallel transcriptional programs intersect during MN differentiation to establish a unique three-dimensional motor coordinate system required to steer movement. Understanding the logic of these transcriptional control programs provides important mechanistic insights into the principles underlying the generation of a diverse array of MN subpopulations, which acquire highly specific peripheral trajectories, stereotypic cell body positions and central connections. We review these findings in the context of the relative contributions of hierarchical and parallel pathways to the coordination and acquisition of distinct phenotypic traits gained by MNs during the course of postmitotic differentiation. Moreover, we discuss how progressive transcriptional specification of MNs establishes their competence to respond to programs initiated at later differentiation steps. How these sequential genetically-determined transcription factor mediated programs interact with activity-dependent processes during development has recently been reviewed elsewhere (Ladle et al., 2007; Hanson et al., 2008).

2.2 Acquisition of motor neuron identity to accommodate target diversity

The establishment of precise connections between MNs and the muscular output system requires their strategic alignment along the body axis. In order to accommodate differences in peripheral targets throughout the body, MN number, identity and connectivity differ significantly along the rostro-caudal axis of the spinal cord. Analyzed anatomically, MN cell bodies are organized into motor columns according to broad projection territories such as limbs (lateral motor column; LMC) or the autonomic nervous system at thoracic levels (preganglionic column; PGC), and these columns are formed only at appropriate segmental levels (Landmesser, 2001) (Figure 1, A). Within motor columns, groups of MNs projecting to individual muscles in the limb are clustered into MN pools, subdividing the vertebrate LMC into approximately 50 defined groups of MNs (Romanes, 1942; Romanes, 1951; Hollyday and Jacobson, 1990; Landmesser, 2001). While many aspects of this sophisticated anatomical organization only emerge gradually during development, the initiation of phenotypical diversification is programmed into MNs at very early stages, long before motor axons first meet their target muscles.

2.2.1 Hox factors and motor neuron specification

Is there a coherent molecular program that drives MNs to differentiate into distinct subpopulations at each segmental level to match the needs of their axonal targets? Several recent studies provide evidence that members of the vertebrate Hox gene family, homeodomain transcription factors consisting of 39 members located on four chromosomal clusters (McGinnis and Krumlauf, 1992; Kmita and Duboule, 2003), play key roles in assigning both columnar and MN pool fate. In the spinal cord as elsewhere in the body, the overall expression of individual Hox genes along the rostro-caudal axis

is closely linked to position within a chromosomal cluster (McGinnis and Krumlauf, 1992; Kmita and Duboule, 2003). This raises the possibility that the combinatorial expression patterns of Hox genes may also contribute to segmental specification of motor circuits. Analysis of Hox expression at the cellular level in combination with recently defined markers for different motor columns and MN pools has made progress possible.

How do Hox proteins program motor column and pool fate? The specification of segmentally-restricted motor columns is controlled by Hox proteins with expression patterns that prefigure their rostro-caudal extents (Figure 3, A). The emergence of brachial LMC MNs in the chick, marked by the expression of the retinaldehyde dehydrogenase-2 (RALDH2) gene requires Hox6 activity (Dasen et al., 2003). Similarly, at thoracic levels of the spinal cord, Hox9 activity is essential to program PGC fate characterized by the expression of bone morphogenetic protein-5 (BMP5). Specific gain- and loss-of-function experiments in the chick demonstrate that Hoxc6 and Hoxc9 activities are sufficient to transform columnar identity not only at the level of molecular markers, but also with respect to column specific establishment of peripheral trajectories (Dasen et al., 2003). The expression patterns of other Hox proteins do not obey the rostro-caudal boundaries set by emerging columns, but act in two distinct ways to specify MN pool identities (Dasen et al., 2005). MN pools occupy specific rostro-caudal subdomains within a single motor column (Figure 3, B), and within the chick brachial LMC, Hox5 proteins are restricted to rostral pools while Hox8 proteins mark caudal pools (Tiret et al., 1998; Dasen et al., 2005; Vermot et al., 2005) (Figure 3, B). In addition, within a single rostro-caudal level, several MN pools emerge in parallel, and this intrasegmental diversification is driven by cross repressive interactions between multiple Hox proteins (Dasen et al., 2005) (Figure 3, C). For

example, the specification of forelimb innervating MN pools within the Hoxc8+ domain requires the actions of Hox4, Hox6, and Hox7 paralogs (Dasen et al., 2005) (Figure 3, C).

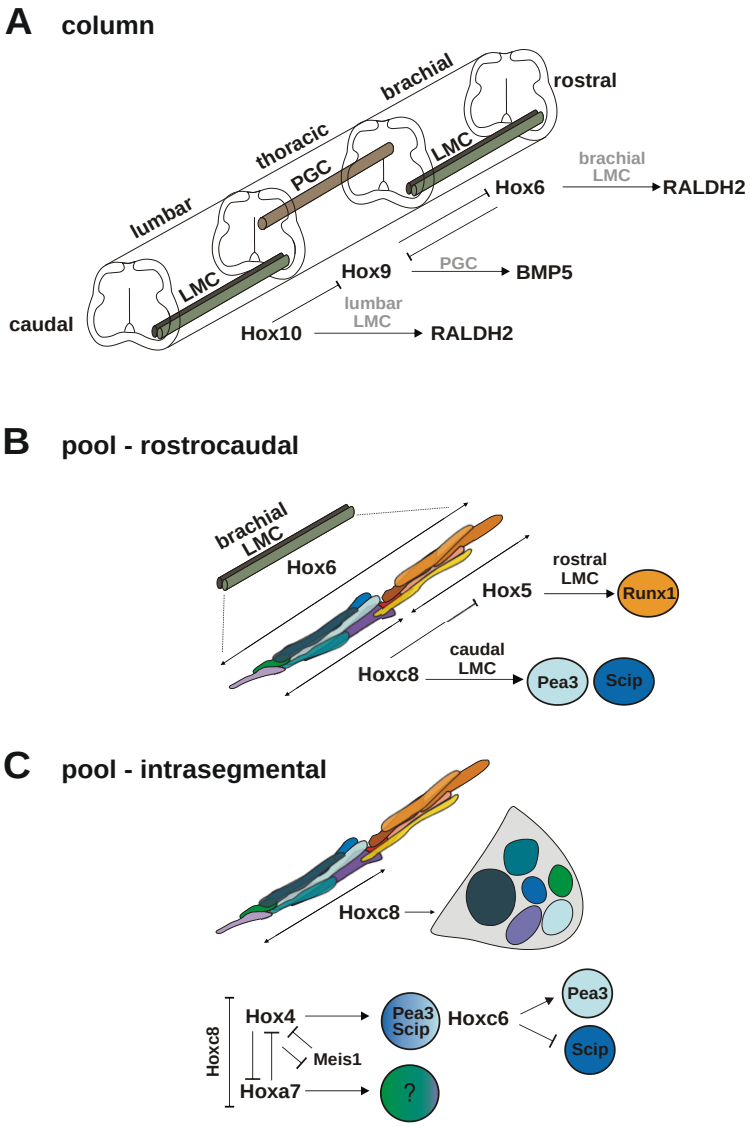

Figure 3: Hox mediated mechanisms controlling MN columnar and pool identities

A: In the developing SC the emergence of MNs at brachial and lumbar segmental levels innervating skeletal limb muscles is characterized by the formation of LMCs. Segmental levels of the thoracic SC lack LMCs but can be identified by their formation of PGCs . In chick the development of brachial and thoracic columnar identities is controlled by the mutually repressive interactions of Hoxc6 and Hoxc9 proteins (Dasen et al., 2005). These proteins are mutually cross-repressive and appear to play instructive roles for the induction of the brachial and thoracic motor column identity markers such as RALDH2 and BMP5, respectively. Similarly, at lumbar LMC levels Hox10 activity directs the establishment of lumbar columnar identity by repressing Hox9. (Lance-Jones et al., 2001; Lin and Carpenter, 2003; Tarchini et al., 2005; Choe et al., 2006; Wu et al., 2008). **B:** At brachial levels Hox5 and Hoxc8 direct the subdivision of the LMC into a rostral Hox5 positive and caudal Hoxc8 positive LMC domain. This rostrocaudal subspecification of the LMC through Hox activities constitutes an early hierarchical step in motor pool differentiation and increases the diversity of transcriptional pool identities required for latter steps of MN pool differentiation (Dasen et al., 2005). **C:** At a specific segmental level multiple Hox proteins are expressed. A fine-tuned regulation of their repressive interactions determines motor pool transcriptional identities. Within the rostrocaudal extent of Hoxc8, the Hoxc4 positive LMC domain is permissive for both, Pea3 and Scip positive MN pools. The terminal specification of the Scip MN pool is obtained by exclusion of Hoxc6 expression (Dasen et al., 2005).

Analysis of the role of Hox transcription factors in fine aspects of MN pool differentiation was heavily dependent on the availability of selective MN pool markers. Within the LMC, anatomically defined MN pools can be identified by expression of specific transcription factors, such as the ETS transcription factor Pea3 or Er81 (Lin et al., 1998; Arber et al., 2000; Livet et al., 2002; Vrieseling and Arber, 2006), the runt-related protein Runx1 (Dasen et al., 2005), or the Pou-domain transcription factor Scip (Helmbacher et al., 2003; Dasen et al., 2005). Functional experiments changing Hox codes in MN pools went hand in hand with specific alterations of MN pool markers, and these gene expression changes were tightly linked to alterations in motor axon trajectories to muscle targets (Dasen et al., 2005).

Together, these findings provide strong evidence for a deterministic role of Hox networks in the diversification of MNs at columnar and pool levels. Hox factor programs play instructive roles for the acquisition of subpopulation-specific gene expression patterns and establishment of peripheral trajectories. Whether this role is also extended to the acquisition of appropriate central connectivity and maturation of late MN pool specific traits is currently unknown. Given the dominant upstream role in programming MN identity, it is most likely that these important aspects of motor circuit assembly lie downstream of Hox transcriptional programs as well.

2.2.2 Mechanisms regulating Hox activities

Are Hox gene networks used to specify all motor columns and pools? At a rough level of analysis, domains of Hox factor expression cover the entire rostro-caudal extent of the spinal cord, but their precise contribution to each segmental level has not been analyzed. At the lumbar level of the spinal cord, Hox10 proteins are expressed and play a crucial role in MN specification (Lance-Jones et al., 2001; Lin and Carpenter, 2003; Tarchini et al., 2005; Choe et al., 2006; Wu et al., 2008). However, how changes in

cellular identity parallel alterations in peripheral trajectory is less clear than at brachial levels where combinatorial expression of Hox proteins at the MN pool level seems to determine target muscle innervation for at least some MN pools (Dasen et al., 2005). Moreover, it is unclear whether all MN subtypes are equally competent to respond to the activity of Hox factors or whether the cellular context programmed at progenitor stages only equips a subset of MNs to be malleable by Hox transcription factors.

It is interesting to note that MNs within the medial motor column (MMC) innervating axial muscles display differentiation properties independent of Hox activity and thus appear to escape Hox-dominated MN differentiation programs (Dasen et al., 2003). In this context, it must be considered that Hox transcription factor activity and function also depend on interaction with a variety of cofactors such as Pbx and Meis homeodomain proteins (Moens and Selleri, 2006), some of which are expressed in subpopulations of spinal neurons during development (Dasen et al., 2005; Rottkamp et al., 2008). Manipulation of their expression not only affects Hox target specificity, but can also result in alterations of Hox gene expression (Dasen et al., 2005) and lead to phenotypes similar to mutation of Hox factors themselves (Moens and Selleri, 2006). Testing for degrees of Hox-responsiveness will therefore require a deeper understanding of the mechanisms through which Hox transcriptional networks regulate MN differentiation.

It is evident that the function of individual Hox proteins cannot be studied in isolation. First, Hox genes are embedded within genomic clusters and expression of at least some members is under the control of long-distance regulatory genomic elements (Kmita and Duboule, 2003). As a consequence, altering Hox loci by mouse genetic strategies can change the expression of other Hox genes in some instances (Carpenter, 2002; Tarchini et al., 2005). Functional redundancy between Hox paralogs also complicates genetic

analysis in mice. In contrast, experiments in chick embryos using *in ovo* electroporation leave the genome intact and can easily assess function of paralogs (Dasen et al., 2003; Dasen et al., 2005). Second, Hox proteins function through transcriptional cross repression or activation of gene expression and these mechanisms ensure that certain columns or MN pools are generated only at specific segmental levels (Dasen et al., 2003; Dasen et al., 2005). Thus, cross-regulatory interactions between different Hox factors must be considered when studying the function of individual transcription factors. Cross-repressive transcriptional mechanisms are also used for dorso-ventral patterning at progenitor cell stages (Jessell, 2000; Muhr et al., 2001), but Hox interactions occur predominantly in postmitotic neurons (Dasen et al., 2005). The mechanisms by which the Hox regulatory network intersects with the output of the dorso-ventral transcriptional program(s) through which MN emerge remains to be determined. Third, Hox gene expression is also tightly regulated through histone modifications and collinear activation of Hox genes is partly the result of a progressive opening of the chromatin structure within their genomic cluster (Soshnikova and Duboule, 2008). Although epigenetic modifications are likely to play a more prominent role in the initial developmental activation of Hox loci, a complete understanding of the regulation of Hox factor activity involved in MN diversification will undoubtedly also require a comprehensive view of the epigenetic mechanisms at play at different developmental stages.

2.2.3 Translating Hox activities to generate motor neuron subtypes

At the level of MN pool specification, interactions between different Hox factors may also play an important role in assigning the neuronal number within a given MN pool, a parameter which has to be set in accordance with the target before motor axons project

to the periphery. Slight alterations in cross-repressive balances may therefore be used to alter neuronal number in homologous MN pools during evolution, to parallel changes in size or identity of muscles. Comparing differences in Hox gene function in MNs innervating anterior extremities of chick (wings) and mice (forelimbs) should provide important insight into evolutionary changes and their relation to Hox transcription factor networks in the future.

Despite the striking diversity of MN subtype identities in the spinal cord, there are also certain molecular features that are reiterated along the rostro-caudal axis. LMCs are generated at both forelimb and hindlimb levels, and these LMCs show remarkable similarities in terms of their anatomical organization and gene expression patterns. Within both brachial and lumbar LMCs, a rough topography between MN pool position and innervated muscle target exists, and MN pools innervating proximal limb muscles are found in more rostral positions than MN pools projecting to distal limb muscles (Romanes, 1951; Landmesser, 1978, 1978; Ryan et al., 1998). Moreover, common columnar markers (e.g. RALDH2 and Lhx1) as well as MN pool markers (e.g. Pea3, Scip, Nkx6.1) are expressed by MNs within both of these columns. Despite these organizational similarities, distinct Hox regulators are involved in cervical and lumbar LMC specification, suggesting that combinatorial expression of different Hox paralogs can result in the control of both common and distinct target genes. The unique combination of Hox factors at brachial and lumbar levels thus regulates generation of MN subtypes required at each segmental level, but in addition allows implementation of essential commonalities. Although the molecular mechanism that allows distinct Hox proteins to regulate common target genes is unknown, it is likely to have its origins in the organization of the cis-regulatory elements within these critical MN-specific genes.

The intersection of the transcriptional programs that determine MN specification along the dorso-ventral and rostro-caudal axes provides important information for the establishment of a three-dimensional coordinate system. These transcriptional networks could equally well be read out by other cell populations in the spinal cord and thereby contribute to diversification of interneuron subpopulations for which essentially nothing is known about possible level-specific function and connectivity. Yet, in order to ensure proper functioning of motor circuits, intersecting neuronal circuit elements such as interneurons or information provided by sensory afferents needs to be matched and coordinated with the respective local environment at a three-dimensional level. Intriguingly, Hox factors are not only expressed in distinct patterns in MNs, but also in yet undefined but restricted patterns in interneurons and dorsal root ganglion (DRG) sensory neurons (Dasen et al., 2003; Dasen et al., 2005). Combinatorial profiles of Hox proteins may therefore contribute to the assembly of spinal motor circuits more generally than only in MN specification.

2.3 Cell-intrinsic and target-induced transcriptional mediators of Hox activities

The observation that Hox factors provide important instructive cues for MN diversification raises the question of how different MNs interpret and translate combinatorial Hox expression into appropriate downstream signaling cascades and effector molecules. Recent evidence suggests that Hox transcription factors function by controlling downstream modules of intermediate transcription factors which in turn orchestrate more refined aspects of MN differentiation. These intermediate transcription factors can be grouped into a class which is cell-intrinsically induced through a Hox factor-mediated program (Figure 4, A, B) and a second class which requires the presence of target-derived cues (Figure 4, C).

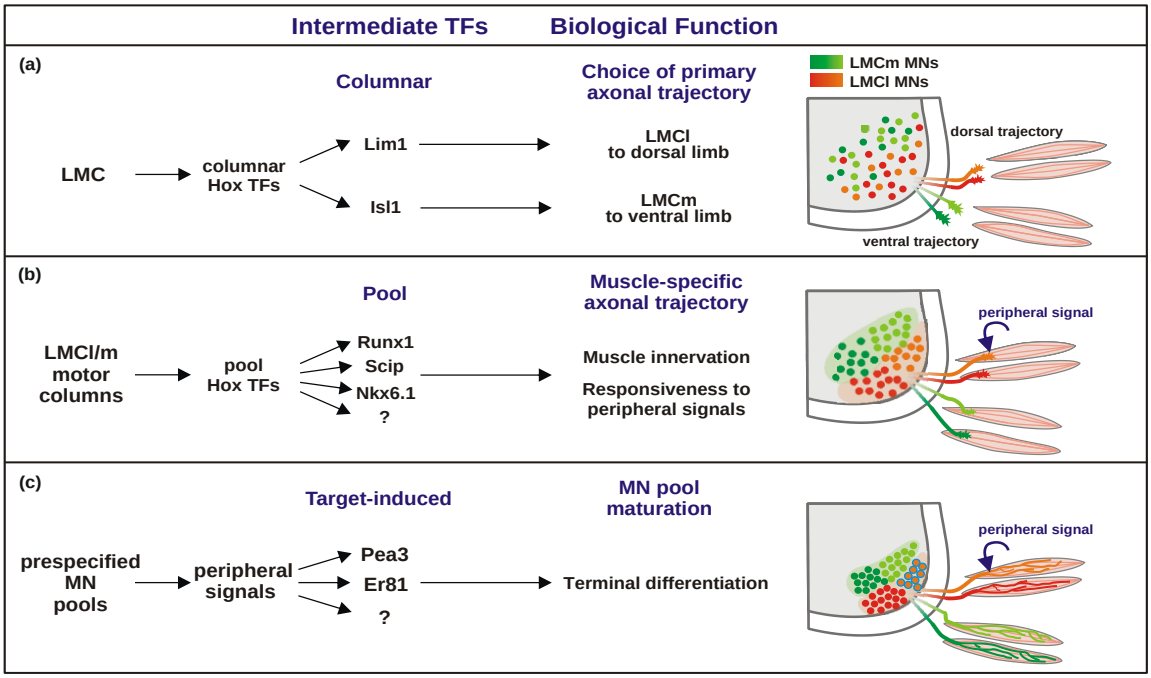

Figure 4: Hierarchical transcriptional programs establish MN pool identities

A: Columnar Hox TFs direct the partition of the LMC into medial and lateral divisions through the activation of LIM-homeodomain TFs Isl1 (LMCm; green) and Lim1 (LMC$_l$; red). These columnar intermediate TFs determine the choice of primary axonal trajectories (Landmesser, 2001; Shirasaki and Pfaff, 2002). Lim1 positive MNs project to ventrally and Isl1 positive MNs to dorsally derived muscles (Kania and Jessell, 2003). **B:** Combinatorial expression of pool Hox TFs directs the activation pool intermediate TFs. Together, the expression of unique combinations of pool Hox and pool intermediate TFs concert the arrangement of motor neurons into prespecified MNs pools with unique peripheral targets and the ability to respond to limb derived signals. **C:** The terminal differentiation of prespecified motor pools can be refined by target induced intermediate TFs. Peripheral signals are encountered and interpreted depending to the diverse axonal trajectories and according to varying cellular contexts of MN pools, respectively. The activities of ETS TFs have been shown to control late aspects of MN pool maturation such as terminal MN pool positioning, axonal branching, dendritic arborization and sensory motor connectivity (Vrieseling and Arber, 2006).

2.3.1 Cell-intrinsic intermediate transcriptional programs

Expression of certain LIM-homeodomain transcription factors defines MN columnar subtypes soon after MNs become postmitotic (Tsuchida et al., 1994; Shirasaki and Pfaff, 2002) and some columnar expression patterns are controlled by Hox transcription factors (Dasen et al., 2003) (Figure 3, A). Combinatorial expression of different LIM-homeodomain transcription factors provides important cues for MN connectivity including the establishment of their initial motor axon trajectories (Landmesser, 2001; Shirasaki and Pfaff, 2002). For limb-innervating LMC MNs, Lhx1 instructs the outgrowth of motor axons towards dorsal limb muscles (Kania et al., 2000) (Figure 4, A) and acts through the control of the Eph/Ephrin signaling system at the choice point at the base of the limb (Kania and Jessell, 2003). Similarly, MNs projecting towards the

dermomyotome (MMC_m) express Lhx3 (Tsuchida et al., 1994) which instructs expression of the fibroblast growth factor (FGF) receptor 1, allowing these MNs to respond to target-derived FGF signals (Shirasaki et al., 2006).

Are there similar intermediate transcription factors acting at the level of MN pools? A recent study provides evidence for a role of the homeodomain transcription factor Nkx6.1 in the establishment of MN pool specific trajectories (Garcia and Jessell, 2008). Nkx6.1 is transiently expressed by all MN progenitors, but its expression is rapidly restricted to MN pools at lumbar levels at the time when motor axons project towards their target muscles. Genetic experiments support the idea that Nkx6.1 is necessary to instruct MNs innervating ventral thigh muscles to correctly grow towards their specific targets (Garcia and Jessell, 2008). MN pool specific expression of Nkx6.1 is independent of limb-derived retrograde signals and appears to emerge through Hox transcriptional control (Garcia and Jessell, 2008) (Figure 4, B). The cell surface molecules which may be controlled by Nkx6.1 and involved in directing axons towards their specified target muscle remain to be identified.

2.3.2 Intermediate transcriptional programs induced by target-derived signals

In contrast to Nkx6.1, the expression of other MN pool specific genes is regulated by target-derived signals (Figure 4, C). Two members of the ETS transcription factor family have been studied extensively (Pea3 and Er81), both with respect to regulatory pathways involved in their induction as well as function. Pea3 and Er81 are expressed in defined MN pools in the vertebrate spinal cord (Lin et al., 1998; Livet et al., 2002; Vrieseling and Arber, 2006) and limb ablation in chick embryos at early stages abolishes their induction (Lin et al., 1998). Whereas glial cell line-derived neurotrophic factor (GDNF) induces expression of Pea3 in specific MN pools (Haase et al., 2002),

the signal inducing Er81 in MNs is currently still unknown, but likely to be of mesenchymal origin (Wang and Scott, 2007). *Pea3* mutant mice exhibit striking alterations in MN cell body positioning, invasion of target muscles, elaboration of MN dendrites and sensory-motor connectivity (Livet et al., 2002; Vrieseling and Arber, 2006). These findings demonstrate that despite the importance of early cell-intrinsic transcriptional programs for MN identity, target-derived programs also exert a profound influence on multiple aspects of MN differentiation.

How are the target-dependent programs linked to the early-established Hox transcriptional networks in MNs? As outlined above, ectopic expression of Hox genes is sufficient to reprogram MN pools and to direct peripheral axonal trajectories. This includes the induction of the ETS transcription factor Pea3 at brachial levels upon missexpression of Hoxc8 (Dasen et al., 2005). However, since Pea3 initiation requires peripheral signals (Lin et al., 1998; Haase et al., 2002), these findings suggest that Hoxc8 expression controls genes that endow MNs with the cellular competence to respond to peripheral cues encountered by Hoxc8^{+} MNs as their axons project towards their target muscles. Consistent with this hypothesis, this domain of competence fails to be established in *Hoxc8* mutant mice and MNs cannot respond by induction of Pea3 (Vermot et al., 2005).

2.3.3 Establishing cellular competence and cell-type specificity

These observations raise the more general question of how distinct MN pools or columns respond to similar transcriptional programs in terms of generating distinct cellular and functional output. While currently available data are still sketchy, they suggest that not all MNs respond equally to expression of the same or similar transcription factors and that the cellular context created by upstream regulatory

pathways represents an important parameter in determining the output that a transcriptional network can generate. The establishment of such a cell-type specific environment will ultimately depend on upstream programs, to which a variety of factors including the combinatorial activities of transcription factors, their cofactors as well as epigenetic mechanisms may contribute.

For example, whereas Nkx6.1 expression controls motor axon trajectories towards defined target muscles, mice mutant for the homologous Nkx6.2 transcription factor expressed in different MN pools do not show defects in target innervation (Garcia and Jessell, 2008). Similarly, while Pea3 expression in two cervical MN pools controls multiple steps in MN differentiation (Livet et al., 2002; Vrieseling and Arber, 2006), expression of the homologous transcription factor Er81 in lumbar MN pools does not influence cell body positioning or target invasion (Garcia and Jessell, 2008). In addition, whether MNs can respond to cues provided by the periphery with the induction of an additional transcriptional program is tightly controlled by their cellular competence. Spinal explants which are confronted with GDNF *in vitro*, only induce Pea3 expression in MNs approximating the normal number *in vivo*, despite the fact that more MNs express functional GDNF receptors (Haase et al., 2002). Moreover, heterochronic limb transplantation experiments in early chick embryos provide evidence that despite the addition of a more mature limb, the onset of ETS transcription factor expression cannot be accelerated through such manipulations (Wang and Scott, 2007). Together, these findings argue that transcriptional programs create a subpopulation-specific cellular context in distinct MN pools which allows them to read out similar signals to create different downstream outputs.

Because our knowledge of the intermediate transcriptional programs acting at the level of MN pool specification is still at an early stage, the currently available data leave

open the possibility that not all MN pools depend on such programs. Some MN pools may inherit sufficient information for differentiation by directly reading out information acquired through Hox transcription factors without intersecting with additional transcriptional programs. Similarly, evolutionary expansion in the number of intermediate transcriptional programs could lead to more sophisticated differentiation programs further diversifying neuronal populations. Yet, only future work will reveal whether and to what extent the differentiation of distinct MN subpopulations occurs through a different number of intermediate transcriptional layers for different MN pools.

The concept of combinatorial cascades of transcription factors acting at distinct steps of neuronal differentiation is not unique to spinal MNs. In the DRG, sensory neuron diversification and aspects of central connectivity are driven by activity of Runx transcription factors (Chen et al., 2006; Chen et al., 2006; Kramer et al., 2006; Ladle et al., 2007). Moreover, the ETS transcription factor Er81 is induced by target-derived neurotrophin 3 (NT-3) in proprioceptive afferent DRG neurons (Arber et al., 2000; Patel et al., 2003) and experiments expressing an ETS transcription regulator at premature stages of differentiation in DRG neurons suggest that the appropriate temporal activation of transcription factors is of key importance for their biological function (Hippenmeyer et al., 2005). Whether and how Hox transcription factors also prespecify DRG neurons to acquire cellular competence to downstream transcriptional intermediates is currently unknown.

2.4 Conclusions

Collectively, the studies discussed in this review provide evidence for the existence of sophisticated transcriptional networks acting in MN subpopulations at postmitotic stages to control their appropriate differentiation and incorporation into motor circuits.

The functionality of different transcription factors at sequential steps of MN maturation depends on the cellular context generated by upstream events and intersects with cues encountered by motor axons on the way to their targets. The strategy of generating distinct cellular competences by intrinsic instructive transcriptional programs allows similar permissive signaling cascades to interact with prespecified neuronal populations and yet to generate distinct outputs in different subpopulations. Due to a stereotypic anatomical organization and easily accessible peripheral axonal trajectories, studies on MNs have been at the forefront in the identification of genetic mechanisms generating neuronal diversity. However, future work should be able to build on this knowledge to address how other neuronal subpopulations are diversified on the basis of transcriptional networks and more broadly, how specificity of connections in the nervous system is generated during development.

2.5 Acknowledgments

We thank Thomas Jessell for numerous discussions on topics covered by this review. S.D.T. and S.A. were supported by a grant from the Swiss National Science Foundation, by the Kanton of Basel-Stadt, and by the Novartis Research Foundation. J. D. was funded by a Burroughs Welcome Fund Career Award in Biomedical Sciences and a Whitehead Fellowship for Junior Faculty.

3 Gene Expression Profiling of Cervical Motor Neuron Pools

3.1 Introduction

3.1.1 An unknown repertoire of cell-surface molecules controls motor neuron fate specification

In the previous chapter we have reviewed the transcriptional mechanisms controlling MN diversity and connectivity. Collectively, the discussed findings suggest hierarchical and intercepting transcriptional networks to generate a combinatorial code endowing MNs sharing the same target muscle with a unique molecular identity. To this end, the presentation of exclusive combinations of receptor and signaling molecules at the cell surface is a precondition. Membrane receptors and secreted proteins constitute the cellular interface permitting neurons to communicate with neighboring cells and signals from the extracellular matrix. In developing CNS, several classes of molecules, including cell surface ligand-receptor pairs, have been implicated in the control of neural positioning (Hatten, 2002; Park et al., 2002) and axonal guidance (Yu and Bargmann, 2001; Dickson, 2002; Grunwald and Klein, 2002). Many of these proteins, including cadherins (Price et al., 2002), Slit/Robo proteins (Nguyen-Ba-Charvet and Chedotal, 2002), netrins and their receptors (Salinas, 2003), ephrins and Eph receptors (Tsuchida et al., 1994; Kania and Jessell, 2003) and semaphorins and their receptors (Eline Pecho-Vrieseling et al., unpublished data) have been shown to direct axon guidance or neural cell migration processes in the SC. However, not all of them are expressed in MNs and if so, they cannot readily account for the degree of MN pool specifications necessary to accommodate target diversity.

At least it could recently be demonstrated that the mutually repressive interactions of the LIM-homeodomain transcription factors Isl1 and Lim1 expressed in the medial and

later division of the LMC, respectively, specify the peripheral trajectory of ventrally and dorsally directed axon through differential regulation of membrane EphA receptors. Presentation of EphA receptor at the cell surface of growth cones endows MNs of the LMC_l with the competence to respond to local repulsive ephrinA secretion in the ventral limb mesenchyme. EphrinA/EphA interactions therefore guide LMC_l axons into the dorsal limb musculature and which constitutes the first basic peripheral pathfinding decision for MNs innervating limb muscles (Tsuchida et al., 1994; Kania and Jessell, 2003; Marquardt et al., 2005). However, at the level of individual MN pools, the effector molecules controlling axonal and dendritic patterning, cell migration or specific sensory-motor connectivity are little understood. At least it has been suggested that MN pool aggregation, which is dependent on cellular migration and cell adhesion events, is controlled by members of the type II cadherin family of cell adhesion molecules. In chick, the combinatorial expression patterns of these cadherins allow classification and distinction of MNs at single pool resolution and ectopic expression of cadherins disturbs MN pool formation (Price et al., 2002). Recent data from our own laboratory also suggest Sema3e to act as a Pea3-dependent repulsive guidance cue involved in the regulation of specific sensory-motor connectivity for distinct cervical MN pools (Eline Pecho-Vrieseling et al., unpublished data). Nonetheless, our understanding of the transcriptional mechanisms governing MN subclass diversification is disproportionate compared to our scarce knowledge about the actual effector molecules translating transcriptional identities into cellular outputs.

Peripheral projections of MNs are organized in a topographic manner such that the axonal trajectories and neuromuscular targets of a MN can be predicted from the settling position of its pool in the SC (Romanes, 1951, 1964; Landmesser, 1978b; Vrieseling and Arber, 2006). During the process of cell migration and simultaneous

axonal outgrowth, growth cones encounter guidance cues which trigger intracellular signaling cascades. Appropriate interpretation of these signals allows a neuron to continuously and quickly adjust its cell-surface repertoire of receptors proteins and secreted signaling molecules to changing extracellular environments and these adaptations are also regulated at the transcriptional level. What remains still largely unclear it how the mutual interdependences of transcriptional activity and presentation of cell surface molecules are linked.

To further improve our knowledge about the genes differentially expressed in spinal MNs pools, we sought to establish a method allowing us to simultaneously gain access to the repertoire of transcriptional codes and cell surface molecules of individual MN pools. To this end we aimed to compare the expression profiles of four chosen cervical MNs pools using a combination of retrograde tracing, laser capture microdissection and Affymetrix gene chip technology. The obtained results led to the identification of genes singularly expressed in individual MN pools, many of the products of which are integrated in or secreted from the cell surface and could therefore lie at the basis of chemotactic signaling interactions directing MN fate specification and connectivity.

3.1.2 Choice of cervical motor neuron pools expressing Pea3 for gene chip analysis

Previous work in our laboratory about the role of the ETS transcription factor Pea3 in cervical MN pool specification has led to the establishment of a relatively comprehensive map of the topographic organization of cervical MN pools using retrograde labeling techniques (Vrieseling and Arber, 2006) (Figures 5 and 6A). Pea3 appears to act as a key regulator for an array of aspects in MN pool specification, including dendritic patterning (Figure 6B), MN pool settling position (Figure 6A),

selectivity of Ia afferent connectivity (Figure 6B) and axonal pathfinding (Livet et al., 2002; Vrieseling and Arber, 2006) (Figure 6C).

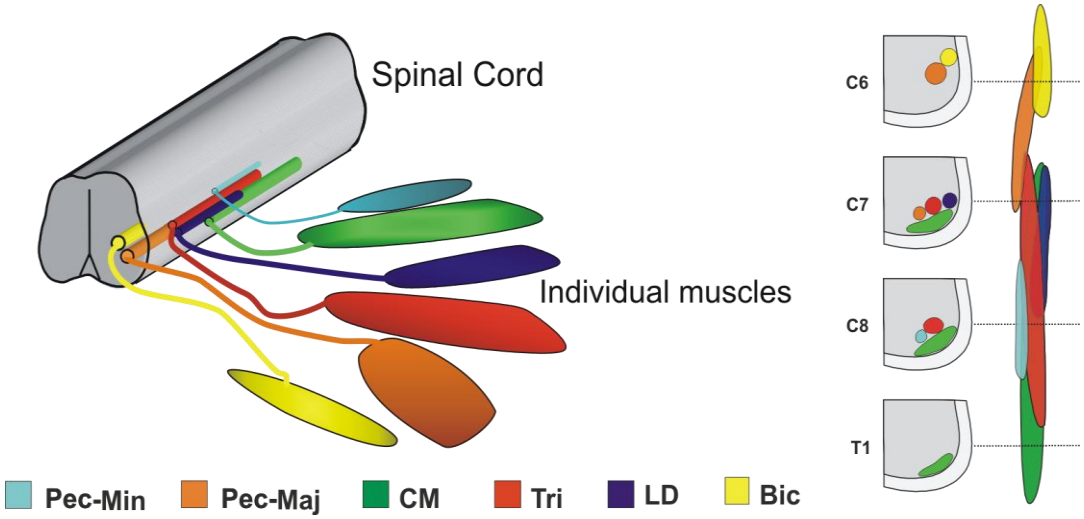

Figure 5: Topographic organization of cervical motor neuron pools

The ensemble of MNs that project to the same muscle and cluster into longitudinal columns in the ventral horn of the SC are referred to as MN pools. The positions of MNs in the SC are arranged in correlation with the location of their muscle targets in the periphery (Romanes, 1942). The relative position of MN pools is highly conserved among different individuals within a species and to some extent also across different species. **Legend:** Pectoralis Minor (Pec-Min), Pectoralis Major (Pec-Maj), Cutaneous Maximus (CM), Triceps (Tri), Latissimus Dorsi (LD), Biceps (Bic).

At the beginning of this study our expertise on transcriptional identities and topographic organization of was most advanced at cervical levels the murine SC as we had acquired knowledge about an ensemble of cervical MN pools comprising their Pea3 expression status and their affiliation with either division of the LMC by means of their Isl1/Lim1 status. At the time only two potential effector molecules, cadherin 8 and Sema3e, had been identified as downstream targets of Pea3 (Livet et al., 2002) and since we disposed of *Pea3* null mutant mice we considered investigations on Pea3 expressing MN pools as particularly promising for the identification of additional cell surface molecules implementing transcriptional codes. Moreover, the cervical motor system is more readily traceable by retrograde labeling techniques than its lumbar counterpart. This is the case, because for most muscles the distance between their somas and the entry points of their axons into the muscle is shorter at cervical than at lumbar levels which greatly facilitates over-night retrograde labeling with dextran-coupled fluorophores employed to mark individual MN pools.

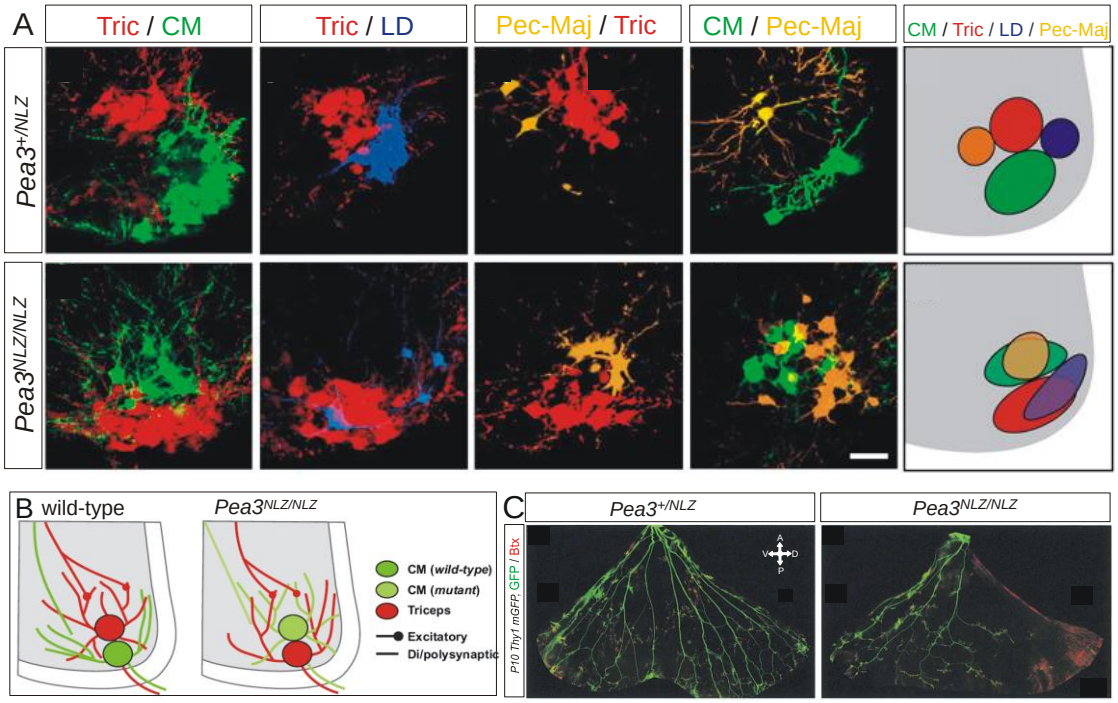

Figure 6: *Pea3* mutant phenotypes in cervical MN pools

A: Retrograde labeling of a selection of cervical MN pools in wild-type and *Pea3* mutant mice. Of all MN pools shown only CM and LD express Pea3, but in mutants pool clustering and settling positions of virtually all other MN pools are affected, too. Adapted from Vrieseling et al. (2006). **B:** *Pea3* mutants exhibit a switch in the settling position of a CM and Tric MNs which results from developmental failure of Pea3 expressing CM MNs to migrate from a dorsal to ventral position. Concurrently, CM MNs adopt a radial dendritic tree and make aberrant monosynaptic connections with Tric group Ia proprioceptive afferents. **C:** In *Pea3* mutant mice CM motor axons fail to establish normal axonal branching patterns and endplate distribution. The number of nerve branches penetrating the muscle is significantly lower and the dorsal half of the muscle lies completely fallow. Adapted from Livet et al. (2002)

We decided to acquire the gene expression profiles of a total of four cervical MN pool covering the medial and lateral divisions of the LMC. We chose Cutaneous Maximus (CM) and Pectoralis Minor (Pec-Min) MN pools as representatives of the LMC_m ($Isl1^+$, $Lim1^-$) innervating ventral muscle mass derived targets and the Triceps (Tric) and Pectoralis Major (Pec-Maj) MN pools as representatives of the LMC_l ($Isl1^-$, $Lim1^+$) innervating targets from the dorsally derived muscle mass. By means of our screens we were also interested in improving our knowledge about genes regulated by Pea3 because the mechanisms directly responsible for its loss of function phenotypes are to a large extent still unknown. For this reason, two of the four chosen MN pools, the CM and the Pec-Min, are known to express Pea3. The Pea3-negative Tric MN pool was of particular interest because *Pea3* mutant CM MNs acquire characteristics of Tric MN

pools, such as similar MN pool position, similar dendritic patterning and aberrant monosynaptic connections with Tric Ia afferents.

In summary, we chose an ensemble of four cervical MN pools for which preliminary information about their transcriptional identity, their morphological appearance, sensory-motor connectivity and axonal projections pattern had been established in wild-type and *Pea3* mutant mice. However, although the role of a few single genes had been investigated, virtually nothing was known about comprehensive gene expression profiles defining the identity of individual MN pools. Thus, our screen aimed to identify genes singularly expressed in individual MN pools and to improve our knowledge about the correlations between the transcriptional fingerprints of these MN pools, their morphological characteristics and the repertoire of expressed cell surface and intracellular signaling molecules.

3.2 Expression profiling of wild-type motor neuron pools

3.2.1 Results

3.2.1.1 Chip quality indicators and data processing

Using a combination of retrograde labeling, Laser Capture Microdissection (LCM) and Affymetrix gene chip technology the expression profiles of CM, Tric, Pec-Min and Pec-Maj MN pools were investigated at P0-P1. For each examined MN pool the mRNA was extracted and amplified from at least three independent retrograde labeling experiments. Affymetrix' "present call" analysis of the CM, Tric, Pec-Min and Pec-Maj gene chips revealed 36%, 31%, 33% and 31% genes of the total 45'000 chip probes (39,000 transcripts and variants) to be expressed above background, respectively. These present call values are relatively low compared to the 45-50%

typically found in Affymetrix experiments using freshly extracted mRNA but they are still within the normal range for LCM applications (Klur et al., 2004). Importantly, the expression of a total of 11'163 genes (25% of total) was shared among the four examined cervical MN pool samples indicating a certain consistency in the produced data.

Statistical analysis of the chip data revealed a total 1646 genes to be at least 2-fold differentially regulated between at least two of the four examined MN pools (N-Way ANOVA; $p \leq 0.01$; $\geq$ 2-fold change). In order to identify transcripts which were enriched in only one of the four examined MN pools, the medians of the expression values of a given MN pool were compared to the averaged expression value medians of the three other MN pools. The resulting "average" fold change over other MN pools was used as a relative measure of transcriptional enrichment and the obtained gene lists were sorted according to this value (Tables 2-5).

The screening results were validated by *in situ* hybridization or when possible by immunocytochemistry on embryonic and early postnatal cervical SC tissue. We set our focus on candidate genes with potential functions in neuronal circuit formation, expressed in a single MN pool. Of particular interest were transcription factors for their well documented roles in the regulation of neuronal subclass diversification discussed above (Livet et al., 2002; Kania and Jessell, 2003; Dasen et al., 2005; Dasen et al., 2008; Garcia and Jessell, 2008) and downstream effector molecules such as membrane bound receptors and secreted signaling molecules translating transcriptional regulation into functional cellular properties (Price et al., 2002; Kania and Jessell, 2003).

3.2.1.2 CM motor neuron pool marker gene candidates

While for most cervical MN pools little is known about MN pool specific gene expression, several studies have addressed the developmental specification of CM

MNs. Livet *et al.* (2002) found the ETS transcription factor Pea3 to be expressed in a distinct subpopulation of cervical MNs consisting of the CM but also of the LD and partly the Pec-Min MN pools. In their study two genes were found to depend on Pea3: cadherin 8 (Cdh8) and Sema3e (Livet et al., 2002). Expression of the latter has meanwhile been shown to be restricted to the CM MN pool where it contributes to the selectivity of sensory-motor connectivity (Eline Pecho-Vrieseling et al., unpublished data). Although expression of Pea3, Cdh8 and Sema3e in MNs is strongest during late embryonic development, their affiliation to CM MNs still proved to be a useful validation for the Affymetrix chip data at P1. The CM screening results revealed *Sema3e* and *Cdh8* to be 10.8-fold and 4.0-fold upregulated compared to the averaged medians of the three other MN pools (Table1). *Pea3* did not pass the criteria of the applied ANOVA test, but ignoring the relatively high internal variance and only judging by the median expression values it is also found 2.0-fold upregulated compared to the other three MN pools (Table 2).

Rank	Gene	Fold change	Medians ± STD			
		CM_{all} wt vs. o. pools wt	CM	Tric	Pec-Min	Pec-Maj
1	Tnfaip8*	21.8	**853.4** ± 98.9	19.7 ± 33.5	68.8 ± 35.2	28.8 ± 3.9
2	Chn2*	19.1	**511.7** ± 110.1	18.5 ± 11.4	33.3 ± 4.6	28.6 ± 16.4
3	Epha3	16.6	**623.3** ± 421.6	15.1 ± 3.5	12.4 ± 18.6	14.8 ± 0.2
4	Asb4*	16.4	**259.1** ± 182.4	16.0 ± 7.9	61.7 ± 10.3	36.1 ± 7.6
5	Areg*	16.2	**354.3** ± 189.0	16.6 ± 4.5	20.4 ± 53.7	11.0 ± 1.1
6	Esr1*	16.1	**843.0** ± 200.7	17.1 ± 13.6	16.5 ± 53.7	32.3 ± 20.6
7	Megf10	15.2	**525.3** ± 217.2	85.1 ± 71.1	31.3 ± 81.4	50.0 ± 9.4
8	Galn13	14.2	**1332.0** ± 136.2	57.7 ± 47.0	25.7 ± 44.3	27.5 ± 2.4
9	Pkr2*	13.8	**969.8** ± 455.7	29.3 ± 11.3	224.0 ± 149.6	35.3 ± 7.5
10	Hoxa9	12.5	**244.5** ± 360.8	168.1 ± 71.3	32.2 ± 10.4	32.7 ± 14.5
13	Sema3e*	10.8	**359.7** ± 122.3	19.1 ± 6.0	67.4 ± 90.6	13.3 ± 2.1
15	Clim1	8.8	**244.5** ± 360.8	168.1 ± 71.3	32.2 ± 10.4	32.7 ± 14.5
21	Narp*	8.2	**622.9** ± 316.7	17.2 ± 1.9	12.9 ± 1.1	12.2 ± 1.0
28	Pkr2*	6.8	**200.7** ± 50.1	15.6 ± 2.8	55.3 ± 19.8	17.5 ± 4.6
30	Del1*	6.5	**5017.7** ± 740.0	271.2 ± 297.3	1346.6 ± 382.6	708.1 ± 3.3
31	Pkr2*	6.3	**5072.1** ± 1052.6	173.4 ± 258.9	2130.3 ± 238.6	106.4 ± 2.2
54	Cckar*	4.9	**241.2** ± 98.8	55.9 ± 19.6	33.4 ± 8.7	59.0 ± 3.4
94	Cdh8*	4.0	**2896.5** ± 1147.1	323.6 ± 252.2	947.6 ± 11.7	901.1 ± 180.5
425	Irx6*	2.1	**234.5** ± 126.8	15.6 ± 1.7	157.3 ± 448.8	162.3 ± 134.6
447	Pea3*	2.0	**56.9** ± 23.1	23.1 ± 21.7	37.6 ± 7.3	23.8 ± 7.7

Table 2: Genes enriched in CM motor neurons

Median gene expression values form CM MNs (n=4 animals) were compared to the average median values of the three other pools (n≥3 for each other MN pool) to calculate fold changes. The top 10 genes most in CM MNs are listed. In addition a selection of genes of particular interest is listed below. Genes marked with an asterisk (*) were tested by *in situ* hybridization.

Legend: Tnfaip8, tumor necrosis factor, alpha-induced protein 8; Chn2, chimerin (chimaerin) 2; Epha3, Eph receptor A3; Asb4, ankyrin repeat and SOCS box-containing 4; Areg, amphiregulin; Esr1, estrogen receptor 1 (alpha); Megf10, multiple EGF-like-domains 10; Galnt13, UDP-N-acetyl-alpha-D-galactosamine:polypeptide N-acetylgalactosaminyltransferase 13; Pkr2, prokineticin Receptor 2; Hoxa9, homeo box A9; Sema3e, semaphorin 3e; Clim, LIM domain binding 2; Narp, neuronal pentraxin 2 (neuronal activity regulated protein); Pkr2, prokineticin receptor 2, Del1, developmental endothelial regulated locus 1, Cckar, cholecystokinin A receptor; Cdh8, cadherin 8; Irx6, Iroquois related homeobox 6 (Drosophila); Pea3, ets variant gene 4.

For the CM MN pool, *in situ* hybridization experiments at P1 confirmed *prokineticin receptor 2* (*Pkr2*, Figure 7, B), *iroquois related homeobox 6* (*Irx6*, Figure 7, B), *amphiregulin* (*Areg*, Figure 7, C), *neuronal activity regulated pentraxin* (*Narp*, Figure 7, D) and *developmental endothelial locus 1*, (*Del1*, Figure 7, E), to be specifically expressed in similar position as *Pea3* (Figure 7 A). Potential biological functions in

MNs of a selection of successfully validated marker genes are discussed below, insofar as published data was available.

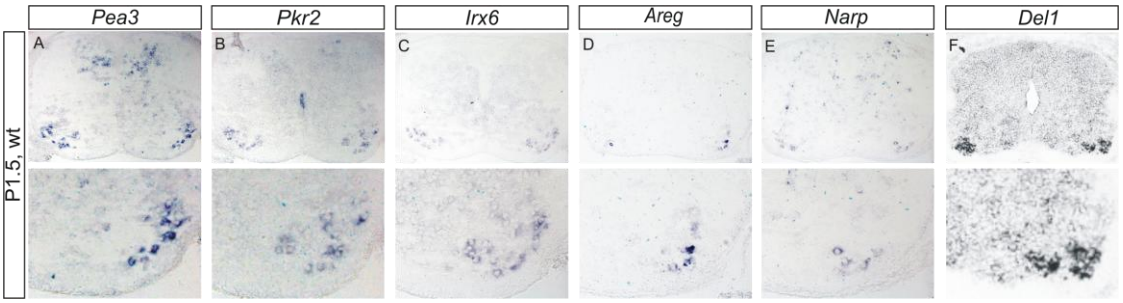

Figure 7: *In Situ* validation of potential CM MN pool marker genes

In Situ hybridization experiments on P1 transverse sections of cervical SCs revealed *Pkr2*, *Irx6*, *Areg, Narp*, and *Del1* to be expressed at the same position as *Pea3* expressing MN pools. Bottom panels display magnifications of the bottom right quadrant of the image above. **A:** Pea3 signal in the ventral horn marks the position of CM but also the LD and to some extent the Pec-Min MNs. Pea3 also marks an uncharacterized population of dorsal interneurons only found at the segmental levels of Pea3 positive MN pools. **B-C:** In MNs *Pkr2* and *Irx6* signals are detected at the same position and in similar numbers as *Pea3*. In addition *Pkr2* expressing cells are lining the central canal. **D:** *Areg* expression is restricted to *Pea3* expressing MNs although generally in slightly smaller numbers than *Pkr2* or *Irx6*. **E:** *Narp* expression was associated with a subpopulation of *Pea3* expressing MNs and a number of dispersed interneurons. **F:** *Del1* expression was generally detected in smaller numbers than *Pea3*, *Pkr2* and *Irx6*, suggesting that it is expressed in a subpopulation of Pea3 expressing MNs.

In order to distinguish genes merely expressed downstream the Pea3 signaling pathway from the ones exclusively expressed in CM MNs, dextran-rhodamine backfills were conducted from the CM muscle nerve to label the cell bodies of all CM MNs (Figure 8, 2nd row). As previously shown, Pea3 expressing LD and Pec-Min MNs differ in that only Pec-Min MNs coexpress Isl1 (Vrieseling and Arber, 2006). Therefore, we tried to exploit the Isl1-status of a MN in combination with retrograde labeling from the CM muscle nerve to distinguish the three cervical Pea3 positive MN pools. Dextran-rhodamine filled cells mark the CM MN pool, Dextran-rhodamine negative Isl1^{+} cells at a dorsal position relative to the CM MN pool are likely Pec-Min MNs and Dextran-rhodamine negative Isl1^{-} neurons at a dorso-lateral position to CM MNs are likely part of the LD MN pool (Figure 8). In our experiment a number of medially positioned MNs expressing Isl1 remained unfilled, but based on a large set of previous data we are convinced that they supply the CM muscle, too. These cells were most likely not labeled in this experiment because a small dorsal side-branch of the CM muscle nerve

must accidentally have been excluded from the suction capillary containing dextran-rhodamine dye (Figure 8, white arrows last row).

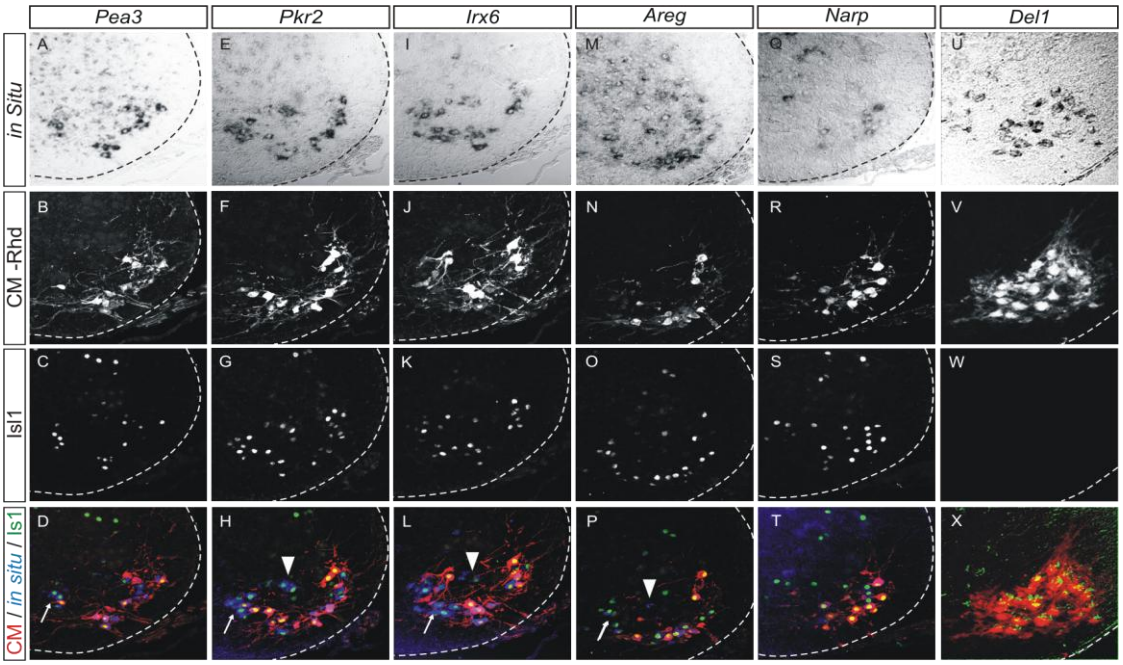

Figure 8: Backfill validation of potential CM MN pool marker genes

A close up of the ventral horn harboring the *Pea3* positive CM MNs. In order to attribute CM marker gene candidates to the CM MN pool *in situ* hybridization experiments were combined with retrograde labeling from the CM muscle nerve. All backfills (except for *Del1*, W) were complemented with Isl1 immunocytochemistry in order to discriminated between CM (backfill, Isl1+), Pec-Min (no backfill, Isl1+, white arrowhead in H, L and P) and LD (no backfill, Isl1-) MN pools. Judging by their position, medially located MNs expressing Pea3 and Isl1 are also CM MNs, but they were accidentally not backfilled (white arrow in D, H, L, and P).
A-D: Virtually all backfilled MNs coexpress *Pea3* and Isl1. **E-P:** *Pkr2*, *Irx6* and *Areg* appear to be expressed in almost all ventral Isl1 positive MNs, including a dorsal cluster most likely belonging to the LD MN pool (white arrowhead in H, L and P). **Q-T:** Compared to its signal in interneurons, *Narp* appeared only weakly expressed in MNs. It does not 100% colocalize with Isl1+ MNs and is thus probably only expressed in a subpopulation of MNs. **U-X:** *Del1* colocalized with virtually all CM MNs. No significant signal was detected outside CM MNs, indicating that Del1 might be a marker for the CM MN pool.

Expression patterns of *Pkr2* and *Irx6* and *Areg* do not appear to be restricted to the CM MN pool. Additional *in situ* signal was observed in a number of $Isl1^{+}$ MNs outside the CM MN pool. These MNs are likely part of to the Pec-Min MN pool (white arrowheads in Figure 8, last-row). *Pkr2* expression was also found to colocalize with *Pea3* at lumbosacral levels of the SC corroborating the notion that Pkr2 requires temporal coexpression of Pea3 (see below). Analysis of independent series of *in situ* hybridization experiments suggest that the number of *Areg* and *Narp* positive MNs are generally lower than number of Pea3 expressing MNs (Figure 7 and 8, data not shown). Especially *Narp* appears to be expressed in only a small ventral subpopulation of CM

MNs. *Del1* is expressed by all CM MNs and virtually no signal was found outside the retrogradely labeled CM MN pool, suggesting that this gene is restricted to the CM and not a generally expressed downstream the Pea3 signaling cascade.

3.2.1.3 Tric motor neuron pool marker gene candidates

A number of the top Tric marker gene candidates (Table 3) were tested by *in situ* hybridization on cervical SC transverse sections. However, only *tachykinin receptor 3* (*Tacr3*, table 3), the very top hit of the list, yielded *in situ* hybridization patterns confined to a small group of MNs dorsal of the *Pea3*-positive domain, which was a first indication that *Tacr3* could effectively label the Tric MNs known to form a small cluster at this position (Figure 9). More significantly, combination of *Tacr3 in situ* hybridization with retrograde labeling from the Tric muscle nerve confirmed *Tacr3* to specifically mark Tric MNs along the entire extent of the Tri MN pool (Figure 10). Due to the switch in settling position between CM and Tric MN pools in Pea3 mutants, we predicted Tacr3 expressing MNs to be found at an aberrant ventro-lateral position in *Pea3* mutant SCs. Accordingly, our *in situ* hybridization results from P1 heterozygous and homozygous *Pea3* mutant tissue strongly supports the notion of *Tacr3* marking only Tric MNs (Figure 14, E). In addition to its signal in Tric MNs a relatively scarce salt and pepper *Tacr3* pattern was observed dorsal layers of the SC (Figure 9).

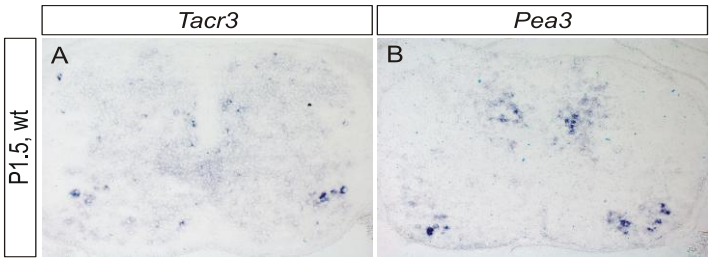

Figure 9: *In situ* hybridization validation of the potential Tric MN pool marker Tacr3

In Situ hybridization experiments on P1 transverse sections of cervical SCs revealed *Tacr3* to be expressed in a distinct population of neurons located dorsal to the Pea3 positive MN pools.
A: *Tacr3* positive MNs are found at a position typical for the Tric MN pool. The number of labeled MNs lies within the expected range for the Tric MN pool on thin sections. **B:** Consecutive section showing the position *Pea3* positive MN pools, here serving as a positional landmark for the allocation of the Tric MN pool.

Rank	Gene	Fold change: Tric wt vs. o. pools wt	Medians ± STD: CM	Tric	Pec-Min	Pec-Maj
1	TacR3*	27.3	51.9 ± 83.1	**853.2** ± 221.1	23.7 ± 5.8	18.0 ± 0.2
2	TacR3*	13.3	545.9± 410.6	**2591.0** ± 516.2	17.4 ± 7.7	20.5 ± 6.3
3	COUP TF II*	9.7	46.6 ± 39.0	**399.3** ± 267.4	35.9 ± 16.5	41.0 ± 12.7
4	C230062K19Rik	8.9	18.0 ± 5.5	**130.3** ± 91.3	12.0 ± 3.3	13.8 ± 3.8
5	1500016L03Rik	7.8	32.7 ± 5.2	**360.9** ± 207.3	22.7 ± 2.3	83.1 ± 19.5
6	Tox3	7.7	49.5 ± 41.7	**427.8** ± 143.0	40.0 ± 35.2	92.0 ± 45.9
7	Lmx1*	6.7	19.6 ± 7.1	**316.8** ± 95.7	20.8 ± 6.2	102.4± 16.2
8	Cbln1*	6.4	44.8± 23.2	**989.4** ± 176.1	137.5±136.3	277.9±184.9
9	Gdap10	6.4	20.3 ± 8.6	**124.1** ± 79.9	20.6 ± 1.0	17.5 ± 6.1
10	1500015O10Rik	6.2	136.8 ± 232.6	**1126.9** ± 333.2	255.3± 84.3	149.3± 3.4

Table 3: Genes enriched in Triceps MNs

Median gene expression values form Tric MNs (n=3 animals) were compared to the average median values of the three other pools (n≥3 for each other MN pool) to calculate the fold-change. The top 10 genes most expressed in Tric MNs are listed. Genes marked with an asterisk (*) were tested by *in situ* hybridization.
Legend: Tacr3, tachykinin receptor 3 tumor necrosis factor, COUP TFII, COUP transcription factor 2; C230062K19Rik, RIKEN clone C230062K19; 1500016L03Rik, RIKEN cDNA 1500016L03 gene, Tox3, TOX high mobility group box family member 3; Lmx1, LIM homeobox protein 1; Cbln1, cerebellin 1 precursor protein; Gdap10, ganglioside-induced dfferentiation-associated-protein 1; 1500015O10Rik, RIKEN cDNA 1500015O10 gene.

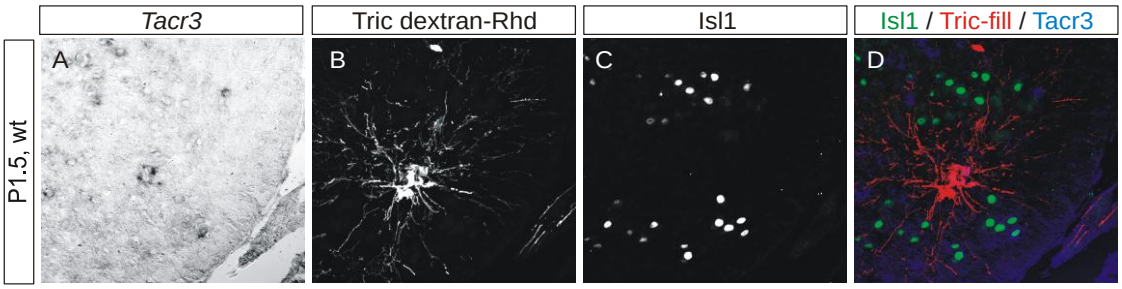

Figure 10: Backfill validation of potential Tric MN pool marker genes

A close up of the ventral horn displaying *Pea3* positive CM MNs. In order to attribute *Tacr3* to the Tric MN pool *in situ* hybridization experiments were combined with retrograde labeling from the Tric muscle nerve.
A-D: *Tacr3 in situ* signal (A) colocalizes with retrogradely labeled Tric MNs (B, D). The Tric MN pool is devoid of Isl1 signal (C, D), which at this segmental level marks dorsal MN pools projecting to forearm muscles and ventrally MN pools of the Pea3 pathway.

3.2.1.4 Pectoralis motor neuron pool marker gene candidates

The two prominent and functionally related muscle heads of the Pectoralis muscle are supplied by nerves from two segmentally overlapping but distinct MN pools named Pec-Min and Pec-Maj MN pools. While part of the Pec-Min MNs coexpress Pea3, MNs of the Pec-Maj MN pool reside at a more anterior and more dorsal location and do not express Pea3. Interestingly, the expression profiles of Pec-Min and CM MNs correlated

more strongly with one another than the two Pec MN pools. The similarity between CM and Pec-Min MNs could be caused by the partly shared pathways controlled by Pea3 and manifested itself in the transcriptional activation of a number of common genes. Possibly, as a consequence, not a single gene identified in the screen (Table 4) could be validated to be exclusively expressed by Pec-Min MNs.

		Fold change	Medians ± STD			
Rank	Gene	Pec-Min wt vs. o. MN pools	CM	Tric	Pec-Min	Pec-Maj
1	Crh	7.6	28.1 ± 33.4	319.0 ± 291.5	**1980.6** ± 519.0	439.7 ± 126.9
2	Plxnc1*	7.5	54.4 ± 17.6	18.3 ± 8.0	**235.0** ± 258.2	20.9 ± 0.6
3	Transcribed Locus	6.2	44.7 ± 18.2	65.6 ± 27.1	**369.1** ± 129.9	69.1 ± 3.1
4	6030445D17Rik	6.1	14.4 ± 9.6	17.0 ± 8.7	**93.6** ± 49.8	15.0 ± 1.0
5	Gramd1b	6.0	31.6 ± 4.7	26.8 ± 6.3	**188.7** ± 163.5	36.7 ± 10.3
6	Bpil2	5.0	19.9 ± 3.3	21.3 ± 5.7	**135.4** ± 56.5	92.0 ± 13.1
7	Ai848100	4.8	20.0 ± 1.9	20.8 ± 40.2	**131.2** ± 68.7	40.6 ± 7.1
8	Gchfr	4.7	21.8 ± 9.8	24.0 ± 5.0	**128.3** ± 64.1	35.5 ± 3.5
9	Dmp1*	4.4	19.0 ± 11.6	265.2 ± 101.1	**459.0** ± 348.8	27.3 ± 6.5
10	Diap2*	4.3	23.0 ± 2.7	47.7 ± 77.2	**211.4** ± 168.0	75.9 ± 51.6
13	Sst*	4.0	729.8 ± 631.1	471.1 ± 267.9	**5524.0** ± 601.6	2963.9 ± 292.3

Table 4: Genes enriched in Pectoralis Minor MNs

Median gene expression values form Pec-Min MNs (n=3 animals) were compared to the average median values of the three other pools (n≥3 for each other MN pool) to calculate the fold-change. The top 10 genes most enriched in Pec-Min are listed. Sst yielded MN pools specific *in situ* patterns lumber levels of the SC but was not confirmed as a Pec-Min marker. Genes marked with an asterisk (*) were tested by *in situ* hybridization.
Legend: Crh, corticotropin releasing hormone; Plxnc1, plexin C1; Transcribed Locus, transcribed locus; 6030445D17Rik, RIKEN cDNA 6030445D17 gene; Gramd1b, GRAM domain containing 1B; Bpil2, bactercidal/permeability-increasing protein-like 2; Ai848100, expressed sequence AI848100; Gchfr, GTP cyclohydrolase / feedback regulator; Dmp1, dentin matrix protein; Diap2, diaphanous homolog 2 (Drosophila), Sst, somatostatin.

For the Pec-Maj MN pool, only *neuropeptide Y* (*Npy*), which emerged as 3-fold upregulated compared to other MN pools (Table 5), could be validated as specifically enriched. Double-backfills from Pec-Min and Pec-Maj muscle nerves indicate that Npy is strongly expressed by most Pec-Maj MNs and weakly by a minor population of Pec-Min MNs (Figure 11). The exact expression pattern of Npy in Pec-Maj MNs, its time point of induction, transcriptional time-course and affiliation to MN pools at other segmental levels has not been investigated.

Rank	Gene	Fold change	Medians ± STD			
		Pec-Maj wt vs. o. pools wt	CM	Tric	Pec-Min	Pec-Maj
1	Ebf3*	16.9	25.6 ± 6.7	58.5 ±14.7	24.2 ± 9.2	**609.1** ± 37.4
2	Slc32a1	14.5	122.6 ±177.9	35.0 ±64.7	14.1 ± 8.2	**830.7** ±129.6
3	Igf1*	12.1	22.2 ± 16.9	16.7 ±62.7	98.4 ±61.1	**553.0** ±180.0
4	FoxP2	11.9	33.2 ± 12.4	13.6 ± 8.5	15.0 ± 2.6	**244.7** ± 83.3
5	Plxdc1	11.8	24.7 ± 33.5	24.5 ±17.8	46.4 ±25.6	**377.3** ± 40.6
6	Igf1*	11.3	28.0 ± 18.5	48.1 ±21.2	33.8 ±20.5	**415.8** ±156.9
7	Sorcs3	10.3	36.6 ± 17.8	32.9 ± 9.2	35.8 ±53.3	**363.1** ± 33.9
8	Mrpl50	10.3	23.4 ± 6.2	24.1 ± 6.0	17.8 ± 3.7	**223.2** ±153.8
9	Timeless*	8.5	13.1 ± 2.1	13.3 ± 6.3	18.8 ± 5.4	**127.5** ± 54.4
10	Klhl14	8.4	15.9 ± 5.3	11.2 ± 5.4	9.7 ± 1.3	**102.7** ± 27.3
18	Igf1*	6.0	17.8 ± 3.6	15.9 ± 2.1	15.7 ± 0.4	**99.1** ± 16.0
62	Npy*	3.0	61.9 ± 79.9	110.2 ±34.9	325.5 ±89.6	**495.8** ±146.9

Table 5: Genes enriched in Pectoralis Major MNs

Median gene expression values form Pec-Maj MNs (n=3 animals) were compared to the average median values of the three other pools (n≥3 for each other MN pool) to calculate the fold-change. The top 10 genes most enriched in Pec-Maj are listed. Additionally, values of Npy are shown as is a validated gene enriched in Pec-Maj MNs. Genes marked with an asterisk (*) were tested by *in situ* hybridization or immunocytochemistry.
Legend: Ebf3, Early B-cell factor; Slc32a1, vesicular inhibitory amino acid transporter; Igf1, insulin-like growth factor 1; FoxP2, forkhead box P2; Plxdc1, plexin C1; Sorcs3, sortilin-related VPS10 domain containing receptor 3 ;Mrpl59, mitochondrial ribosomal protein L5; Timeless, timeless homolog (Drosophila); Klhl14, kelch-like 14 (Drosophila); Npy, Neuropeptide Y.

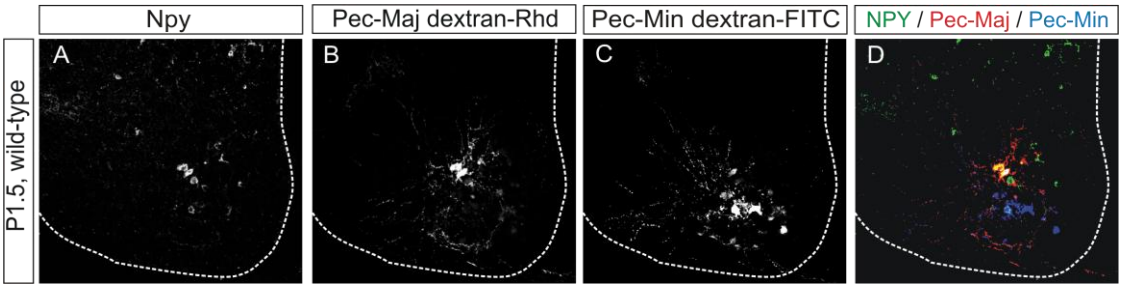

Figure 11: Backfill validation of potential Pec-Maj MN pool marker genes

Sections display the ventral horn of the SC harboring Pec-Maj and Pec-Min MN pools. In order to attribute Npy to Pec-Maj MN pool *in situ* hybridization experiments were combined with backfills from both Pec-Min and Pec-Maj muscle nerves. **A-D**: NPY (A) colocalizes with retrogradely labeled Pec-Maj MNs (B, D). Most Pec-Min MNs do not express Npy, few express it weakly (C, D).

3.2.1.5 Time course of motor neuron pool marker gene expression

Many of the developmental events leading to the formation of selectively interconnected neuronal networks controlling the locomotion take place at defined time periods between MN generation (E9-E11) and P0. Because MN pool gene profiling was performed at P0-P1, it was important to determine whether the identified MN pool marker candidates could be involved in earlier events of sensory-motor circuit

assembly. For this purpose a selection of the MN pool marker genes were tested on consecutive SC sections at different embryonic developmental stages and compared to the expression pattern of *Pea3* (Figure 12). Expression of *Pkr2* starts between E13 and E14, displays a striking similarity to the *Pea3* expression pattern and persists until at least P1 (Figure 12, A). Similarly, *Irx6* also appears to match *Pea3* expression patterns throughout all examined stages but in contrast to *Pkr2* its mRNA can already be detected at ~E12, shortly after the onset of *Pea3* itself (Figure 12, B). *Del1* exhibited a similar expression time-course as *Irx6*, however, the number of labeled cell was always smaller than the number of Pea3 expressing cells and especially at the position where $Pea3^+$ LD MNs usually reside expression patterns diverged (Figure 12, D). These observations strengthen the notion that *Del1* could specifically mark CM MNs rather than all Pea3 expressing MNs. *Areg*, which was first detected at E13.5, is expressed in a subpopulation of the $Pea3^+$ MN pools, yet in insufficient numbers to be a general CM marker gene (Figure 12, C). The exact identity of the *Areg* expressing subpopulation of MNs was not investigated.

All of the examined marker gene candidates fulfill the basic criteria to potentially play a role in the developmental processes connecting, shaping or refining the spinal motor system. With the exception of *Del1*, expression of genes identified as enriched in CM MNs, are unlikely restricted to the CM MN pool (*Pkr2*, *Irx6*) or as the case for *Areg* expressed in all CM MNs. However, because their expression patterns are overlapping and induction of these genes is subsequent to the onset of *Pea3,* there are indications for them being downstream targets of the Pea3 program. This possibility was tested by means of a second screen comparing the expression profiles of CM MNs in *Pea3* mutant and heterozygous animals (see chapter below).

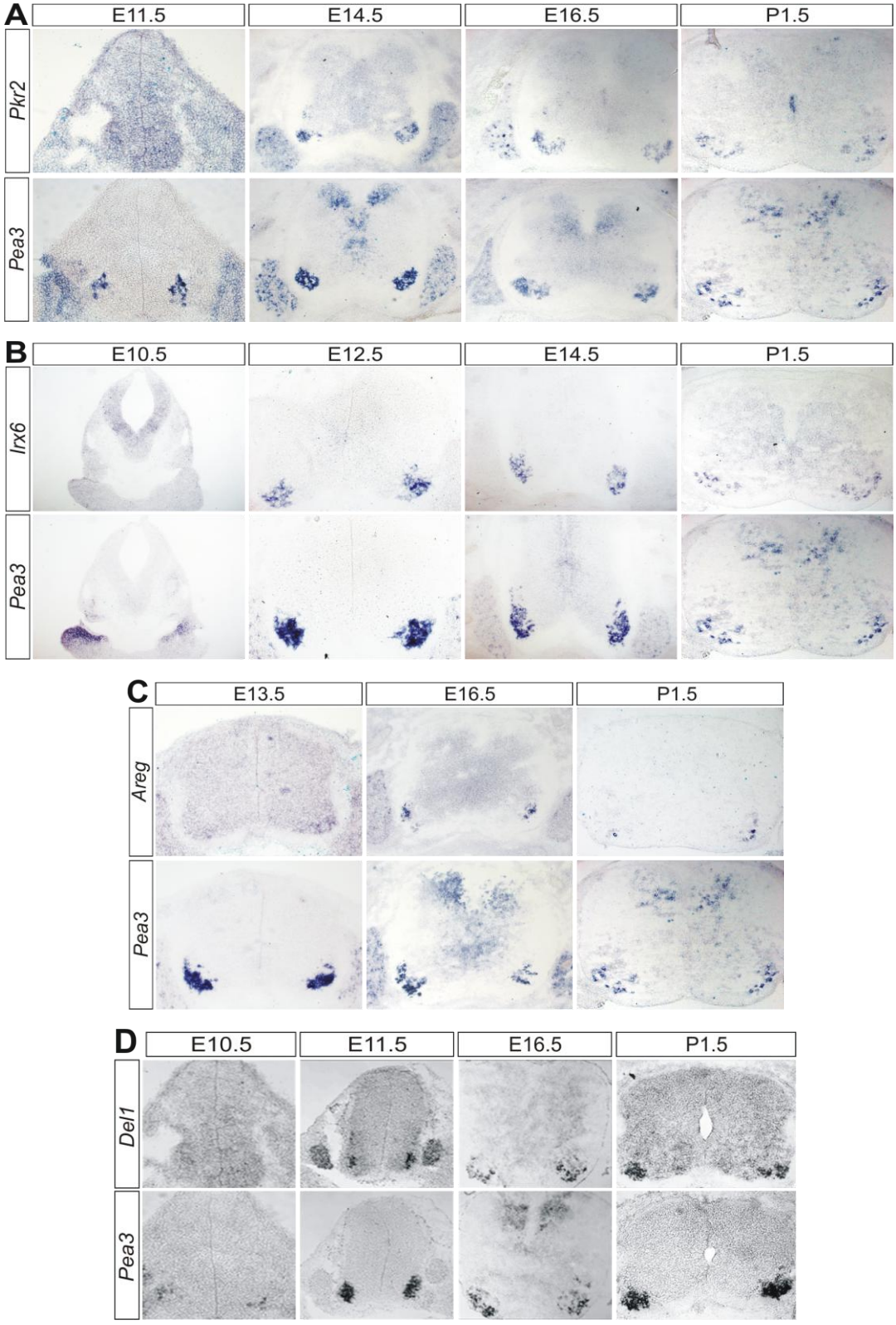

Figure 12: Developmental time-course of potential CM markers genes *Pkr2*, *Irx6*, *Areg* and *Del1*

In situ hybridization experiments of *Pkr2, Irx6, Areg* and Del1 were each performed on consecutive sections with *Pea3* (except *Areg* at P1). None of the examined MN marker gene transcripts was detected before onset of Pea3 (~E11). **A:** *Pkr2* mRNA is first detected at about E14 and the number of labeled cells remains comparable to the number of *Pea3* positive cells until birth. **B:** The induction of *Irx6* takes place between E10.5 and E12.5. Although its *in situ* signal is slightly weaker the number of labeled cells is comparable to *Pea3* from the onset on. **C:** The onset of *Areg* takes place at around E13.5 when the first weakly labeled cells can be detected. At all examined stages *Areg* appears to label only a subpopulation of the *Pea3* positive MNs. **D:** Onset of *Del1* occurs shortly after *Pea3* at about E11. The number of *Del1* labeled cell appears smaller than the number of *Pea3* positive cells.

The Tric marker gene *Tacr3* was first detected at E11.5 and its expression pattern remained mutually exclusive to *Pea3* until P0, which is the last time point we tested (Figure 13). The rostro-caudal extent of *Tacr3* positive MNs and their relative position to *Pea3*$^{+}$ MN pools further strengthens the notion of Tacr3 being a specific marker of the Tric MN pool.

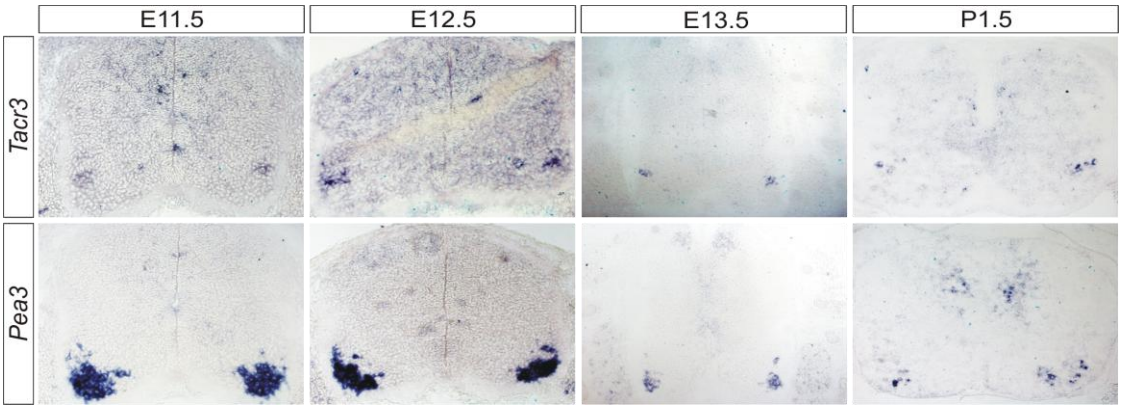

Figure 13: Developmental time-course of *Tacr3*

Faint *Tacr3* expression was first detected at E11.5 and strong signal was detected until P1.5 which was the last time point we tested. Throughout all examined stages, no detectable overlap between the expression patterns of *Tacr3* and *Pea3* was detected.

3.3 CM motor neuron pool gene profiling in Pea3 mutant mice

3.3.1 Introduction

Previous studies had provided evidence that Pea3 is essential in at least two cervical MN pools for the establishment of MN soma positions, dendritic patterning, axon pathfinding and selective Ia proprioceptive afferent connectivity (Haase et al., 2002; Livet et al., 2002; Vrieseling and Arber, 2006) (Figure 6). Recent findings have shown that Sema3e expressing MNs repel Plexin D1 expressing Ia proprioceptive afferents and hinder them from making direct synaptic contact with CM MNs. Yet in *Sema3e* mutant mice neither CM MN pool position nor dendritic arborization or neuromuscular innervation pattern were in a major way affected (Eline Pecho-Vrieseling et al, unpublished data). These results indicate that a number of different effector molecules

must be in charge of establishing central and peripheral specification of developing Pea3 expressing MN pools. Coincidentally, a relatively high proportion of the genes we identified as enriched in distinct MN pools, displayed strikingly similar expression patterns to Pea3. We therefore sought to determine whether these genes were also regulated by Pea3 and, at a later step, to explore their relative contributions to the maturation of cervical motor circuits. For this purpose, we performed a second Affymetrix screen, comparing the expression profile of the CM MN pool between *Pea3* mutants and wild-type controls. In *Pea3* mutants only the ventral most segment of the CM muscle is innervated through a few distinct nerve branches (Livet et al., 2002) (Figure 6, D). Consequently, in order to collect most comparable control data sets only these lateral nerve branches were used for retrograde labeling in wild-type, too.

3.3.2 Results

3.3.2.1 Chip quality indicators and data processing

Using LCM, the expression profiles of four biological replicates of the mRNA of both CM MNs of *Pea3* mutant mice and the lateral (ventral) branch of CM wild-type MNs (CM_{lat} MNs) mice were investigated. Affymetrix' "present call" analysis of wild-type CM_{lat} and *Pea3* mutant CM MNs gene chips revealed 20.5% and 20.3% of the total 45'000 chip probes to be expressed above background, respectively. The present call values of this mutant vs. wild-type screen are therefore significantly lower than the ones obtained in the wt screen (average 33%) which cannot be explained readily. Statistical analysis of the chip data revealed a total of 470 genes to be at least 2-fold differentially regulated between mutant and wild-type (ANOVA, $p \leq 0.01$; $\geq$ 2-fold change). Considering that due to normalization, 50% of all gene probes displayed expression raw values higher than 20 and taking into account the average present call value of 20.4%, the expression raw values of Pea3 (wt: 28.5; *Pea3*-mutant: 17.9) are

too low at P1 to be used for chip validation purposes. In contrast, *Cdh8* and *Sema3e* both appeared among the top hits of genes positively regulated by Pea3 (Livet et al., 2002) validating the informative value of our screening data (Table 6).

Rank	Gene	Fold Change		Medians ± STD	
		CM_{lat} wt vs. *Pea3*$^{NLZ/NLZ}$	CM_{all} wt vs. o. pools wt	CM_{lat} wt	CM_{lat} *Pea3*$^{NLZ/NLZ}$
1	Sema3e*,1	64.0	10.8	3833.8 ± 338.8.1	59.9 ± 150.1
2	Asb4*,1	32.7	16.4	671.4 ± 387.7	20.6 ± 17.7
3	Xist	15.2	--	1725.7 ± 870.7	113.6 ± 567.8
4	Pkr2*,1	13.6	13.8	506.0 ± 225.7	37.1 ± 2.3
5	Cubn	13.0	--	178.5 ± 526.9	13.7 ± 3.0
6	AI503301	12.0	--	427.1 ± 307.0	35.6 ± 6.4
7	Gpr50	10.6	--	126.3 ± 160.9	11.9.0 ± 1.7
8	Ptprk*	10.2	5.1	291.3 ± 149.3	28.6 ± 3.5
9	S100a11	10.0	5.0	383.2 ± 238.8	38.2 ± 13.8
10	Odz3	9.8	2.1	938.0 ± 117.5	95.6 ± 38.4
29	Del1*	6.3	6.5	2148 ± 440.7	339.1 ± 76.6
31	Epha3[1]	5.8	7.4	786.3 ± 260.7	134.7 ± 47.1
32	Hoxa9[1]	5.8	12.5	829.6 ± 496.7	143.2 ± 251.1
33	Esr1*,1	5.8	16.1	135.9 ± 127.5	23.6 ± 12.6
37	Galnt13[1]	5.4	14.2	321.4 ± 137.8	59.5 ± 51.7
38	Megf10[1]	5.3	15.2	255.2 ± 105.8	47.9 ± 17.0
40	Cdh8	5.3	4.0	161.8 ± 143.3.7	30.7 ± 26.4
53	Chn2*	4.6	19.1	86.0 ± 23.1	18.9 ± 2.5
63	Sema3e*,1	4.0	6.3	67.3 ± 30.5	16.8 ± 2.4
74	Irx6*	3.6	2.1	74.8 ± 35.8	20.8 ± 12.5
76	Cbln2*	3.5	3.5	2171.3 ± 606.0	614.1 ± 211.8
81	Narp*	3.4	8.2	487.9 ± 322.2	142.0 ± 25.4
138	Cutl2*	2.7	–	2656.0 ± 464.4	1000.3 ± 360.2
235	Tnfaip8*,1	1.8	21.8	34.8 ± 39.4	19.5 ± 6.5
X	Pea3*,2	1.6	2.0	28.5 ± 11.0	17.9 ± 3.6
X	Areg*,1,2	1.4	16.2	16.6 ± 280.4	11.6 ± 0.9

Table 6: Genes positively regulated by Pea3 in CM motor neurons

Gene expression values between MNs projecting to the lateral branches of the CM muscle in wild-type (CM_{lat} wt, n=4) and *Pea3* mutant (CM_{lat} *Pea3*$^{NLZ/NLZ}$, n=4) mice were compared. The top 10 genes most downregulated in *Pea3* mutant tissue are listed. In addition, a selection of genes found to be enriched in CM MNs (2nd column "Fold Change"), including the complete top ten from table 2 are listed for comparison. Most of the genes enriched in CM MNs appear to be regulated by Pea3. Genes marked with an asterisk (*) were tested by *in situ* hybridization or immunocytochemistry. Genes marked with a (1) are among top ten genes enriched in CM MNs vs. other pools (table 2).Genes marked with a (2) did not pass the ANOVA test, but are listed for interest.

Legend: Sema3e, semaphorin 3e; Asb4, ankyrin repeat and SOCS box-containing 4; Xist, inactive x-specific transcripts; Pkr2, prokineticin Receptor 2; Cubn, cubilin; AI503301, expressed sequence AI503301; Gpr50, G-protein-coupled receptor 50; Ptprk, protein tyrosine phosphatase, receptor type, K; S100a11, S100 calcium binding protein A11 (calgizzarin); Odz3, odd Oz/ten-m homolog 3 (Drosophila); Del1, developmental endothelial locus 1; Epha3, Eph receptor A3; Hoxa9, homeo box A9; Esr1, estrogen receptor 1 (alpha); Galnt13, UDP-N-acetyl-alpha-D-galactosamine:polypeptide N-acetylgalactosaminyltransferase 13; Megf10, multiple EGF-like-domains 10, Cdh8, cadherin 8; Chn2, chimerin (chimaerin) 2; Sema3e, semaphorin 3e, Irx6, Iroquois related homeobox 6 (Drosophila); Cbln2, cerebellin 2 precursor protein; Narp, neuronal pentraxin 2 (neuronal activity regulated protein); Cutl2, Cut-like 2 (Drosophila); Tnfaip8, tumor necrosis factor, alpha-induced protein 8; Pea3, ets variant gene 4; Areg, amphiregulin.

3.3.2.2 Validation of genes positively regulated by Pea3

On the basis of our *Pea3* mutant screening results, the previously identified CM-enriched genes *Pkr2*, *Del1*, *Sema3e*, *Irx6*, *Cdh8* and *Narp* all appear to be positively regulated by Pea3. The only exception is *Areg* the median expression values of which are low in CM_{lat} compared to the CM values obtained in the wild-type screen and the variance among its replicates is high (Table 6, bottom). Of the top ten genes enriched in the CM MN pool (Table 2) nine appear to be positively regulated by Pea3 (Table 6). On the contrary, expression of most of the genes regulated by Pea3 also appear to be enriched the CM MN pool (Table 6, second fold-change column).

The validation of the *Pea3* mutant screen was for the most part conducted by Joachim Luginbühl, who was working as a Master's student under my supervision during that time. On the basis of our screen a number of candidate genes indicative of positive regulation by Pea3 were tested by *in situ* hybridization and/or immunohistochemistry. In addition to the previously identified CM markers genes mentioned above *cut-like 2 (Drosophila), tumor necrosis factor, alpha-induced protein 8, protein tyrosine phosphatase receptor type K,* were tested on wild-type and $Pea3^{NLZ/NLZ}$ SC tissue. Despite clear detection of mRNA on control tissue, none of the newly tested genes could be validated as Pea3 target genes (data not shown). In addition to *Sema3e* and *Cdh8*, only previously identified *Pkr2*, *Del1* and *Irx6* genes yielded clear *in situ* results as virtually no signal was detectable on level matched *Pea3* mutant SC sections (Figure X8). At the same time, it remains uncertain if the CM-enriched genes *Areg* and *Narp* are also positively regulated by Pea3 as they could not be reliably tested.

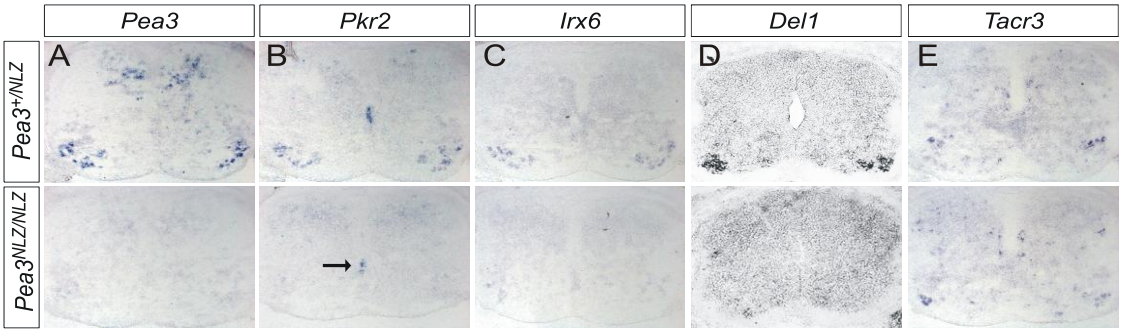

Figure 14: Validation of *Pea3* mutant mouse screen by *in situ* hybridization

In situ hybridization experiments demonstrating the dependence of *Pkr2, Irx6* and *Del1* on Pea3. P1 SCs of *Pea3*$^{+/NLZ}$ and *Pea3*$^{NLZ/NLZ}$ mice were level matched using the exit point of ventral roots as positional landmarks. Except for *Del1* (D) consecutive sections are shown. **A:** *Pea3* was used as a control for CM MN pool position. **B:** *Pkr2* expression in MNs is eliminated in the absence of Pea3. In contrast, *Pkr2* expression around the central canal remains unaffected by (black arrow). **C:** Some residual *Irx6* expression can be detected on *Pea3* mutant tissue, but the signal is clearly weaker than in heterozygous controls. **D:** *Del1* expression on *Pea3* mutant MNs was abolished while in DRG and other MN pools the signal remained unchanged (not shown). **E:** *Tacr3* expression is displayed as a positive control for the integrity of *Pea3*$^{NLZ/NLZ}$ tissue: As anticipated the *Tacr3* expressing Tric MNs exhibit a swap in pool position on *Pea3* mutant tissue and settle at the ventro-lateral boarder instead of more dorsally (also see Figure 6), while the signal intensity remained unchanged.

3.3.2.3 Validation of genes negatively regulated by Pea3 – focus on Scip

Our efforts to validate genes negatively regulated by Pea3 were less extensive. Of the top ten candidates (Table 7) only Scip was more thoroughly examined. In wild-type MNs a number of the identified genes were expressed in all except CM MN pools, supporting the notion of them being negatively regulated by Pea3.

		Fold Change		Medians ± STD	
Rank	Gene	CM *Pea3*$^{NLZ/NLZ}$ vs. CM_{lat} wt	o. pools wt vs. CM_{all} wt	CM_{lat} wt	CM *Pea3*$^{NLZ/NLZ}$
1	Bcl11b	26.7	--	31.8 ± 62.0	849.4 ± 412.0
2	Gabra1	23.4	7.7	22.0 ± 18.6	513.0 ± 154.8
3	Sema5b	22.8	6.7	17.9 ± 1.6	407.1 ± 273.9
4	Crh	17.6	32.5	108.6 ± 62.2	1915.1 ± 871.6
5	Acaa1b	17.6	--	44.0 ± 153.8	772.7 ± 479.5
6	Scip*	17.2	--	40.1 ± 137.6	690.8 ± 197.4
7	Cdh9	16.0	20.8	130.9 ± 11.7	2093.0 ± 591.2
8	Fign	11.4	--	31.4 ± 6.2	28.6 ± 3.5
9	Gabra2	11.2	--	27.9 ± 61.0	314.2 ± 72.2
10	Gabra1	10.1	--	38.8 ± 14.7	392.0 ± 107.8
19	Cryab*	7.3	4.3	61.1 ± 24.7	441.6 ± 124.0

Table 7: Genes negatively regulated by Pea3

Gene expression values between MNs projecting to the lateral branches of the CM muscle in wild-type (CMlat, wt, n=4)) and *Pea3* mutant (CMlat, *Pea3*$^{NLZ/NLZ}$, n=4) mice were compared using ANOVA (p≤0.01, ≥2-fold change) statistical analysis. The top ten genes upregulated in *Pea3* mutant CM MNs are shown. Genes marked with an asterisk (*) were tested by *in situ* hybridization or immunohistochemistry.
Legend: Bcl11b,B-cell leukemia/lymphoma 11B; Gabra1, gamma-aminobutyric acid (GABA-A) receptor, subunit alpha 1; Sema5b, semaphorin 5b; Crh, corticotropin releasing hormone; Acaa1b, acetyl-Coenzyme A acyltransferase 1B; Scip, POU domain, class 3, transcription factor 1; Cdh9, cadherin 9; Fign, fidgetin; Gabra2, gamma-aminobutyric acid (GABA-A) receptor, subunit alpha 2, Cryab, Crystalin alpha, B;

The availability of ABs against Scip protein allowed a thorough analysis using immunocytochemistry. In order to establish the expression pattern of Scip in the context of *Pea3* mutant mice, we made use of the nuclear LacZ cassette (NLZ) knocked into exon 6 of the *Pea3* locus (Livet et al., 2002). However, expression of Pea3-LacZ in homozygous *Pea3*^{NLZ} mutants can only be used at early embryonic stages E10.5-E12.5, since at later developmental stages loss of Pea3 leads to deregulation of its own transcription and the LacZ signal is lost.

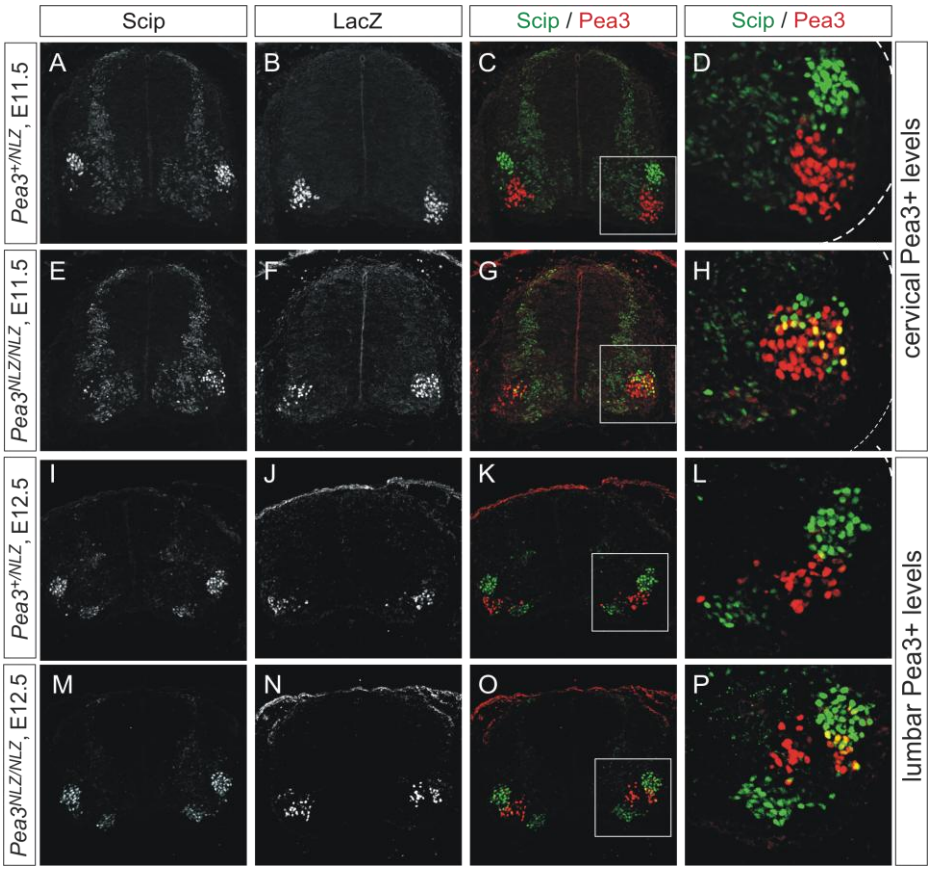

Figure 15: Scip expression in *Pea3* wild-type and mutant mice at E11.5

Scip and Pea3 expression at E11.5 in *Pea3*^{NLZ} heterozygous and mutant cervical SC. **A-C:** In *Pea3*^{NLZ} heterozygous animals Pea3-LacZ and Scip positive MNs settle at their typical ventral and dorsal positions, respectively. The two populations to not intermingle and no double positive neurons are found. (D) depicts a magnification of the in C indicated area. **E-G:** In contrast, in *Pea3* mutant animals Pea3-LacZ and Scip positive MNs intermingle due to the described dorsal shift of CM motor neurons. Colocalization of Scip and Pea3-LacZ indicates that in the absence of Pea3 prospective CM MNs are capable of inducing Scip. A magnification of the in G indicated area is provided in (H). **I-L:** Similar to cervical levels, lumbar Pea3 populations segregate from Scip positive MNs. **M-P:** Loss of Pea3 leads to intermingling and colocalization of Scip and Pea3-LacZ labeled MNs at lumbar levels, too.

At E11.5 combined immunocytochemistry to Pea3 and Scip at CM MN pools levels of *Pea3*$^{+/NLZ}$ animals revealed a Scip positive population of MNs residing at a position dorsal to Pea3-NLZ positive MN pools (Figure 15, A-D). In contrast, in *Pea3* mutants,

Pea3-LacZ expressing MNs exhibit a marked dorsal shift in their settling position and some of them clearly coexpress Scip (Figure 15, E-H). Similar results were found at E12.5 at lumbar levels where Scip and Pea3 are also expressed at the same rostro-caudal levels (Figure 15, I-P). In order to clarify the identity of Scip expressing MNs, we performed backfills from a number of cervical muscle nerves at E16.5. At Pea3-negative cervical levels (~C1-C5) a distinct clusters of Scip expressing MNs could be assigned to the diaphragm muscle by retrograde labeling form the phrenic nerve (Figure 16, A). At more posterior levels we established that the Scip^{+} column of MNs, which expands in parallel to Pea3^{+} MN pools, projects through ulnar and median nerves to innervate forearm muscles (Figure 16, B).

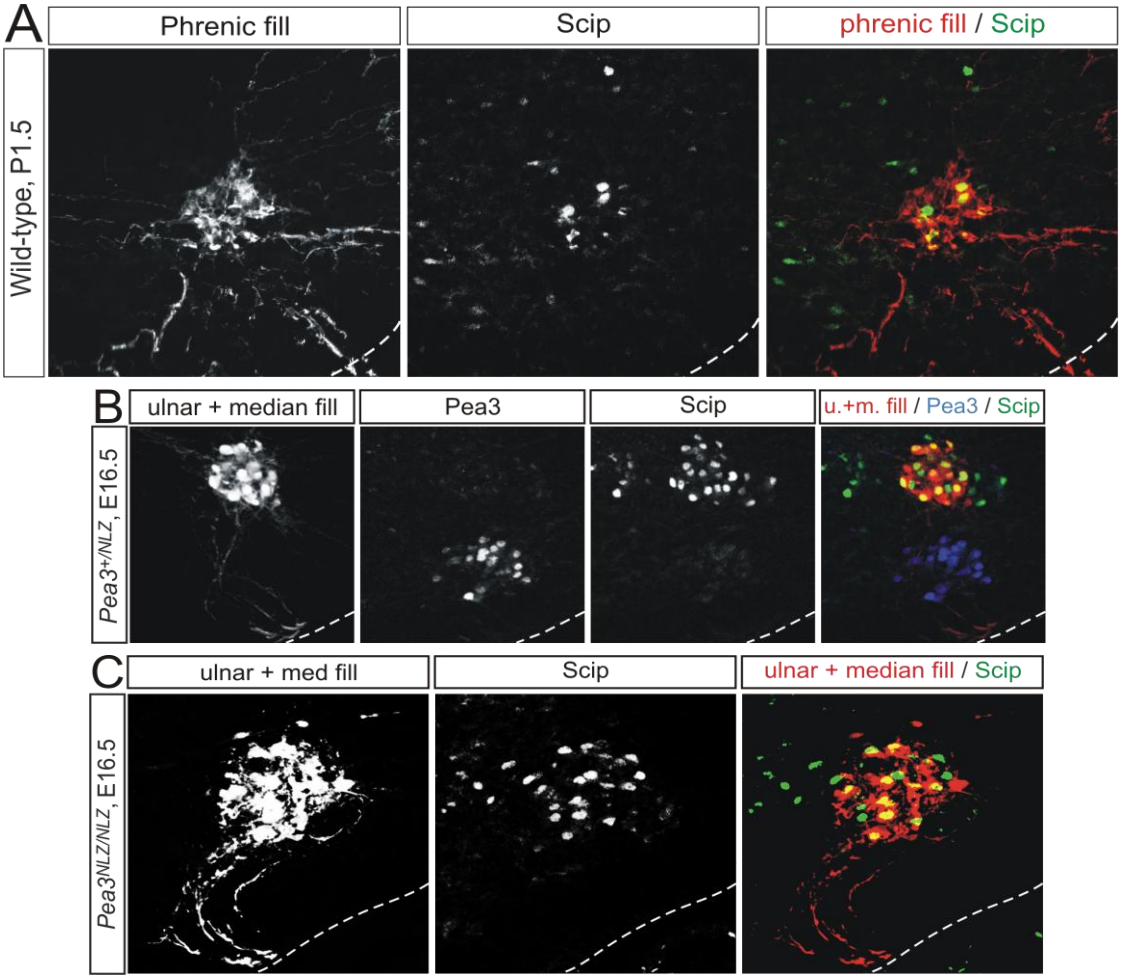

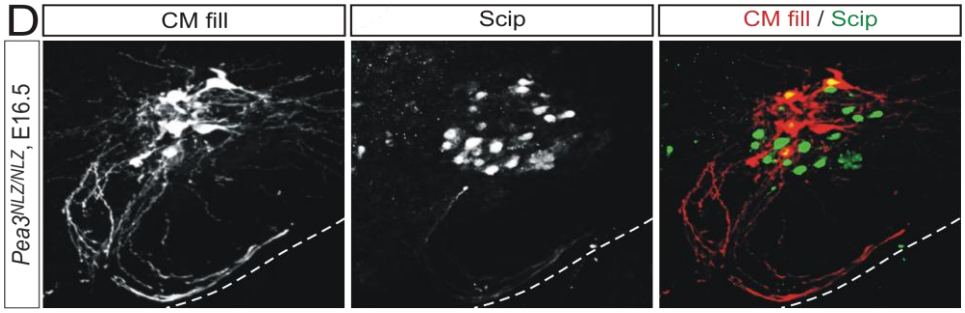

Figure 16: Scip expression in *Pea3* wild-type and mutant mice at E16.5

Mapping of Scip and Pea3 expression patterns in combination with retrograde labeling from CM, phrenic, ulnar and median nerves in wild-type and *Pea3* mutant animals. **A:** Rostral Scip expressing MNs innervate the diaphragm through the phrenic nerve. **B:** Retrogradly labeled ulnar and median MNs express Scip at a position dorsal to Pea3+ MN pools. At Pea3 positive segmental levels of the SC almost no Scip positive MNs are found outside retrogradely labeled MNs. Additionally, a subpopulation of interneurons express Scip at more medial and dorsal positions. **C:** Scip expression in forearm MN pools appears unaffected in *Pea3* mutant mice. **D:** In contrast to wild-type, in *Pea3* mutants Scip immunoreactivity is detected in virtually all retrogradely labeled CM MNs.

Retrograde labeling from CM and median/ulnar nerves in *Pea3* mutant animals revealed that the transcriptional identities (Scip$^+$, Isl1$^+$) and pool positions of forearm projecting MNs remain unaffected by the loss of Pea3 (Figure 16, C), while at the same time CM MNs, in accordance with their shift in pool position, responded with a pronounced upregulation of Scip (Figure 16, D). These results raised the possibility that Scip, which is expressed at low levels in all newborn MNs, is normally downregulated in prospective CM MNs upon induction of Pea3. Supporting this idea, CM and Scip positive MNs both belong to the medial Isl1$^+$ division of the LMC and prospective Scip and Pea3 positive MN pools might therefore originate from a common Isl1$^+$, Scip$^+$ "precursor" MN pool in the LMC. According to this theory, in *Pea3* mutant animals CM MNs would fail to engage new transcriptional modalities, remain in an aberrant dorsal position and maintain/enhance expression of Scip.

In order to provide direct evidence for a repressive function Pea3, we sought to determine whether Pea3 is sufficient to repress Scip by *in ovo* chick electroporation experiments. Stage HH 15 chick embryos were transfected with β-actin promotor driven murine Pea3-LacZ expression vector and colocalization of Pea3 and Scip was monitored 48 hours later by immunocytochemistry. Unfortunately, too few Scip$^+$ MNs

expressed sufficient levels of ectopic Pea3 to perform a quantitative analysis (data not shown).

In order to gain deeper insight into the regulation of Scip in differentiating MNs we also investigated its expression in *Hb9* mutant mice. *Hb9* mutant mice share a number of features with mice lacking *FoxP1* which exhibit strong upregulation of Scip in virtually all MNs (see discussion). Both *FoxP1* and *Hb9* mutant genotypes cause a reduction of Raldh2, Er81 and Pea3 expression levels, deregulation of LIM-homeodomain transcription factors, misrouting of axon trajectories and aberrant (or lack of) limb muscles innervation (Arber et al., 1999; Dasen et al., 2008; Rousso et al., 2008).

Hb9 mutant embryos were analyzed for Scip expression at SC levels where diaphragm and forearm muscle projecting MNs are located and at levels usually devoid of Scip. At the level of the phrenic MN pool, Scip positive MNs were detectable in approximately normal numbers, but compared to heterozygous controls, failed to aggregate into a tight cluster (Figure 17, B). The observed reduction of Isl1 positive cells is in accordance with the original characterization of the *Hb9* mutants (Arber et al., 1999). At the level of the CM MN pool some residual expression of Pea3 was detected in $Hb9^{NLZ/NLZ}$ embryos. However, similarly to our observations at segmental levels of the phrenic pool, $Scip^{+}$ MNs were broadly scattered instead of clustered. In summary, unlike in $FoxP1^{-/-}$ the total number of Scip positive cells appeared unchanged and despite the lack of MN pool organization, Scip in no instance colocalized with Pea3 expressing cells, which is consistent with the idea of Pea3 suppressing Scip. However, little is understood about the transcriptional regulation and inductive potentials of maturating MNs in *Hb9* mutants and since its differentiation program is likely affected at multiple levels our results cannot readily be assigned to a wild-type situation.

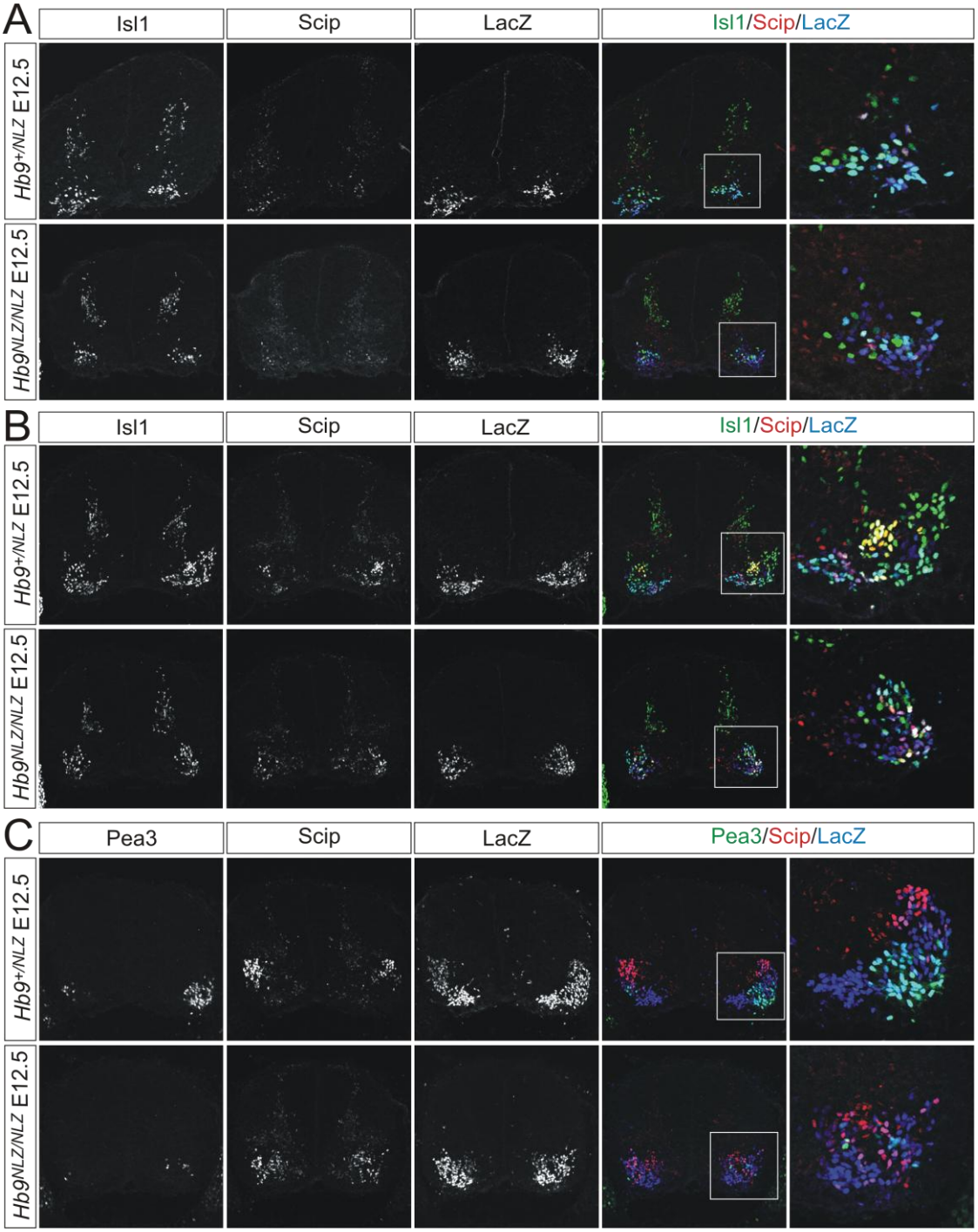

Figure 17: Evaluation of Scip expression in *Hb9* mutant mice

Scip expression was mapped at cervical SC levels of E11.5 embryos in *Hb9*$^{+/NLZ}$ and *Hb9*$^{NLZ/NLZ}$ mice. Sections of *Hb9* mutant and het MNs were level matched using Pea3 and Scip as positional landmarks. **A:** At segmental levels harboring almost no Scip+ cell in wild-type, neither their numbers nor their level of expression increased in *Hb9* mutants. **B:** At the level of the Scip expressing phrenic MN pool we found no apparent change in the number of Scip expressing cells in *Hb9* mutants. Compared to *Hb9* heterozygous SCs, Scip cells were however more scattered and did not aggregate into distinct MN clusters. **C:** The reduction of Pea3 expression in *Hb9*$^{NLZ/NLZ}$ did not lead to detectable increase in the number of Scip expressing MNs. In contrast to wild-type, Scip+ cells did not aggregate into MN pools but intermingled with Pea3 expressing cells throughout the ventral horn. Notably, no colocalization of Scip and Pea3 was found on any of the examined sections.

3.4 Discussion

3.4.1 Considerations on possible limitations of approach

Many of the key processes of sensory-motor circuit assembly, including neuronal cell migration, MN pool aggregation, axonal pathfinding, dendritic tree patterning, target recognition and synapse formation occur during embryonic stages (Chen et al., 2003; Ladle et al., 2007). For this reason genes which are expressed and deploy their function during embryogenesis are of particular interest as they are active during the time when most of the key processes underlying spinal motor circuit formation take place. Genes expressed at later time points might still play essential roles for the maintenance of neuronal properties and function, but they were not the primary focus of this study. However, in order to visually discern and dissect free the peripheral muscle nerves of the MN pools of interest, we were technically limited to use early postnatal tissue for our Affymetrix screening. As a consequence, our screen only comprises expression data of genes (still) transcribed at P1 but lacks information about transcriptional activity at time-periods when key processes controlling MN pool diversification and synaptic connectivity take place.

Developmentally activated genes do not necessarily have to play a role in the maintenance of specific neuronal identities and can be downregulated at postnatal stages. *Pea3,* for instance, is progressively downregulated during early postnatal development. In accordance with *in situ* hybridization and immunocytochemistry experiments, our Affymetrix chip data indicated *Pea3* expression at P1, but in some of the chip replicates the signal was not readily distinguishable from background noise. The example of Pea3 illustrates that, by sampling gene expression profiles at P1, it is in principle possible to lose tightly regulated developmentally active genes with significant roles in neuronal circuit formation. Moreover, during embryogenesis

members of the Hox gene family have been shown to be expressed in dynamic patterns across differentiating neuronal populations in the SC and it has been suggested that the same paralogs might play different roles, in different neural populations at different time points (Choe et al., 2006; Wu et al., 2008).

However, in favor of our approach argues the fact that a number of previously identified genes, such as members of the Hox family, LIM homeodomain transcription factor Isl1 and Lim1, ETS transcription factors Er81, Pea3 or the Runt domain transcription factor Runx1 known to regulate important aspects of sensory-motor circuit formation in the SC are still expressed at P1 in DRG or the SC. Similarly, cell surface effector molecules such as Sema3e, ret proto oncogene (c-Ret), calcitonin gene related protein (CGRP) and neurotrophic factor receptors, including Trks in DRG are induced at embryonic stages but remain strongly expressed until at least early postnatal stages. Moreover, our own *in situ* time-course experiments demonstrated that all of the marker genes detected at P1 were already expressed at embryonic stages.

In summary, virtually all previously identified proteins with documented roles in developmental aspects of motor circuit assembly could be identified in the expected expression patterns in the four pools sampled at P1. Thus the present screening data provides a suitable entry point into the transcriptomes of individual MN pools. A more through evaluation, including sampling at multiple time-points during embryonic development, could still complement our data in the future.

Nerve transection studies with DRG sensory afferents demonstrated that the transcriptional machinery reacts within as little as 15 hours to peripheral nerve injuries, possibly in even less time (Zhang et al., 1995). This is of relevance, because the incubation time of over-night backfills was in the range of 12-15 hours, too. These concerns were met, in that expression profiles of different MN pools were only

analyzed comparatively, canceling out most of the transcriptional deregulation bias caused by nerve injury. However, if in some MN pools transcriptional adaptations due to nerve damage is for some reason disproportionate, the effect would be reflected by inclined MN pool gene lists. More importantly, genes which are downregulated in response to nerve injury will misleadingly appear as unexpressed. An additional source for false negative results is naturally the relatively low present call values which might be inherent to tissue undergoing over-night ex-vivo retrograde labeling.

Taken together the addressed reservations of our method emphasize the importance to validate Affymetrix chip data by *in situ* hybridization experiments or immunohistochemistry. Nonetheless, our results indicate that the time point of the screen also allows the identification to genes strongly active during earlier developmental stages.

3.4.2 Potential functionalities of validated genes in motor circuit formation

The identification and validation of motor pool markers permitted us to choose candidate genes of particular interest for analysis at functional level. To this end we searched our screening data for genes which are the most likely to play important roles in the regulation of motor circuit assembly.

An extraction of the published findings about a number of validated genes with potentially interesting functions is recapitulated below. We are currently exploring the functionality of the Pea3 downstream targets *Pkr2* and *Del1* by analysis of their genomic null mutants. A more thorough discussion about the functions of Pkr2 and Del1 in other systems is found at the beginning of the respective chapters which also include our own findings on their roles in motor circuit formation.

3.4.2.1 Iroquois 6

Irx6 initially aroused our interest when it appeared 15.6-fold upregulated in CM MNs compared to Tric MNs (Table 2) and because it could be confirmed as a downstream target of Pea3 (Figure 14). Interestingly, Irx5 and Irx3 which are both located on the same chromosomal cluster as Irx6 display a largely overlapping expression pattern in CM MNs (Houweling et al., 2001) but our *in situ* hybridization indicated that in contrast to Irx6, Irx5 is not regulated by Pea3 (data not shown).

In human and mouse *iroquois* genes encode a family of homeodomain transcription factors comprising six genes (*Irx1-Irx6*) organized in two paralogous genomic clusters (Peters et al., 2000). *Iroquois* genes were first discovered and characterized as body patterning molecules in *Drosophila.* Essentially identical patterns of expression between *Araucan* (the *Drosophila Irx1/Irx3* homolog) and *Caupolican* (the *Drosophila Irx2/Irx5* homolog) paired with results from loss of function and genetic overexpression experiments suggested a high degree of functional redundancy within the iroquois gene family (Gomez-Skarmeta et al., 1996; Cavodeassi et al., 2001).

In vertebrates iroquois transcription factors have been studied for their roles in the specification of neuroectoderm in *Xenopus* and the regulation of the dorso-ventral subdivision of the chick and mouse neural plate (Gomez-Skarmeta et al., 2001). Here, Irx3 acts as a class I repressor gene defining the boundary between V2 interneurons and oligodendrocyte transcription factor 2 (Olig2) expressing MN precursors (Briscoe et al., 2000). Similarly, Irx3 is also involved in the establishment of anterior-posterior subdivisions in that it contributes to differentiation of the forebrain-midbrain boundary through mutually repressive interactions with other homeodomain transcription factors (Kobayashi et al., 2002). Moreover, Irx2 contributes to early specification events

required for the formation of the cerebellum in chick (Gomez-Skarmeta and Modolell, 2002).

Of all examined *Iroquois* genes *Irx6* displays the most restricted expression in developing mouse embryos. Its coexpression with Irx5 in MNs but diverging pattern in interneurons have also been documented by others (Mummenhoff et al., 2001). Interestingly, while in *Xenopus Irx5* could be identified a direct target of Hoxb4 (Theokli et al., 2003) in chick Hox4 paralogs are involved in the specification of Pea3 expressing MN pools (Dasen et al., 2005). Together these data raise the possibility that in the context of Pea3, murine *Irx* genes may also be direct targets of Hox transcription factors and Irx6 could figure as a pool intermediate transcription factor and play a role the molding of CM MN identity.

Until now virtually nothing is known about the downstream targets employed by Irx5 and Irx6. A functional analysis of Irx6 by means of a genetic mull mutant has not been described to date and there is a risk that in MNs, potential phenotypes could be masked by Irx3 or Irx5 compensating for the loss of Irx6. Ideally, the functions of iroquois transcription factors should be addressed by multiple conditional genetic mutants, which might be the scope of future studies.

3.4.2.2 Neuronal activity induced pentraxin

Narp was found 8.2 times enriched in CM MNs (Table 2) compared to other MN pools and the chip data also indicated *Narp* to be positively regulated by Pea3, (Table 6).

Narp protein belongs to the pentraxin family of secreted lectins and was originally identified through differential screening as an immediate early gene upregulated by induced brain seizure (Tsui et al., 1996). *In vitro* experiments addressed its role in the promotion of dendritic neurite outgrowth and neuronal migration in the developing and adult CNS (Tsui et al., 1996). More recently Narp has been shown to be secreted by

both pre- and postsynaptic neurons and to associate with AMPA receptors on aspiny hippocampal interneurons and spinal neurons *in vitro*. Analysis of the distribution and accumulation of AMPA receptors in Narp overexpression assays provided strong evidence that Narp protein stimulates AMPA receptor aggregation and the formation of new synaptic contact sites (O'Brien et al., 1999; Mi et al., 2002; O'Brien et al., 2002). In addition to its role in developmental and adult synaptogenesis, Narp emerges as an activity-regulated extracellular protein. It has been shown to interact with neuronal pentraxin1 and may play an important role in the regulation of excitatory synaptic plasticity in the developing and adult brain (Xu et al., 2003). However, a recent analysis of *Narp* mutants revealed that these mice were performing normally in a number of basic Pavlovian learning paradigms and only displayed statistically significant defects in their ability to process sensory-specific incentive values (Johnson et al., 2007).

Although several reports make mention of Narp expression in spinal neurons, no *in situ* hybridization patterns have been published until now. Based on the available data one can only speculate about potential functions of Narp in MNs. Despite functional parallels, it is unlikely to play a major in the aggregation of acetylcholine receptors (AChR) at NMJs, a process which has been well explored and attributed to the agrin–MuSK–rapsyn pathway (Madhavan and Peng, 2005). Instead, in MNs Narp likely fulfills their best understood "classical" role, which is the facilitation of AMPA receptor recruitment to sites of synaptic contact.

In this context it should be noted that the CM motor units differ functionally from the bulk of other skeletal muscles' motor units. CM MNs probably receive the largest part of their input through polysynaptically connected somatosensory afferents innervating a major proportion of the skin covering the trunk (Blight et al., 1990). In contrast to other

MN pools, CM MNs do not receive direct Ia proprioceptive afferent feedback from muscles (Vrieseling and Arber, 2006) and the CM muscle is unlikely to play a key role in locomotion. Although MN pools projecting to other limb muscles also receive information from sensory modalities of the body surface, it has been shown that the CM MN pools is the only cervical MN pool which receives major input from long ascending propriospinal projections neurons (Holstege and Blok, 1989).

But why would Narp predominantly be expressed in CM MNs? During the first postnatal weeks, when mice grow fur, receptive fields and synaptic contacts of somatosensory neurons and reflex encoders conveying stimuli from the skin to MNs undergo significant refinements (Granmo et al., 2008). Therefore, the enhanced expression of Narp in CM MNs could in some way reflect the dynamic regulation of sensory circuit refinement which must be of particular importance for the functionality of CM muscle controlling twitching of the skin (Blight et al., 1990).

Taken together, based on the functional spectrum of Narp, including its stimulatory effects on dendritic neurite outgrowth and neuronal migration (Tsui et al., 1996), it might be of interest to examine *Narp* mutants for phenotypes in CM MNs.

3.4.2.3 Amphiregulin

Areg figured among the top five hits of genes enriched in CM MNs (Table 2) and displayed an expression pattern strikingly similar to *Pea3* from E13 to P1.

Areg is a member of the epidermal growth factor family and has been shown to signal through the epidermal growth factor receptor ErbB1 (Maher and Schubert, 1995). Available information on the of Areg/ErbB1 signaling in the nervous system is scarce and largely based on *in vitro* experiments using DRG sensory neurons where Areg was initially identified as a gene upregulated upon sciatic nerve transection (Nilsson and Kanje, 2005; Nilsson et al., 2005). The same research group showed that Areg

stimulates axonal outgrowth and survival of adult sensory neurons *in vitro*. Moreover, Areg immunoreactivity colocalized with cells expressing its receptor ErbB1, indicating an autocrine or paracrine action as a neurotrophic factor for adult sensory neurons (Nilsson and Kanje, 2005).

In brief, despite its remarkable *in situ* pattern in CM MNs, the lack of functionally significant data on Areg/ErbB1 signaling led to the decision to put further investigation about Areg function on hold for the moment.

3.4.2.4 Tachykinin Receptor 3

Affymetrix chip data indicated *Tacr3* to be highly upregulated in Tric MNs, a finding which was confirmed by *in situ* hybridization experiments at embryonic and early postnatal stages. Tacr3 is the third member of the tachykinin family of G-protein coupled receptors mediating neuronal excitability and is activated by binding of the neuropeptide tachykinin 3 (Tac3, formerly neurokinin B). Two low affinity ligands, the neuropeptides Tac1 (also neurokinin1 or substance P) and Tac2 (neurokinin A) display preferential selectivity for Tacr1 (Substance P receptor) and Tacr2, respectively, but at higher concentrations also induce Tacr3 (Maggi, 1995; Maggi and Schwartz, 1997). Tachykinin receptors have mostly been investigated for their roles in central sensitization of pain perception following peripheral tissue injury or inflammation. Accordingly, Tac1 and Tac3 are most prominently expressed in laminae I and II of the dorsal horn, the termination zone of tactile and nociceptive sensory afferents. Tacr2 expression appears to be more restricted to the lamina I, where mostly peptidergic sensory afferents terminate. Over all the most pronounced and broad pattern of expression is detected for the substance P receptor Tacr1 which was for instance also found in the more ventrally located lamina X (Yashpal et al., 1990). Tac1 and Tac2 are the product of a single gene and as a result are often found to be coexpressed in and

coreleased from the same cells, including primary sensory afferents and spinal interneurons (Hokfelt et al., 1977; Todd and Spike, 1993). Epression of Tac3 is restricted to interneurons (Too and Maggio, 1991; Moussaoui et al., 1992). Central sensitization, a characteristic of hyperalgesia and allodynia, is triggered by peripheral inflammation and tissue injury and causes an increase in sensory-motor reflex response. The resulting activation of C-fibers leads to a release of Tac1 and Tac2 into the grey matter of the dorsal SC (Duggan and Hendry, 1986; Brodin et al., 1987). Tacr2 expressing neurons appear to integrate mostly inputs from muscle C-fibers while Tacr1 predominantly responds to inputs from skin C-fibers (Ma and Woolf, 1995) but other differences in their time-course and range of action of these receptors have been described as well (Xu et al., 1991). Recently, *in vivo* experiments on limb withdrawal reflexes with rabbits using specific Tacr3 inhibitors suggested a critical role in late stages of central sensitization (Houghton et al., 2000).

In summary, tachykinin signaling appears to exert an excitatory neuromodulatory role on spinal networks processing peripheral pain perception. All of these studies focused on the distribution and function of tachykinins in adult animals and receptor expression in subpopulation of MNs was not described. It appears plausible that Tacr3 modulate neuronal excitability in embryonic MNs, too. To what extent neuronal activity in developing SCs contributes to the establishment of neuronal networks is however controversial, as at least in chick specific monosynaptic sensory-motor connections also form in the absence of patterned neural activity (Mendelson and Frank, 1991). Tacr3 could also play diverse function at different developmental time points and neuronal populations. Unfortunately, there are currently no *Tacr3* mutant mice available to explore these different scenarios in more detail.

3.4.2.5 Neuropeptide Y

In Pec-Maj MN pools, *Npy* transcript emerged as 3-fold upregulated compared to other wild-type MN pools (Table 5) and these gene profiling results could be confirmed by experiments showing *Npy* specifically colocalization with retrogradely labeled Pec-Maj MNs (Figure 11).

NPY is a 36 amino acid neuropeptide with high affinity for five types of membrane receptor (Y_1-Y_5) of which Y_1 and Y_2 are most prevalent pre- and postsynaptic terminals of spinal interneurons and DRG sensory neurons (Tatemoto et al., 1982). In mouse DRG, expression of type Y_1 receptors appears to be restricted to the peptidergic ($CGRP^+$) subpopulation of small nociceptive sensory neurons while Y_2 receptor is equally expressed in also non-peptidergic ($IB4^+$) sensory neurons (Zhang et al., 1997). Expression in proprioceptive subpopulations of sensory neurons, central terminals of which could directly interact with NPY secreted from spinal MNs, has not been reported. In the SC, Y_1 receptors are expressed in seven morphologically distinct populations of interneurons distributed across almost all laminae, yet not in MN occupied areas of the ventral horn (Brumovsky et al., 2007).

In contrast NPY is strongly expressed in interneurons of the first three dorsal most laminae of the SC, where they are in direct contact with primary sensory terminals (Snider and McMahon, 1998). Moreover, NPY is strongly induced in sensory neurons of all modalities after nerve axotomy. However, despite a wealth of studies investigating the roles of NPY and its receptors in somatosensory system of the SC, we are the first to report NPY expression in spinal MNs.

Interestingly, *in vitro* results have indicated NPY to increase the growth rates of sensory axons and elicit a attractive turning response (Hokfelt et al., 2008) and recent *in vivo* findings on mice deficient in the Y_1 and Y_2 receptor further support a role for

NPY in axon guidance (Hokfelt et al., 2008). Although it is generally accepted that NPY exerts an inhibitory effect when acting through type Y_1 receptors and that binding to type Y_2 receptors increases the excitability of neurons (Smith et al., 2007), data about the functionality of NPY signaling in the nervous system remains controversial. For instance, in 2006 a survey in pubmed (www.ncbi.nlm.nih.gov/pubmed/) indicated that 52% of all studies attributed NPY an anti-nociceptive role, 29% a pro-nociceptive role and 19% report bilateral effects (Brumovsky et al., 2007).

Since secretion of NPY from Pec-Maj MNs could exert neuromodulatory control over an array of interneuronal populations expressing NPY receptors, the connectivity and role of which is yet little defined, we could only speculate about its potential roles in developing MNs. However, in a more general perspective, the fact that many of the identified MN pool marker genes bear the potential to regulate cellular excitability indicates the developmental role of neuronal activity in differentiating populations of MNs could be more important than hitherto assumed.

3.4.2.6 Scip

Scip (Pou3f1, Oct-6 or Tst-1) is a member of the vertebrate class III POU transcription factors which also comprises Pou3f2, Pou3f3 (Brain-1), and Pou3f4 (Brain-4). The most extensive investigations have addressed Scip's role in peripheral myelination of motor and sensory axons by Schwann cells. For this purpose, *Scip* null mutants were generated of which most homozygous animals die soon after birth due to respiratory failure. In surviving animals loss of Scip led to a pronounced delay in Schwann cell differentiation, with a transient arrest at the promyelination stage before axonal wrapping, suggesting that Scip is required for the transition of promyelin cells to myelinating cells (Bermingham et al., 1996; Jaegle et al., 1996). In Schwann cells, Scip is first induced at E14, expression peaks at about P0 and it is almost undetectable in

adult mice. Initial *in vitro* characterization of Scip revealed that it can bind to and repress the promotor of myelin protein zero and myelin basic protein (Monuki et al., 1989; Monuki et al., 1993). However, *in vivo* experiments imply that Scip usually figures as a transcriptional activator of a number of key regulators of myelination, but some of the data still remain conflicting (Jaegle et al., 1996; Bermingham et al., 2002; Ryu et al., 2007). More recently, the role of Scip has been explored by ectopic expression in Schwann cells which resulted in hypomyelination and axonal loss (Ryu et al., 2007). The current consensus about Scip function advocates that a precisely timed transient expression of Scip is crucial for the normal development of peripheral myelin.

In the CNS Scip expression has been described in the cortex layers II/III and V, the CA1 region of the hippocampus, the nucleus of the lateral olfactory tract (NLOT), a number of nuclei of the brainstem, including the nucleus of the solitary tract (NTS), the nucleus ambiguous, the glossopharyngeal nucleus and the facial nucleus VII and a cluster of cervical MNs, suggested to supply the diaphragm (Bermingham et al., 1996).

A recent study on FoxP1 function detected Scip expression in spinal MNs of the MMC_l (and weakly in MMC_m) division of the SC (Rousso et al., 2008). In *FoxP1* mutant mice, the Scip expressing MMC_l strongly expands at the expense of the LMC (Dasen et al., 2008; Rousso et al., 2008). Dasen et al. (2008) hold the view that loss of FoxP1 reverts the spinal motor system to an ancestral state when undulatory locomotion controlled by MNs supplying axial muscles was predominant in vertebrates and Scip could therefore function as a marker for the transcriptional default state of early postmitotic MNs. In wild-type, Scip positive LMC MNs projecting to limb muscles could thus comprise a population of MNs reading out information acquired through Hox transcription factors without intersecting with additional transcriptional programs. Accordingly, loss of Pea3 directed differentiation programs in prospective CM MNs

could simply retain these MNs in an original Hox/Scip controlled state, which could contribute to their pausing in aberrant dorsal position in the SC and their changes in sensory-motor connectivity (Vrieseling and Arber, 2006).

Since the high early postnatal mortality of *Scip*$^{-/-}$ mice is most likely a direct cause of defects in breathing (reduced frequency and gasping) Bermingham *et al.* examined whether the loss of Scip leads to a disorganization of phrenic MN pools or defects in Scip expressing nuclei of the hindbrain known to be involved the respiratory regulation. While the gross structural organization of hindbrain nuclei appears unaffected, whole-mount β-galactosidase stainings in *Scip* mutant mice revealed a subtle disordering and possible reduction in the number of Scip^{+} MNs (Bermingham et al., 1996). In the same study good evidence was presented that Scip is required for the proper migration of NLOT neurons which at E18.5 and P0 are found at aberrant position and by P4 were missing altogether in *Scip*$^{-/-}$.

In the context of the SC, Scip became of interest for mainly two reasons. Firstly, with its early developmental induction, restriction to distinct subpopulations of MNs and function as a transcription factor, Scip disposes of the typical features of a pool intermediate transcription factor, such as to Nkx6.1 (Garcia and Jessell, 2008). As mentioned above Bermingham *et al.*'s account of *Scip* mutant mice only makes mention of a slight disordering of the phrenic MN pool but no data about Scip expression in MN pools of the LMC or an examination of the peripheral nerve projections are presented. Since most *Scip* mutant mice die shortly after birth due to respiratory failure and the few survivors display severe reduction in body weight and size, subtle abnormalities in forearm coordination due to innervation defects may have escaped the authors' attention. Future studies should therefore address the function of Scip in MNs of the LMC. As a starting point, the effect of ectopic Scip expression in

MNs, by crossing *Olig2*^{Cre} or *Hb9*^{Cre} mice with the conditional transgenic *Scip* mouse (Ryu et al., 2007) on the specification of MN pool fate and muscle innervation should be analyzed. The same set of experiments could be applied to embryonic and early postnatal *Scip* mutant mice. We anticipate that the combined analysis of mice lacking or ectopically expressing Scip should provide new insights in its potential roles in neuronal migration, MN specification and pool assembly.

Secondly, Scip could also be involved in the establishment of sensory-motor connections. As described above, in *Pea3* mutants CM MNs express Scip and receive non-homonymous monosynaptic inputs via group Ia proprioceptive afferent sensory neurons. Ectopic expression of Scip in all MNs could therefore also be exploited to address the question of whether Scip is sufficient to change the specificity of Ia afferent inputs, which could be verified by intracellular recordings from CM MNs. Similarly, intracellular recordings from Scip positive MNs in wild-type mice should provide valuable information about the spectrum Ia proprioceptive afferent inputs from other muscle of the forelimb connecting to Scip MNs, a comparison of which with previously recorded connectivity data of CM MNs in *Pea3* mutant mice (Vrieseling and Arber, 2006) could disclose commonalities imposed by Scip.

While the analysis of ectopic Scip expression from MNs should be straightforward, examination of sensory-motor connectivity in *Scip* null mutant mice could be complicated by the retardation of myelination. In our laboratory intracellular recordings are typically performed between P5 and P7, time points when myelination defects become distinct in *Scip*$^{-/-}$ mice (Bermingham et al., 1996; Jaegle et al., 1996). Since in intracellular recordings from MNs, monosynaptic Ia proprioceptive afferent inputs are recognized and defined by their short onset latencies of 2 to 3.6ms (Vrieseling and Arber, 2006), analysis of mice exhibiting compromised AP propagation due to

myelination defects might not be possible. Therefore, to investigate the impact of loss of Scip on sensory-motor connectivity conditional *Scip* mutants would have to be used. Since to our knowledge no such mouse has been generated, a thorough analysis of potential phenotypes regarding MN pool differentiation and peripheral connectivity should be of priority.

3.5 Materials and Methods

3.5.1 Gene expression profiling

3.5.1.1 Retrograde tracing of individual motor neuron pools.

P0-P1 mice were used in retrograde tracing experiments for Affymetrix gene expression profiling and gene candidate validations (E16.5 for Scip). Mice were anesthetized on ice, perfused with artificial cerebral spinal fluid (ACSF), decapitated and transferred to a chamber containing ice-cold circulating oxygenated (95% O_2 / 5% CO_2) ACSF as described previously (Mears and Frank, 1997). In order to decrease O_2 diffusion distances, cervical SCs were exposed by dorsal laminectomy. Muscle nerves were dissected from brachial nerve plexus to their entry point into respective muscles. Tetramethylrhodamine-labeled dextran (Invitrogen) supplemented with isolecitin was applied to detached nerve endings using tightly fitting fire polished glass capillaries. These ex-vivo preparations were incubated over night at room temperature.

For immunohistochemistry, retrogradely labeled SC were fix in 4% paraformaldehyde (Baker, Deventer, NL) and dehydrated by over-night immersion in 30% sucrose, before embedding in Tissue Tek O.C.T (Sakura, Zoeterwoulde, NL). For laser capture microdissection experiments, SCs were fresh frozen in Tissue-Tek O.C.T.

3.5.1.2 Laser Capture Microdissection

14 µm transverse cryosections containing motor pools of interest were collected on membrane slides for laser microdissection (Molecular Machines and Industries (MMI), Glattbrugg, CH). Before downstream processing membrane slides were dehydrated by 30 seconds sequential immersion into ice-cold 70% and 100% ethanol. Individual fluorescently labeled MNs were excised using a fluorescent Olympus IX81 laser microdissection microscope (MMI, Glattbrugg, CH). Laser-dissected cells were almost immediately covered with 50 µl extraction buffer (Arcturus, USA), left to lyse on the lid of the tube at RT for at least 15 minutes, and stored at -80°C. Total cellular RNA was isolated with the PicoPure RNA isolation kit (Arcturus, USA) and for samples the RNA-integrity was validated using a 2100 Bioanalyzer (Agilent). After two rounds of amplification, preparation of *in vitro* transcription products was performed according to Affymetrix protocols (GeneChip Expression Analysis Technical manual). The fragmented cRNA (15 µg) was used in a hybridization cocktail containing spiked controls (Affymetrix). A total of 200 µl of this hybridization cocktail was hybridized at 45°C for 16 hours to GeneChip Mouse Genome 430 2.0 Arrays (Affymetrix). Following hybridization, the arrays were processed using a GeneChip Fluidics Station 400 according to recommended protocols (FS450_0001, Affymetrix). Fluorescent images of arrays were captured using the GeneChip Scanner 3000 7G (Affymetrix), and image data were acquired and analyzed using the GeneChip Operating Software (GCOS, Affymetrix).

3.5.1.3 Statistical Analysis

Expression values and detection p-values were calculated using the GC-RMA implementation found in Genedata's (Basel, Switzerland) Refiner array 4.1 package. Expression values were quantile normalized and median scaled to a value of 20 in

Genedata's Analyst 4.1 package. To reduce the number of genes in the analysis, we performed either a 2-fold filter on the genes present in at least one condition and constructed a union list of these genes. This list was then used to identify statistically significant effects in the data set using an N-way ANOVA ($p<0.01$). In order to identify genes enriched in single MN pool, the subpopulations passing the previous filters were subjected to Self-Organizing-Map (SOM) clustering algorithms. Fold change values of the wild-type screen were calculate by dividing median expression values of a selected MN pool with the average median expression values of the other pools.

3.5.2 *In situ* hybridization

In situ hybridization with digoxigenin-labeled probes was performed on fixed and unfixed tissue according to previously described protocols (Schaeren-Wiemers and Gerfin-Moser, 1993; Wright and Snider, 1995). Antisense riboprobes used in this chapter were produced from plasmids harboring the following cDNAs: *mPea3* (Livet et al., 2002), *Pkr2* (Genebank accession number BC055730), *Irx6* (AA709522), *Tacr3* (BC066845), *Narp* (BC026054), *Areg* (BC009138), *Del1* (BC056386). Images from *in situ* hybridization experiments were recorded using a mountable Leica DFC480 digital camera.

3.5.3 Immunohistochemistry

Cryostat sections were processed for immunohistochemistry as previously described (Arber et al., 1999). In this chapter the following antibodies were used: rabbit anti-Pea3 (c-term) (Arber et al., 2000); guinea pig-anti-Scip (kindly provided by Jeremy Dasen); rabbit anti-GFP (Molecular Probes); rabbit anti-rhodamine (Molecular Probes); rabbit anti-Hb9 (Arber et al., 1999); goat anti-LacZ (Biogenesis Ltd), guinea pig anti-Isl1 (Arber et al., 2000). As secondary antibodies we used Alexa488-, Cy3- and C5-

conjugated fluorophores (Molecular Probes). Fluorescently labeled tissue sections were imaged using an Olympus BX61 scanning microscope (Olympus).

4 Functional Analysis of Pkr2 in Motor and Sensory Systems

4.1 Introduction

Since the elucidation of Pkr2 function in spinal MNs constituted a major goal of my thesis, the following account of published data will primarily cover findings on its role in the nervous system. Even in this limited context a vast amount of information has been collected over the last few years and I will therefore set the focus on data which could contribute to the understanding of Prk2's role in MNs.

The molecular characterization and functional analysis of prokineticins and their cognate receptors was initiated by three independent research groups investigating their roles as selective mitogens for endocrine gland endothelial cells and their stimulatory effect on the gastrointestinal tract (LeCouter et al., 2001; Li et al., 2001; Lin et al., 2002; Masuda et al., 2002; Soga et al., 2002). Subsequent studies began to explore the roles of prokineticin receptors in neural cell migration in the CNS (Ng et al., 2005; Matsumoto et al., 2006; Prosser et al., 2007a; Hardelin and Dode, 2008), pain perception in the peripheral nervous system (Negri et al., 2002; Hu et al., 2006; Negri et al., 2006; Vellani et al., 2006) and the regulation of autoimmune response (LeCouter et al., 2004; Martucci et al., 2006; Shojaei et al., 2007).

4.1.1 General characterization of prokineticin ligand receptor interactions

Prokineticin receptors belong to the superfamily of G-protein coupled receptors and are about 85% identical in their amino acid composition. Their name reflects the functionality of their ligands as potent stimulators of gastrointestinal cell motility (thus pro-kineticin) through activation of smooth muscle cells. As discussed in more detail below prokineticin receptors mainly act as Gq-coupled receptors and usually promote

intracellular Ca^{2+} mobilization, but examples of signaling through Gs and Gi mediated transduction pathways have been demonstrated, too (Li et al., 2001; Lin et al., 2002; Chen et al., 2005; Vellani et al., 2006).

Homologs of murine Pk1 and Pk2 have been identified in humans, monkey, rats and cattle as well as in skin-derived secretions of the frog *Bombina variegata* (Bv8), *Takifugu* fishes (Fugu1 and 2), lizards (Var1) and the venom of the black mamba snake (MIT-1) (Mollay et al., 1999; Negri et al., 2007). The two most important molecular characteristics of these proteins are a highly conserved amino acid sequence at the N-terminal, AVITGA, which is critical for their bioactivity, (Bullock et al., 2004) and ten conserved cysteine residues which assemble into a so called colipase-fold motif through five internal disulfide bridges. This motif is also found in members of the Dickkopf family of extracellular signaling molecules. Prokineticin, however, do not display Dickkopf-like activity nor do Dickkopf proteins display Prokineticin-like activity in their respective assays (Kaser et al., 2003). Until now, two different splice variants of Pk2 have been characterized, a long 102 amino acid form including an additional exon harboring 19 basic amino acids and a short variant of 82 amino acids. However, differences in their receptor binding affinities or regulation of their alternative splicing mechanisms have not been investigated.

Both prokineticin receptors display a higher affinity for Pk2 than Pk1 while neither of the ligands exhibits a significant preference for Pkr1 or Pkr2 (Negri et al., 2007). This apparent non-selectivity implies that in a given tissue it is primarily the availability of the respective ligand/receptors pair which determines the signaling interactions and physiological output rather than selective binding preference. In the CNS Pkr2 and Pk2 gene expression has been demonstrated in a number of distinct nuclei, and ligand receptor interactions have been shown to be implicated in neurogenesis, neuronal

excitability, neuronal survival, neuronal migration, cellular differentiation and regulation of circadian rhythm. In contrast, Pkr1 is only weakly expressed in the neocortex (reviewed by Negri et al, 2007). In non-neuronal tissues, Pkr1 and Pkr2 are both abundantly expressed in mostly non-overlapping patterns and often seem to fulfill related physiological functions, including stimulation of angiogenesis in reproductive and endocrine organs, gastro-intestinal cell motility, ingestive behavior, hormone release, and the regulation of immune responses (Negri et al., 2007).

4.1.2 Prokineticin functions in neuronal excitability

A number of research groups have explored the neuroregulatory role of Pkr1 and Pkr2 in DRG where prokineticin signaling appears to play a major role in the sensitization of pain perception by sensory neurons. Activation of Pkr1 and/or Pkr2 results in stimulation and translocation of protein kinase Cε (PKCε) to the plasma membrane. Membrane associated PKCε can increase the excitability of sensory neurons through phosphorylation of transient receptor potential cation channel, subfamily V, member 1 (Trpv1), which triggers Ca^{2+} influx into the cell (Negri et al., 2002; Hu et al., 2006; Negri et al., 2006; Vellani et al., 2006). A more thorough discussion about the role of prokineticin receptors in DRG in chapters 4.1.4 below.

In the mouse suprachiasmatic nucleus (SCN), Cheng *et al*. (2002) found *Pk2* mRNA to oscillate in a light-regulated manner: Pk2 is upregulated during the course of the day and is rapidly downregulated at night. However, studies using *Pk2* and *Pkr2* null mutants have provided evidence that Pk2/Pkr2 signaling does not regulated timekeeping or entrainment within SCN nuclei themselves, but results in deregulation of circadian output behavior such as disturbance of the activity/rest cycle and thermoregulation, suggesting Pk2 to act as a most downstream mediator of circadian clocking (Li et al., 2006; Hu et al., 2007; Prosser et al., 2007b). Intriguingly, *Pkr2*

mRNA has been detected in virtually all areas targeted by Pk2 expressing SCN efferents, including the paraventricular hypothalamic nucleus (PVN), dorsal medial hypothalamic nucleus (DMH), paraventricular an paratenial thalamic nuclei (PVT/PT), lateral habenula (LHb), paracentral thalamic nucleus (PC), but also in other regions such as the lateral gloubus pallidus (LGP) and the subfornical organ (SFO) (Figure 18). Evidence indicating a stimulatory role of Pk2 on neuronal excitability stem from intracerebroventricular injections of the Pk2 homolog Bv8 which resulted in strong increase of FBJ osteosarcoma oncogene (c-fos) immunoreactivity in the SCN target nuclei PVN, DMN, ARC and SFO (Negri et al., 2007).

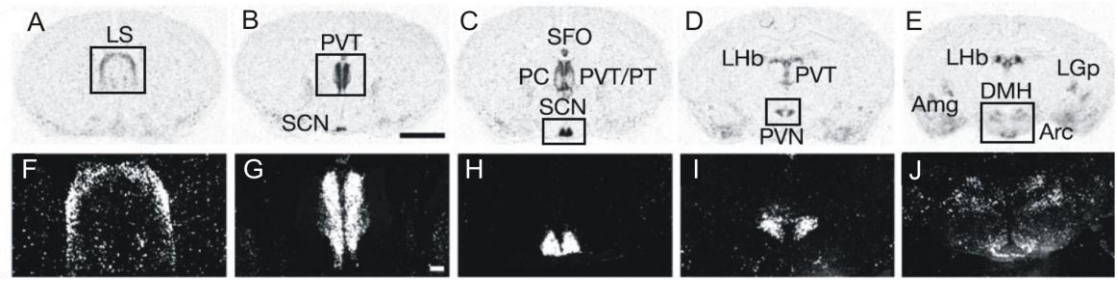

Figure 18: *Pkr2 In situ* hybridization patterns in adult mouse brain

A-E: *Pkr2 in situ* hybridization patterns in the lateral septum (LS), paraventricular thalamic nucleus (PVN), suprachiasmatic nucleus (SCN), paratenial nucleus (PT), subfornical organ (SFO), paracentral nucleus (PC), lateral habenula (LHb), amygdala (Amg), lateral globus pallidus (LGp), dorsal medial hypothalamic nucleus (DMH), arcuate nucleus (Arc). **F-J:** Dark-field images of *Pkr2* mRNA from boxed regions in A–E. Adapted from (Cheng et al., 2002).

Interestingly, Pkr2 is also expressed by Pk2 positive cells of the SCN itself, where it has been shown to be part of a positive feedback loop enhancing the expression of Pk2 upon its activation (Cheng et al., 2002).

The complementary expression patterns of Pk2 and Pkr2 in the SCN and its target structures, respectively, raised the question of whether Pk2 expressing projection neurons make direct synaptic contacts with Pkr2 expressing neurons and whether Pk2 could thus exert its effect on postsynaptic cells by direct release from axon terminals. To this end, it has recently been demonstrated that Pk2 can indeed directly increase excitatory postsynaptic potentials (EPSPs) and the AP frequency in two types of Pkr2 expressing projection neurons of the PVN, a direct target of $Pk2^{+}$ SCN projection

neurons implicated in the modulation of daily autonomic biological patterns. Depolarization of these neurons remained unaffected by tetrodotoxin, but were abolished after addition of prokineticin receptor antagonists or inhibitors of mitogen-activated protein kinase (MAPK), suggesting Pk2 to act through direct synaptic contacts on PVN projection neurons (Yuill et al., 2007). Interestingly, one of the examined populations of PVN projection neurons expressing Pkr2, the parvocellular preautonomic neurons, terminate in NTS comprising a number of nuclei expressing Pk1 and Pk2 (Negri et al., 2004). Similarly, electrophysiological recordings from dissociated SFO neurons, another termination zone of SCN efferents, also indicated that Pk2 exerts a strong depolarizing effect and greatly increases AP frequencies (Cottrell et al., 2004; Fry et al., 2008).

4.1.3 Prokineticin signaling pathways

The stimulatory effect of Pk2 on neuronal excitability of SFO neurons appears to be mediated via the MAPK signaling cascade, which increased AP frequencies by modulation of Na^+ and K^+ channel conductance (Fry et al., 2008). Experimental findings from the same group also demonstrated that increase of intracellular Ca^{2+} concentrations in SFO was independent of intracellular Ca^{2+} stores but mediated through voltage-gated L-type Ca^{2+} channels. Unlike in PVN projection neuron, Ca^{2+} influx was only a secondary effect of increased AP frequency (tetrodotoxin-sensitive) rather than a direct modulatory effect of Pk2 on Ca^{2+}-channel properties (Fry et al., 2008).

Nonetheless, the observed commonalities of Pk2/Pkr2 signaling in the PVN and the SFO raise the question of whether the described signaling pathway involving phosphorylation of MAPK and subsequent increase of intracellular Ca^{2+} are also at play in other neuronal or non-neuronal systems expressing prokineticin receptors. Although

several studies in different cellular contexts have described the activation of p44/42 MAPK by Pk2 (Melchiorri et al., 2001; Lin et al., 2002; Masuda et al., 2002; LeCouter et al., 2003), there are also examples of MAPK independent pathways that regulate membrane depolarization upon prokineticin receptor activation. For instance, Pk2 induced contraction of gastrointestinal smooth muscles via L-type voltage-gated Ca^{2+} channels (as observed in SFO neurons) could not be blocked by inhibitors of MAPK (Li et al., 2001) suggesting that a different downstream signaling pathway is engaged. In addition, in DRG sensory neurons of the peripheral nervous system, sensitization of pain perception upon Pk2/Pkr interactions is also associated with an increase in intracellular Ca^{2+}. In this case, the inward current of Ca^{2+} appears to result from the activation of PKCε mediated phosphorylation and potentiation of Trpv1 (Negri et al., 2002; Negri et al., 2006; Vellani et al., 2006). Similar to gastrointestinal smooth muscle contractions, no link between L-type Ca^{2+} channels and increases in intracellular Ca^{2+} could be shown by pharmacological manipulation (Li et al., 2001; Vellani et al., 2006).

4.1.4 Prokineticin signaling and cell migration

Genetic studies have demonstrated Pk2/Pkr2 interactions to play essential roles for the development of the olfactory bulb (OB), where neurogenesis persists into adulthood. In the olfactory system Pk2 is expressed in the ependymal and subependymal layers of the olfactory ventrical of the mouse embryo as well as the granule cell layer, the periglomerular layer and the mitral cell layers in developing and adult mice (Prosser et al., 2007a). There is strong evidence that Pk2 acts as a chemoattractant guiding Pkr2 expressing neuronal progenitors from the subventricular zone through the rostral migratory stream to their target regions in the OB. Interestingly, olfactory neurons normally move along a migration pathway previously established by sprouting olfactory axons (Gonzalez-Martinez et al., 2004; Yoshihara et al., 2005). In *Pkr2*

mutant mice, these axons fail to reach the forebrain as they form a large tangled sphere-shape structure in the upper nasal region (Matsumoto et al., 2006). It was therefore speculated that the observed cell migration defect is secondary to an axon pathfinding deficiency, insofar as Pkr2 expressing growth cones fail to detect chemoattractant Pk2 gradients in the rostral migratory stream and OB (Matsumoto et al., 2006).

As a result, both, *Pk2* and *Pkr2* loss of function mice, OB sizes are reduced and their cellular architecture is severely disordered (Ng et al., 2005; Matsumoto et al., 2006; Prosser et al., 2007a). The hypothesis that Pk2 can function as a chemoattractant is further supported by *in vitro* assays demonstrating Pkr2 expressing neuronal progenitors cells to migrate towards a local source of Pk2 (Ng et al., 2005). Moreover, the phenotypes observed in *Pkr2* mutant mice bear striking resemblance with clinical manifestations of human Kallmann syndrome, a form of hypothalamic hypogonadism leading to defects in sexual maturation. In mice lacking Pkr2, gonadotrophin releasing hormone (GnRH) neurons fail to migrate from the olfactory epithelium to hypothalamic target area which is indicated by the absence of GnRH immunoreactivity in preoptic area of the hypothalamus (Matsumoto et al., 2006). The implication of Pkr2 signaling is further supported by recent findings in humans, showing that a number of missense mutations that impair human Pkr2 activity are associated with Kallmann syndrome (Monnier et al., 2009).

4.1.5 Prokineticin signaling in the sensitization of pain perception

Experiments investigating the role of prokineticin signaling in pain perception have shown that Pk2 is released at sites of inflammation, where, among other, it interacts with Pkr1 and Pkr2 expressed in non-overlapping subpopulations of peptidergic DRG sensory neurons. Both of these populations have been shown to coexpress the heat and

capsaicin sensitive channel Trpv1 (Negri et al., 2006; Vellani et al., 2006). In average, 68.5% of Trpv1 positive sensory neurons coexpress Pkr1 and 9.4% coexpress Pkr2 (Negri et al., 2006). Several lines of evidence strongly indicate that the loss of Pk2/Pkr signaling results in an impairment of pain sensation (Negri et al., 2002; Hu et al., 2006; Negri et al., 2006; Vellani et al., 2006; Negri et al., 2007). While systemic and local injections of Pk2 lead to intense sensitization of sensory neurons to thermal and mechanical stimuli (Negri et al., 2002), mice lacking Pkr1 displayed impaired responsiveness to noxious heat, mechanical stimuli and capsaicin. Accordingly, *Pkr1*$^{-/-}$ mice exhibited reduced thermal hyperalgesia after acute inflammation. The current model suggests that activation of prokineticin receptors by Pk2 causes immediate influx of Ca^{2+} into sensory neurons, activation of protein kinase Cε (PKCε) and its translocation to the plasma membrane where it phosphorylates and potentiates the activity of Trpv1. Since *Pkr1* mutant mice also exhibit a reduced pain perception in normal (uninflamed) tissue, ligand binding is likely involved in a tonic baseline activation of Trpv1.

At sites of inflammation, expression of Pk2 was found to be 15 to 29 times higher than in normal tissue (Negri et al., 2006). It has been demonstrated that Pk2 is strongly secreted from mature peripheral blood cells including neutrophils, monocytes and dendritic cells and can reach high local concentrations (LeCouter et al., 2004). Besides its role in the regulation of pain perception, there is also evidence that locally secreted Pk2 can function as a stimulant for the maturation and chemoattractant for the migration of prokineticin receptor expressing monocytes to sites of inflammation, respectively (LeCouter et al., 2004; Martucci et al., 2006).

Conversely, little published information is available about pain perception defects of *Pkr2* mutant mice. It was however pointed out that tactile allodynia was equally evoked

by Bv8 in wild-type mice and *Pkr1* mutants (Negri et al., 2006) but reduced in *Pkr2* mutant mice (Negri et al., 2007) suggesting a possible role of Pkr2 in receptor sensitization to punctuate stimuli.

4.1.6 Potential functions of Pkr2 in CM motor circuit assembly

Taken together, a major function of prokineticin receptor signaling in the CNS appears to be modulation of neuronal excitability, a role which seems to be conserved in somatosensory neurons of the peripheral nervous system as well as in subgroups of smooth muscle fibers, yet at times by means of diverging signaling pathways. The biological relevance of a neuromodulatory role in the development of motor circuitry is not immediately intuitive. Unlike for the establishment of other topographically organized neuronal networks, such the visual system, activity does not appear to be important for the initial wiring of selective proprioceptive sensory-motor connections in the SC (Mendelson and Frank, 1991) or neuromuscular connectivity in the periphery. In contrast, the question of whether cellular excitability of MNs might influence the development of other components of motor circuit assembly has not been addressed yet.

As discussed, in the developing olfactory system, Pk2 has also been shown to act as a chemoattractant on migrating neuronal precursors expressing Pkr2 and the employed mechanism appears to involve axon pathfinding (Matsumoto et al., 2006). A chemotactic role for Pkr2 in motor circuit assembly is appealing because many of the phenotypes observed in *Pea3* mutant mice, including axon pathfinding, neuronal migration and the establishment of selective group Ia afferent connectivity (Haase et al., 2002; Livet et al., 2002; Vrieseling and Arber, 2006) are likely caused by misregulation of chemotactic effector molecules implementing such processes. For example, Sema3e acts as a repellent on proprioceptive sensory terminals expressing

plexinD1. Loss of Sema3e signaling in CM MNs abolishes the repellant cue and causes aberrant formation of monosynaptic connections with homonymous Ia proprioceptive afferents (Eline Pecho-Vrieseling et al., unpublished data). Moreover, in *Pea3* mutant mice, CM MNs also exhibit migration defects and fail to reach their normal settling position at the ventral edge of the grey matter (Haase et al., 2002; Livet et al., 2002). As Pea3 is induced through cues from peripheral target tissue, Pkr2 as a downstream molecule cannot be involved in the earliest processes controlling MN specification. It may instead play a role in later events such as terminal cell migration, control of "self" recognition required for MN pool clustering and the formation of gap junctions, and elaboration of MN pool specific dendritic and peripheral axon branching patterns.

Taken together, the Pkr2 signaling pathway disposes of all necessary characteristics to play a role in multiple aspects of MN pool differentiation and motor circuit assembly. Thorough evaluation of Pkr2 function in CM MNs should, therefore, comprise an assessment of their differentiation from cell cycle exit (E9.5 –E11.5), to the moment of Pkr2 induction (~E14) and the assembly of functionally integrated MN pools at the end of embryonic development.

4.2 Results

4.2.1 Pk2 expression in embryonic and adult mice

4.2.1.1 Validation of *Pk2^{GFP}* BAC transgenics

An understanding of the activity and function of Pkr2 signaling requires information about the temporal regulation and special distribution of its natural ligands Pk1 and Pk2. Since Pk2 is the ligand predominantly interacting with Pkr2 *in vivo,* we analyzed bacterial artificial chromosome (BAC) transgenic mice expressing enhanced GFP protein under the control of *Pk2* promotor elements (*Pk2^{GFP}*) (Gong et al., 2003).

Genomic DNA of such BAC transgenics are modified to contain multiple insertions of a modified BAC, in which enhanced GFP reporter cDNA replaces the coding sequence of a protein of interest, but ideally remains under the control of all its endogenous regulatory elements. Since 15% of today's BAC transgenic lines do not exactly reflect the endogenous gene expression patterns (Gong et al., 2003), we examined a selection of sites expressing GFP for their consistency with *in situ* hybridization data from the literature.

In $Pk2^{GFP}$ transgenic mice Pk2-GFP protein was readily detected in the NTS (not shown), OB and the SCN (Figure 19), all structures where the prevalence of Pk2 has been documented by others (Ng et al., 2005; Li et al., 2006; Masumoto et al., 2006; Maldonado-Perez et al., 2007; Yuill et al., 2007; Fry et al., 2008). At embryonic and early postnatal stages we also detected strong Pk2 expression in the epididymis and the ductus deferens of male genitals. Previously, Pk2 expression in the male reproductive system had only been described in adult mice and appeared to be restricted to primary spermatocytes and the prostate (Wechselberger et al., 1999; LeCouter et al., 2003). In BAC transgenics, however, weak transcriptional activation of a gene can result in disproportionally strong GFP signal (Gong et al., 2003), which could explain why early postnatal expression of Pk2 in male genital organs may have escaped other investigators' attention using *in situ* hybridization. Moreover, it remains unclear if sexually immature animals were examined in these studies at all.

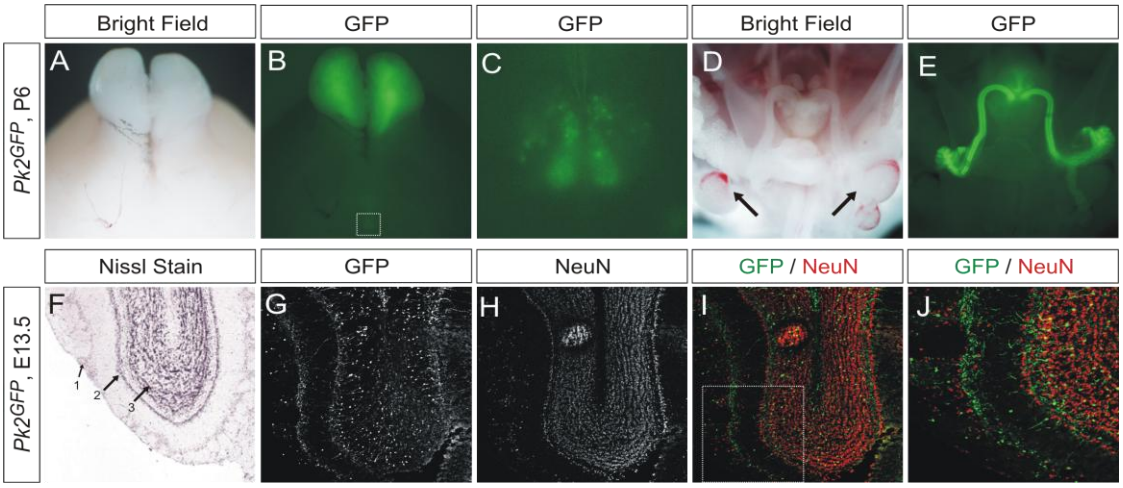

Figure 19: *Pk2*^{GFP} signal is detected in the OB, the SCN and structures of the mouse reproductive system.

Pk2-GFP expression was analyzed for comparison with *Pk2* expression patterns from *in situ* hybridization experiments. **A-C:** P6 brain reveals strong Pk2-GFP expression in OB and SCN. (C) depicts a close up view of the SCN, the position of which is indicated by the boxed area in (B). **D-E:** Structures of the male reproductive system were exposed by removing guts and the bladder. The position of the testicles is marked by black arrows (D). In (E) the same aperture was used to display GFP fluorescence under UV. The signal could be assigned to cauda epididymis and the ductus deferens but not the testicles per se. **F-J:** Sagittal sections of the OB at E13.5. Adult Nissl stain in (F) is adapted from the Allen Brain Atlas to demonstrate the structural organization of the OB which is similar to E13.5 (H). Arrow 1 points at the epiglomerular cell layer, arrow 2 at the mitral cell layer and arrow 3 at the granule cell layer, all of which have been described to express Pk2 (Ng et al., 2005; Negri et al., 2007). Pk2-GFP signal is primarily distributed in the granule cell layer and the epiglomerular layer. Few cell are also found in the mitral cell layer, suggesting that Pk2-GFP reliably reflect endogenous Pk2 expression in the OB. (J) depicts a magnification of the area indicated in (I).

Taken together, we can not be absolutely sure that the *Pk2* BAC transgenic reliably represents endogenous Pk2 expression. RT-PCR experiments on RNA extracted from sorted Pk2-GFP cells of neuronal and non-neuronal sources intended to clarify this critical point did unfortunately not yield clear results (data not shown). We will hereafter assume that GFP expression in our *Pk2*^{GFP} mice reflects the endogenous regulation of *Pk2*, but it should be kept in mind that this can not be taken for granted.

4.2.1.2 Developmental expression of Pk2 in the peripheral target area of CM MNs

In order to design experiments addressing the function of Pkr2 in MNs the spatiotemporal expression pattern of Pk2 must be investigated with respect to two main scenarios of actions. Firstly, Pk2 could act centrally on MN somas and dendrites and, secondly, Pk2 may be secreted by non-neuronal cell peripherally and signal through Pkr2 presented by axon branches and terminals in the target muscle.

To verify central Pk2 expression transverse sections of embryonic and adult *Pk2*^{GFP} mice were analyzed. Few GFP positive interneurons (<100 per SC) were found dispersed along the rostrocaudal extent of the SC (Figure 20, H). The small number and their broad distribution also with respect to the dorsoventral axis, make it unlikely that these interneurons represent a population specifically connected with Pkr2 expressing cervical MN pools such as of the CM muscle (Blight et al., 1990). For this reason, we focused on the possibility of a peripheral source of Pk2.

In this second scenario, peripherally secreted Pk2 could at embryonic stages play a role in axon guidance and in adults mediate neuronal excitability. To investigate these possibilities we performed transverse sections of disemboweled embryos at E13.5 and E15.5 as well as of CM muscles and adjacent skin tissue layers at P3 and P6. At E13.5 and E15.5 but not at postnatal stages (P3, P6, adult), strong Pk2-GFP signal was found in tissue layers flanking the CM muscle but not in the muscle itself (Figure 20, A-D). The exact identity of the GFP positive cells was not determined. A morphologically similar layer of Pk2-GFP expressing cells was found on the inner side of the ribcage at embryonic stages (Figure 20, E). Although the CM muscle was not entirely wrapped by GFP expressing tissue, the relative spatial vicinity of Pkr2 expressing axons and Pk2 secreting dermal tissue is striking.

A peripheral source of Pk2 in the target area of Pkr2 expressing motor and sensory axons raises the possibility that prokineticin ligand-receptor interactions could be employed in axon guidance, for instance by controlling the terminal ramification in the CM muscle or its overlaying skin, respectively. Consequently, *Pkr2* mutants should be explored for abnormalities in these processes.

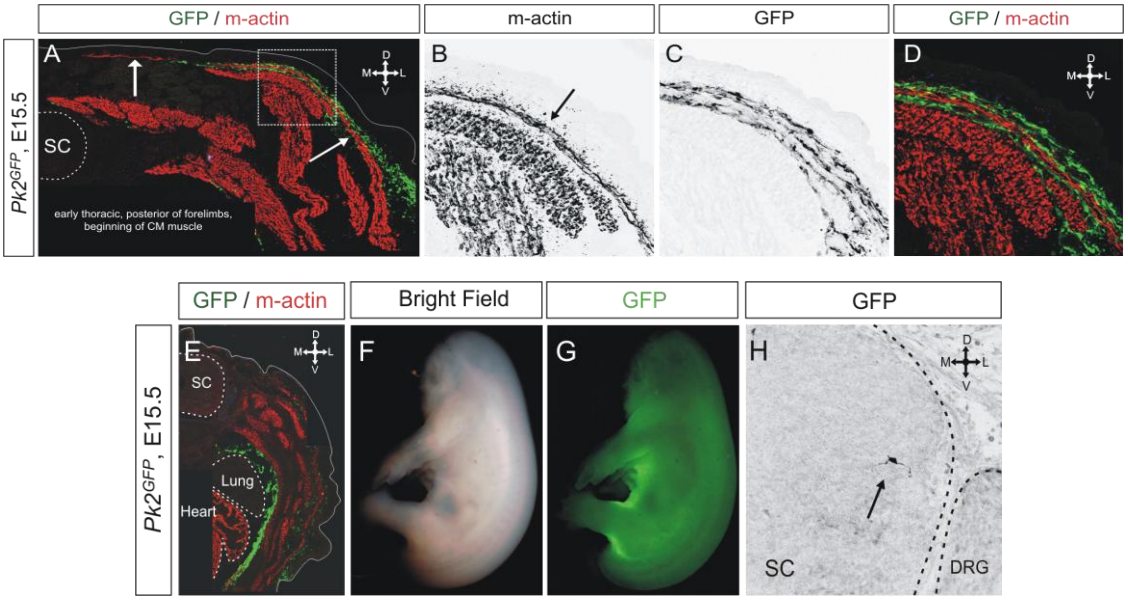

Figure 20: Potential central and peripheral sources of Pk2 for CM MNs

Pk2^{GFP} mice were analyzed for central and peripheral expression of Pk2 potentially interacting with Pkr2 expressing MNs. **A:** Transverse sections through embryonic trunks at E15.5 using antibodies against GFP to reveal potential sites of Pk2 expression and muscle-actin (m-actin) staining all limb muscles. The CM muscle can be identified by its typical location immediately directly underneath the skin (white arrows). **B-D:** Magnifications of the area indicated in (A), illustrates how the CM muscle (white arrows in A, black arrow in B) is embedded in dermal tissue expressing Pk2-GFP. The outmost layers of the skin do not appear to express Pk2-GFP. **E:** Pk2-GFP staining at thoracic levels reveals a distinct layer of cells lining inner side of the rib-cage. Weak Pk2-GFP signal can again be detected in superficial skin layers. **F-G:** Bright-field (F) and GFP channel (G) views of whole-mount E15.5 embryos. Pk2-GFP is relatively uniformly express in superficial layers of the skin spanning the trunk. Stronger Pk2-GFP signal is detected at the base of the limbs. **H:** An example of an interneuron expressing Pk2-GFP (black arrow) in the central grey matter of the cervical SC at E15.5.

4.2.2 Cloning of *Pkr2* mutant mice

None of the previously published *Pkr2* null mutants contain a reporter cassette and no reliable Pkr2 antibody is so far available to resolve endogenous translation and subcellular protein distribution. Therefore, we genetically engineered our own *Pkr2* loss of function allele, custom tailored to fulfill our needs.

The endogenous *Pkr2* locus consists of three exons, with the ATG being located in the second and the stop codon in the third exon. We disrupted the *Pkr2* locus by replacing the open reading frame in exon 2 with Cre recombinase cDNA followed by an internal ribosome entry site (IRES), allowing a nuclear LacZ reporter (NLZ) to be translated from the same mRNA (Figure 21, A). Depending on the experimental context mutant alleles will be abbreviated *Pkr2*^{NLZ} or *Pkr2*^{Cre}.

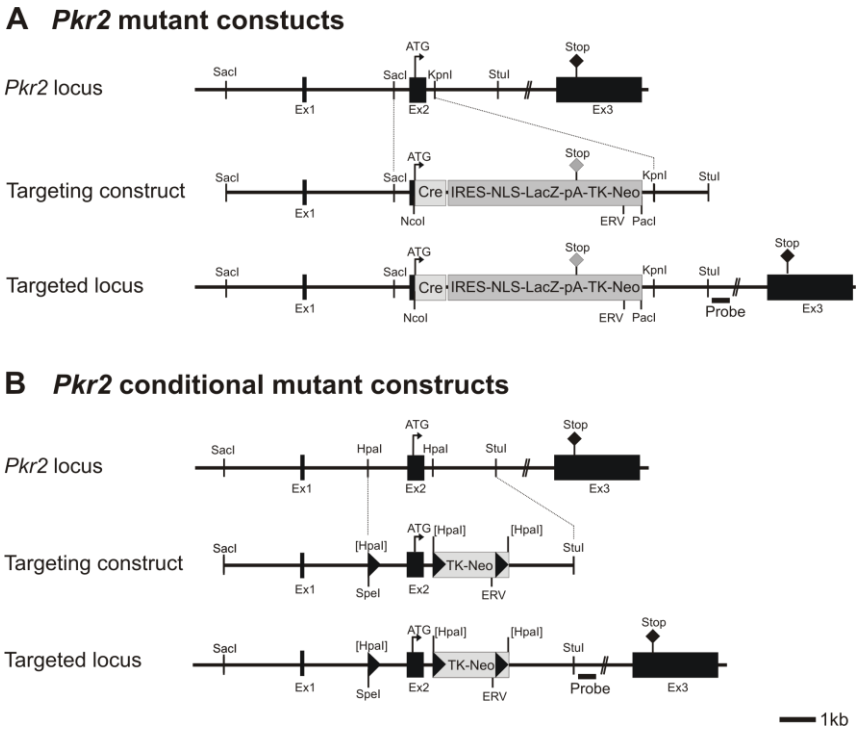

Figure 21: *Pkr2* mutant constructs

Diagrams show the cloning strategies for the generation of the *Pkr2* null and conditional mutant mice. **A:** To disrupt the *Pkr2* locus, Cre-IRES-NLS-LacZ-pA-TK-Neo targeting cassettes were integrated into NcoI site, which had been created by point mutations at the endogenous ATG start codon, and an artificially introduced PacI site ~100bps downstream of the end of Exon2 (Ex2). A 6.5 kb 5' region (SacI–NcoI) and a 2.4 kb 3' region (PacI–StuI) were used to generate the targeting construct into which the reporter and (Tk)-Neo resistance cassettes (gray) were integrated. The Southern probes used to screen for homologous recombination in ES cells consisted of a 270bp PCR fragment (solid black line at 3' StuI site) fragment located 3' to the region used for the generation of the targeting construct. Homologous integration at the targeted locus of homozygous and heterozygous $Pkr2^{NLZ}$ mutant mice was tested by Southern blotting using ERV restriction enzyme. **B:** To generate a floxed conditional *Pkr2* mutant allele, a floxP flanked TK-Neo targeting cassette was integrated into the HpaI site 3' of exon 2, and a floxP site containing an additional cloned SpeI site into the HpaI site 5' of Exon2. The same stretch of genomic DNA and the same Southern probe as in (A) was used for targeting of the endogenous *Pkr2* locus and validation of its correct insertion, respectively. 5' loxP sites were tested by SpeI restriction digests (wt: 15.2 vs. KO 9.5 kb) and of 3' floxed TK-Neo cassettes with ERV digests (wt: 19 vs. KO 12.4 kb). Brackets indicate blunt end ligations.

Cre expression from *Pkr2* locus was used in conjunction with a conditional GFP reporter line, expressing GFP and NLZ from the genomic *Tau* locus (*Tau-lox-STOP-lox-mGFP-IRES-NLS-LacZ-pA*) upon removal of a floxed transcriptional stop signal by Cre recombinase. In $Pkr2^{Cre}Tau^{GFP.IRES.NLZ}$ double heterozygous mice, all MNs normally expressing *Pkr2* at any time during development prior to the experimental time point should express GFP in the membrane of their cell bodies and processes, making it possible to identify muscles innervated by CM and LD MNs and to characterize the terminal arborization pattern of their axons. In addition, the use of a bicistronic cDNA should allow us to monitor the identity of Pkr2 expressing cells by staining for NLZ.

In order to discriminate between phenotypes caused by the loss of Pkr2 in sensory neurons from defects caused by its loss in MNs we also cloned a conditional *Pkr2* mutant allele. For this purpose the ATG harboring exon 2 of the genomic *Pkr2* locus was flanked by floxP sites, which permits disruption of *Pkr2* by Cre recombinase activity (Figure 21, B).

4.2.3 Differences in Pkr2-LacZ expression between *Pkr2* chimeras and heterozygous offspring

ES cell clones #10 and #92 carrying *Pkr2* mutant alleles were used to produce *Pkr2* chimeric mice. While chimeric pups from ES cell clone #92 were all born dead, chimeras from ES cell clone #10 were raised for breeding with wild-type females. Offspring from these matings yielded heterozygous $Pkr2^{+/NLZ}$ pups in F1 and homozygous $Pkr2^{NLZNLZ}$ in F2, both in Mendelian ratios. Unfortunately, SCs of $Pkr2^{+/NLZ}$ mice were completely devoid of LacZ signal while Pkr2-LacZ signals of dead born #92 chimera pups reliably reflected *Pkr2 in situ* hybridization patterns (compare Figure 22, A and B with Figure 7, B). Total loss of LacZ signal was restricted to the SC. In other parts of the CNS and in DRG sensory neurons Pkr2-LacZ expression was detected in the expected cell types, however not in the expected abundance. For instance in DRG sensory neurons Pkr2-LacZ expression was still specific to peptidergic sensory neurons, but compared to our *in situ* hybridization or immunocytochemistry results of clone #92 *Pkr2* chimera pups, the number of Pkr2-LacZ positive neurons was greatly reduced (Figure 22, compare F with G and H).

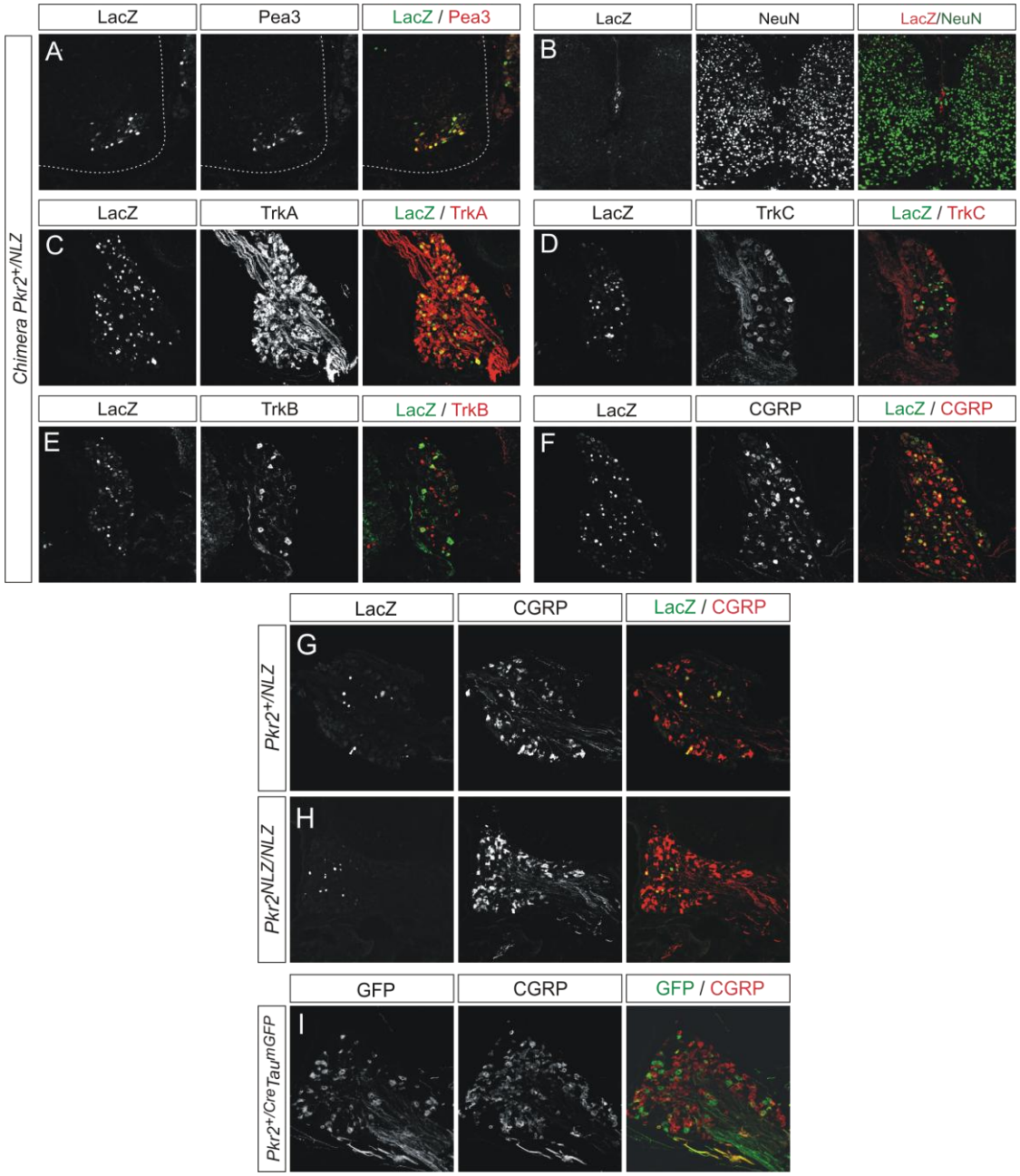

Figure 22: Pkr2-LacZ reflects the endogenous Pkr2 expression pattern in chimeras

Analysis of Pkr2-LacZ expression patterns in Pkr2 chimera pups **A:** Pkr2-LacZ immunoreactivity colocalized with Pea3 signal in CM MNs at cervical levels of the SC. **B:** In accordance with *in situ* hybridization data Pkr2-LacZ was also detected in a population of NeuN negative cells located around the central canal. **C-F:** Pkr2-LaZ expression is restricted to peptidergic subpopulation of TrkA positive DRG sensory neurons, marked by antibodies against CGRP. **G-H:** In *Pkr2*^{NLZ} heterozygous (F1) and homozygous mutants (F2) the number of LacZ expressing DRG sensory neurons was strongly reduced, but association with the CGRP expressing peptidergic subpopulation of sensory neurons remained intact. **I:** In contrast, Pkr2-Cre induced activation of Tau-mGFP is not restricted to the peptidergic subpopulation of DRG sensory neurons, suggesting broader Cre recombinase activity at earlier developmental stages.

It is not unusual that mice expressing LacZ from bicistronic mRNAs using IRES exhibit incomplete LacZ expression patterns. What is atypical in our *Pkr2* mutants is that Pkr2-LacZ stainings in chimera pups reflected the anticipated Pkr2 expression pattern perfectly, but not heterozygous offspring of the following generations. Either

chimera clones #10 and #92 were genetically not identical or epigenetic events disturbed parts of the regulatory elements controlling *Pkr2* transcription in chimera offspring. Two additional attempts to remake *Pkr2* chimeras from ES cell clone #92 and other positive clones failed. Altogether, it remains unclear how the observed discrepancies in Pkr2 expression patterns arose.

4.2.4 Analysis of *Pkr2* mutant mice

4.2.4.1 Validation of loss of Pkr2 function

Homologous recombination at the *Pkr2* genetic locus was confirmed by Southern Blotting and PCR on genomic DNA (data not shown). In addition, homozygous $Pkr2^{NLZ}$ mice were examined for phenotypes previously described in the literature. As expected loss of Pkr2 signaling led to abnormalities in OB development including disruption of OB layer formation (Ng et al., 2005; Matsumoto et al., 2006; Prosser et al., 2007b) (Figure 23). Significant increase in early postnatal mortality, reduced size and body weight and atrophic formation of sexual organs in females and males causing infertility (reviewed by Negri et al., 2007) were also observed. The complete consistency of Pkr2 phenotypes described by others with observations from our own *Pkr2* null mutants provided concrete evidence for the functional elimination of Pkr2 protein, despite inconsistencies in Pkr2-LacZ expression patterns.

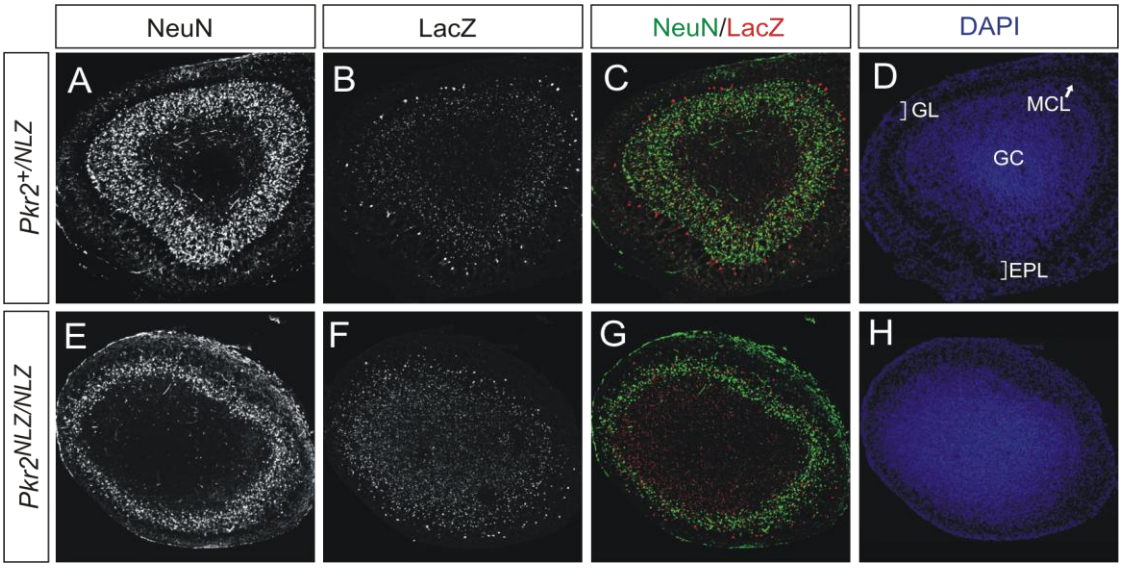

Figure 23: Loss of Pkr2 causes abnormalities in the architecture of OB layers

Coronal sections of OBs from homozygous *Pkr2*^{NLZ} and heterozygous P3 littermates **A-D:** OBs of heterozygous pups display typical features of OB architecture, including a high density central area containing granule cells (GC), a low density external plexiform layer (EPL) and a peripheral glomerular layer (GL). **E-H:** OBs of *Pkr2* mutant mice are characterized by a complete absence of a discernable glomerular layer, mitral cell layer (MCL) and inner plexiform layer. OBs appear to be composed of an extensive GC layer and an EPL (Prosser et al., 2007a).

4.2.4.2 Assessment of motor neuron pool organization in *Pkr2* mutants

CM MN pool position and the morphological characteristics of its dendritic tree were compared between homozygous *Pkr2* mutants, littermate controls and previously collected data from *Pea3* mutant mice. The relative position of Pkr2 expressing MN pools was determined by staining for Pea3. Isl1 was used as a marker of the LMC_m and choline acetyltransferase (ChAT) to display the position of the ensemble of MNs. No difference between control and *Pkr2* mutant animals could be detected (Figure 24). To investigate the morphologies of dendritic trees, CM MNs were retrogradely labeled at P1 using dextran-rhodamine. While loss of Pea3 causes pronounced changes in the receptive field of CM dendrites (Vrieseling and Arber, 2006), genetic elimination of Pkr2 did not result in significant changes in the morphology of dendritic arborizations (Compare Figure 24 I, J and K).

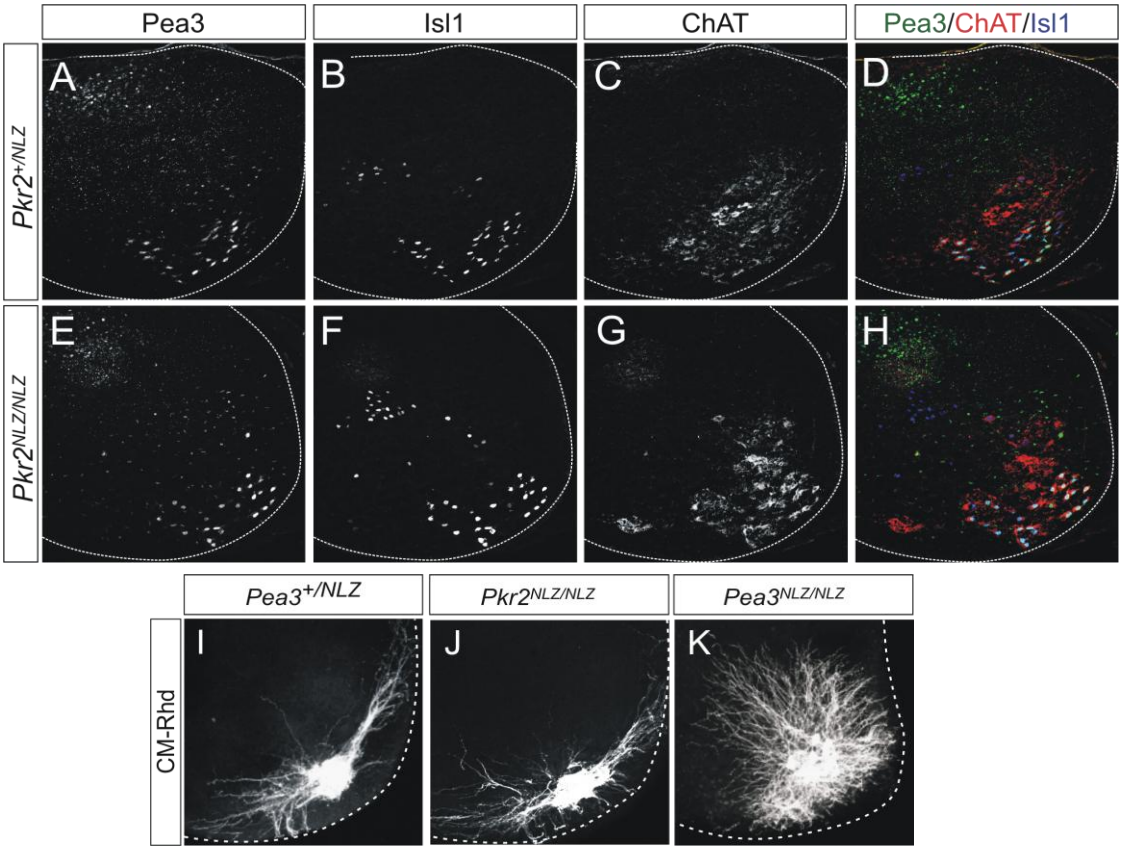

Figure 24: Anatomical organization of cervical MN pools and dendritic arborization of CM MNs in *Pkr2*$^{NLZ/NLZ}$

The settling position of CM MNs was assessed using Pea3 antibody stainings in combination with Isl1 marking the LMC_m and ChAT immunoreactivity marking cholinergic MNs. **A-D:** At rostral levels of the CM MN pool (~C7) virtually all Pea3 positive MNs coexpress Isl1. Dorsally located Isl1-negative MNs of the LCM_l include Tric and Pec-Maj MNs. **E-H:** Unlike loss of Pea3 (Figure 6A), loss of Pkr2 signaling does not cause apparent changes in the settling positions of $Pea3^+$ and $ChAT^+$ MNs. **I-K:** Dendritic arborizations of CM MNs in wild-type (I), *Pkr2* mutant (J) and *Pea3* mutant mice (K) were revealed by retrograde labeling from CM muscle nerves. In *Pea3*$^{NLZ/NLZ}$ mice only the lateral branch was used for retrograde labeling. CM typical bundles of dendrites avoiding the central grey matter are evident in *Pkr2* mutant mice, indicating that Pkr2 is not a downstream target of Pea3 controlling dendritic arborization. (I) and (K) are a courtesy of Eline Pecho Vrieseling.

Taken together, these results argue against the hypothesized potential role of Pkr2 in neuronal cell migration or an influence of prokineticin signaling on the morphology of dendritic trees in CM MNs and these processes must therefore be mediated by other downstream targets of Pea3.

4.2.4.3 Evaluation of CM and LD muscle innervation

In wild-type mice, LD and CM muscle are innervated by Pea3 expressing MNs and genetic elimination of Pea3 leads to compromised axonal penetration and arborization in both muscles (Figure 6, C for CM) (Livet et al., 2002). Developmental expression of Pk2 in the peripheral target area of CM MNs at developmental periods of limb

innervation raises the possibility of an interaction between Pkr2 expressing motor axons and secreted Pk2. Therefore, we explored the innervation of CM and LD muscles and their terminal branching patterns in homozygous *Pkr2* mutants and heterozygous controls. Originally, we meant to exploit $Pkr2^{Cre}Tau^{GFP.IRES.NLZ}$ reporter crosses for this purpose, but similar to the lack of Pkr2-LacZ expression in SCs, Pkr2-Cre induced recombination did not yield the expected Tau-mGFP expression pattern at cervical levels (data not shown). Instead, we crossed $Pkr2^{NLZ}$ mutants with $Hb9^{mGFP}$ transgenic mice, offspring of which ($Pkr2^{NLZ}Hb9^{mGFP}$) permitted the analysis of whole-mount dissected CM and LD muscle innervation patterns using GFP.

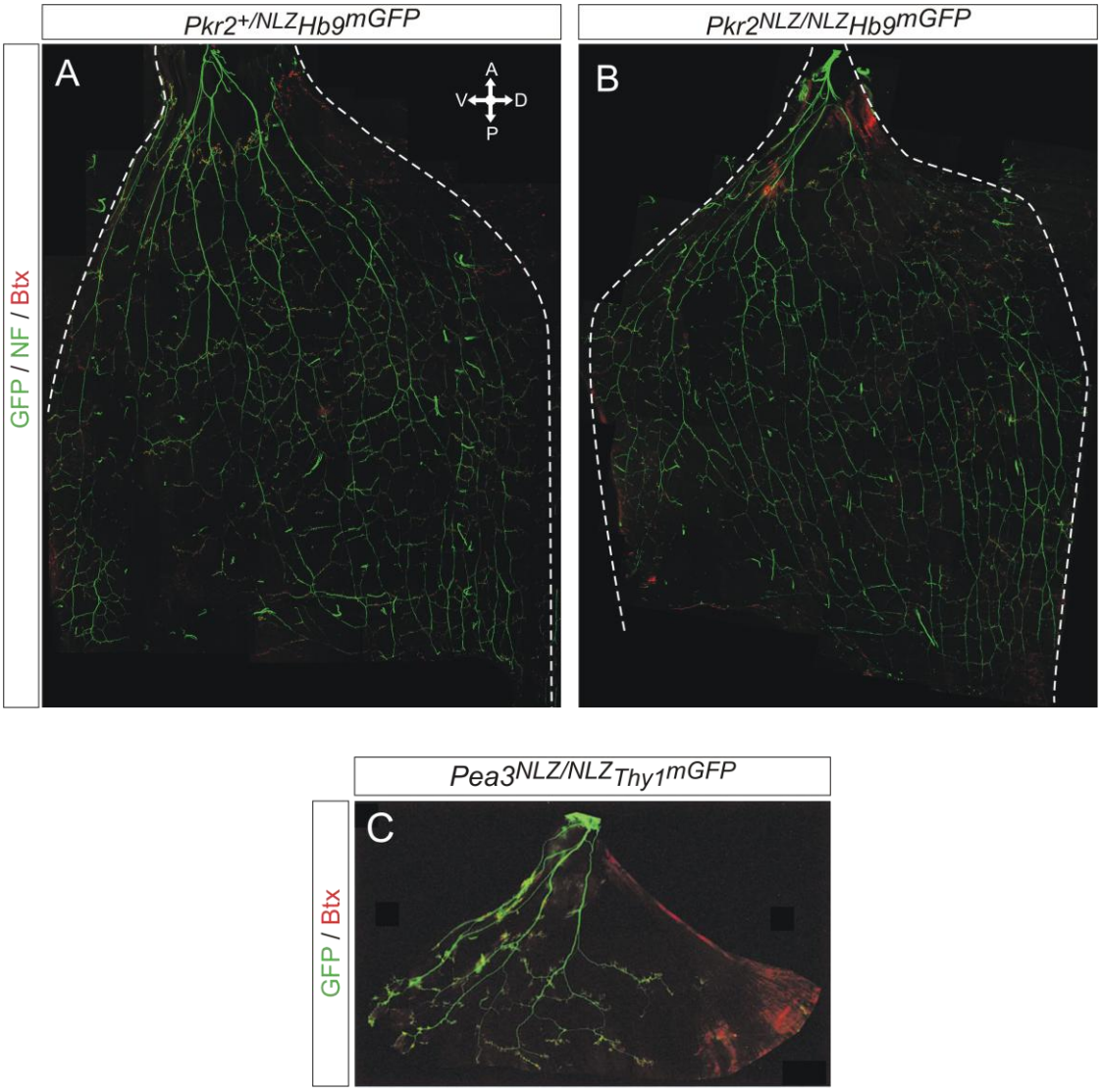

Figure 25: Loss of Pkr2 causes no apparent defects in CM innervation patterns

Analysis of terminal branching and neuromuscular endplate patterns of CM motor axons in $Pkr2^{+/NLZ}$ and $Pkr2^{NLZ/NLZ}$ CM muscles at P1. To visualize motor axons, animals were crossed with $Hb9^{mGFP}$ transgenic mice and additionally stained

with neurofilament-H antibodies. Neuromuscular junctions are revealed by Btx-rhodamin. **A-B:** The axonal branching and neuromuscular endplate pattern in CM muscles of *Pkr2* mutants (B, n=2) is not significantly different from heterozygous controls (A, n=2). **C:** For comparison the top part of the CM innervation pattern in *Pea3* mutants (P14) is shown. Adapted from Livet et al. (2002).

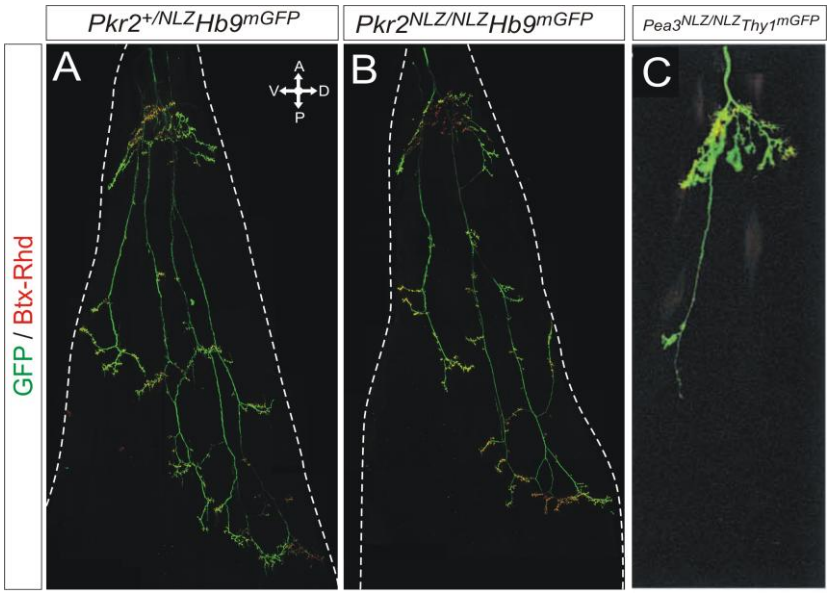

Figure 26: Loss of Pkr2 causes no apparent defects in LD innervation patterns

Analysis of terminal branching and neuromuscular endplate patterns of LD motor axons in *Pkr2*$^{+/NLZ}$ and *Pkr2*$^{NLZ/NLZ}$ LD muscles at P1. To visualize motor axons, animals were crossed with *Hb9*^{mGFP} transgenic mice. Neuromuscular junctions are displayed by Btx-rhodamine staining. **A-B:** The overall innervation and neuromuscular endplate pattern of the LD muscle appears unaffected in *Pkr2*$^{NLZ/NLZ}$ (n=2) when compared to controls (n=2). **C:** For comparison the LD innervation patter of *Pea3* mutant mice in conjunction with Thy1 driven reporter GFP (P14, adapted from Livet et al., 2002) is shown.

To reveal the overall patterns of axonal arborization and NMJs, bungarotoxin (Btx) was used in combination with antibodies to GFP and neurofilament H (NF) at P1 and P14. In *Pkr2* mutants, neither CM (Figure 25, B) nor LD muscles (Figure 26, B) (n=2 each) exhibited significant differences in their innervation and NMJ patterns as compared to controls (n=2 each) (Figures 25, A and 26, A). The lack of a phenotypical manifestation thus strongly argues against a critical role of Pkr2 in axon guidance in spinal MNs despite the spatial and temporal apposition of receptor and ligand.

4.2.4.4 Assessment sensory-motor connectivity in *Pkr2* mutant mice

At cervical levels loss of Pea3 leads to drastic changes in Ia proprioceptive afferent selectivity in that CM MNs receive monosynaptic sensory input from non-homonymous muscles (Vrieseling and Arber, 2006). As described above, recent findings form our lab provide strong evidence that Sema3e, which is specifically

expressed by CM MNs, acts as a repellent on proprioceptive sensory terminals, causing them to avoid most ventral areas of the SC harboring CM MNs (Eline Pecho-Vrieseling et al., unpublished data). However, despite these compelling new findings, a number of aspects regarding sensory-motor connectivity remain unclear and the currently emerging model suggests also molecules other than Sema3e to be involved in the control of selective sensory-motor synapse formation.

Therefore, we sought to explore the influence of Pkr2 on anatomical organization of Ia proprioceptive afferent ingrowth pattern at segmental levels of the CM MN pool. Since in wild-type mice the absence of monosynaptic proprioceptive input to CM MNs is reflected by a lack of vesicular glutamate transporter vGlut1 positive sensory terminals on CM MNs, we used the distribution of vGlut1 patterns to assess the effect of genetic Pkr2 elimination. Cervical SCs were sampled from C6 to T1 and the relative fraction of the total area occupied by MNs, revealed by ChAT staining, contacted by vGlut1 positive proprioceptive sensory neurons was calculated. Our quantification did not reveal significant differences between *Pkr2* mutant mice (n=3) and controls (n=3) (Figure 27) and we conclude that, unlike Sema3e, Pkr2 exerts no distinguishable influence on Ia proprioceptive afferent terminals or the formation of monosynaptic sensory-motor contacts with CM MNs.

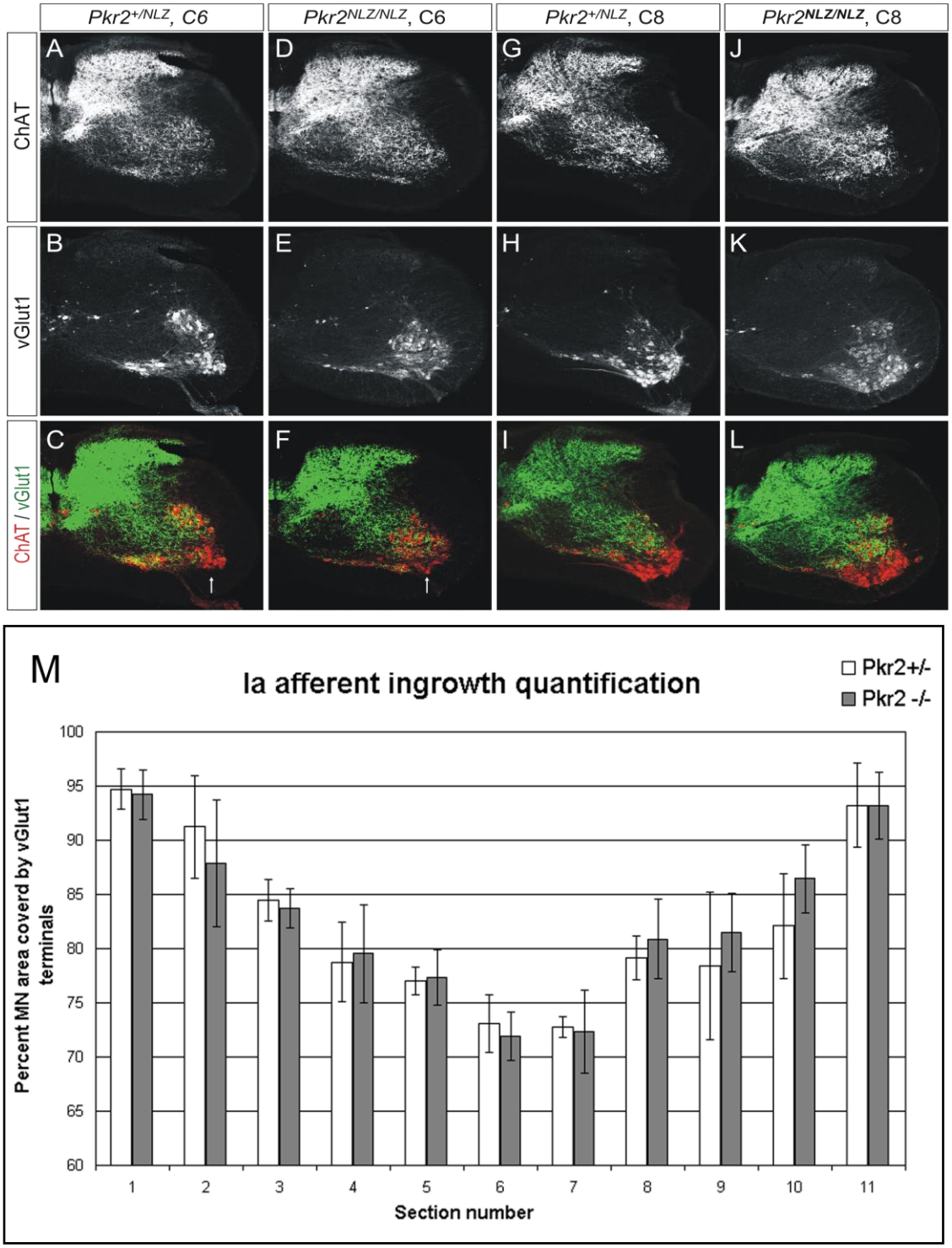

Figure 27: Loss of Pkr2 causes no gross defects in group Ia afferent projection patterns

At P14, ingrowth of group Ia proprioceptive afferents was assessed by comparing the distributions of Ia proprioceptive terminals, using antibodies to vGlut1, relative to the ensemble of MNs, using antibodies to ChAT. **A-F:** At C6 levels of the SC most MNs are covered by vGlut1 terminals. The beginning of the CM motor pools can be identified by the absence of Ia afferent terminals synaptic contacts on ventral MNs (white arrow in C and F). Similar patterns were found in *Pkr2*$^{+/NLZ}$ (n=3, A-C) and *Pkr2*$^{NLZ/NLZ}$ animals (n=3, D-F). Slight differences in shape and cell number are artifacts of section processing and/or imperfect level matching. **G-L:** At C8 levels of the SC, CM MNs devoid of vGlut1 terminals have reached their maximal extension and occupy a significant fraction of the ventral horn. No apparent differences between *Pkr2*$^{+/NLZ}$ and *Pkr2*$^{NLZ/NLZ}$ animals were found. **M:** Quantification of percent vGlut1 coverage of the total area occupied by MNs from C6 (Section 1) to T1 (Section 11). *Pkr2* homozygous (n=3) and heterozygous mutants (n=3) were not significantly different.

Considering Pkr2's published range of biological functions, a role of Pkr2 in Ia proprioceptive afferent connectivity would have required the existence of additional modes of actions. However, since in other developing neuronal systems activity is a crucial factor contributing to the refinement of synaptic connectivity it remains a possibility that loss of Pkr2 affects other components of the spinal motor circuitry.

4.2.4.5 Assessment of central and peripheral innervation patterns of Pkr2 expressing peptidergic sensory neurons

During embryonic development, Pk2 is expressed in dermal layers of the skin, where somatosensory neurons branch and form peripheral receptive terminals (Figure 20, A-D). This finding raised the question of whether during embryogenesis Pkr2 expressing peptidergic sensory neurons use Pk2 gradients as chemoattractant guidance cues to reach and ramify in the skin. While defects in pain perception through prokineticin signaling has been documented extensively (Negri et al., 2002; Hu et al., 2006; Negri et al., 2006; Vellani et al., 2006), a developmental component involving chemotactic Pk2/Pkr2 interactions for sensory axon guidance had not been considered. To verify this hypothesis we had intended to map skin innervation patterns using $Pkr2^{Cre}Tau^{mGFP.IRES.NLZ}$ mice, but, unfortunately, early developmental Cre activity led to additional Tau-mGFP signal in non-peptidergic neurons, making this line uninformative (Figure 22, I). Instead, we had to resort to $Pkr2^{NLZ}Isl^{Cre}Tau^{mGFP}$ mice, in which Cre and consequently Tau-mGFP is expressed in all DRG sensory neurons.

For our analysis $Pkr2^{NLZ/NLZ}Isl1^{Cre}Tau^{mGFP.IRES.NLZ}$ mice were sacrificed at E16.5 and compared to littermates heterozygous for Pkr2-NLZ. Neither cross-sections at predefined position of thoracic skin (Figure 28, G, H) nor horizontal whole-mount preparations (Figure 28, A-F) revealed any distinguishable difference in skin innervations patterns between the two genotypes. Taken together, these results suggest

that Pkr2 is not required for sensory or motor axon guidance and terminal arborization at these peripheral targets.

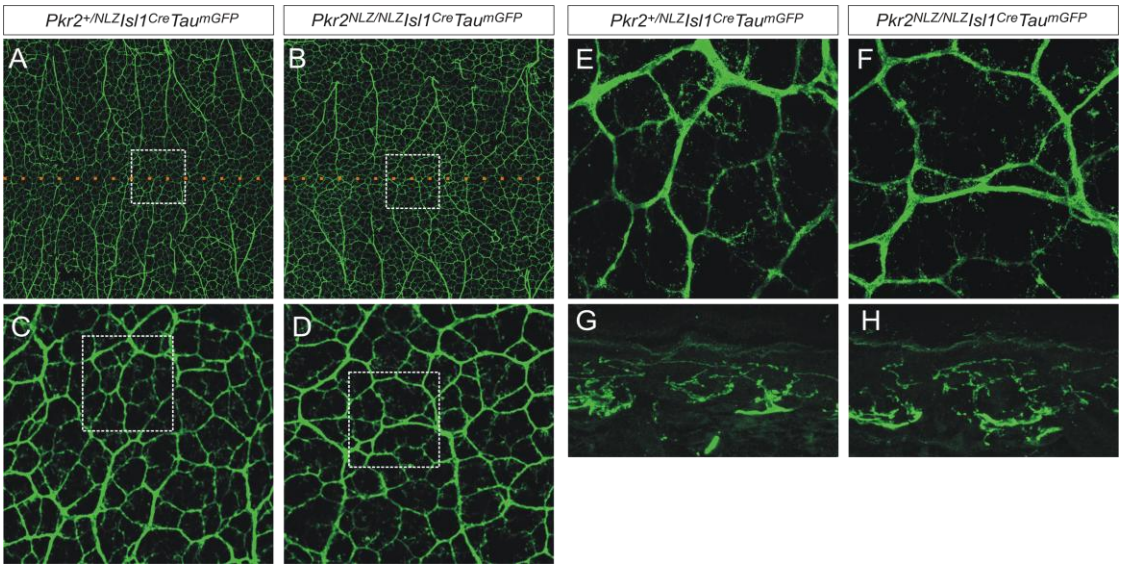

Figure 28. Loss of Pkr2 causes no abnormalities in skin innervation patterns

Sensory afferent projection pattern in dorsal skin were analyzed at different magnifications in whole mount preparations at E16.5 (A-F) and thoracic cross sections of the skin at P6 (G-H). **A-B:** Comparison of whole mount skin innervation between *Pkr2* heterozygous and homozygous E16.5 $Pkr2^{NLZ}Isl1^{Cre}Tau^{mGFP}$ embryos revealed no gross structural abnormalities in mutant genotypes. The dorsal midline is indicated by orange doted lines (A, B). **C-D:** Magnifications of the areas indicated by white boxes (A,B) reveal morphological details of the terminal innervation pattern at the dorsal midline (C,D), but no significant differences can be detected. **E-F:** High resolution imaging of the areas indicated in (C) and (D) allows analysis of skin innervation patterns at single axon resolution. Yet, no differences in innervation density or other morphological characteristics could be detected. **G-H:** Skin cross sections of P6 $Pkr2^{NLZ}$ pups of both phenotypes were labeled using antibodies against PGP9.5 at high magnification. No apparent abnormalities in the innervation pattern could be detected in *Pkr2* mutants (H) relative to controls (G).

We also analyzed whether loss of Pkr2 impacts on the establishment of the central laminar terminations of sensory afferents. In the SC, CGRP staining was used to specifically label the peptidergic subpopulation of sensory neurons, which includes the Pkr2 expressing subpopulation (Figure 22, G, H). As an independent marker for dorso-ventral position in the dorsal SC an antibody to ladybird homeobox homolog 1 (Lbx1) transcription factor was applied to reveal deep layer dorsal horn interneurons (Figure 29, B, F) (Muller et al., 2002). In agreement with previous observations (Snider and McMahon, 1998), we found that in wild-type the great majority of TrkA sensory afferents terminated in Lbx1-negative superficial layers of the dorsal horn and within this population peptidergic afferent terminals were further restricted to the outer part of the $TrkA^{+}$ $Lbx1^{-}$ dorsal layer I (Figure 29, D). To compare the terminal innervation

patterns of *Pkr2*$^{NLZ/NLZ}$ with heterozygous controls, cross-sections of P1 SCs were level matched using cervical Pea3 MN pools as a rostrocaudal marker. However, no significant differences in the establishment of laminar termination were detected between *Pkr2* mutants (Figure 29) and heterozygous littermates.

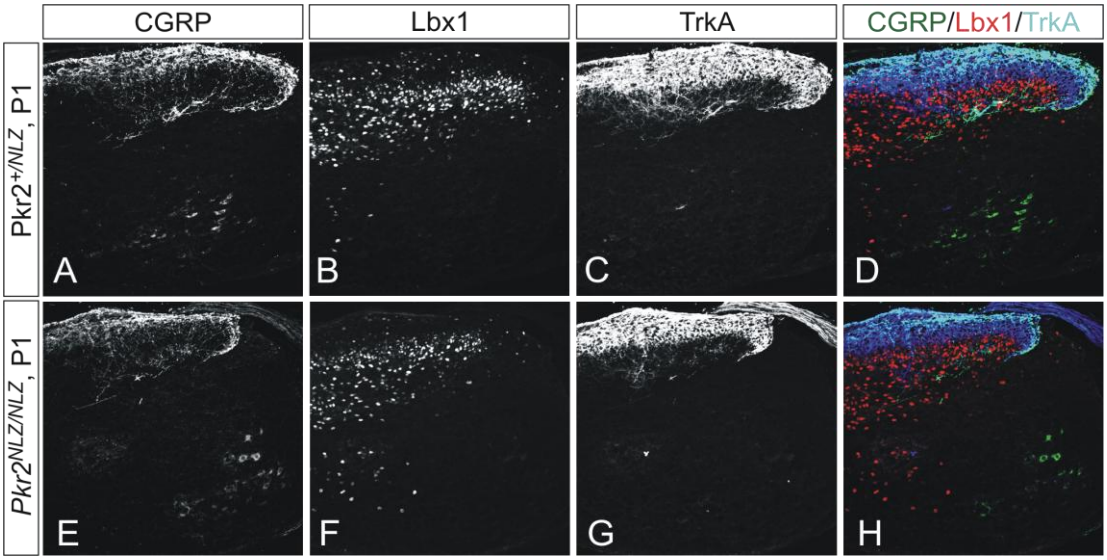

Figure 29: Assessment of laminar termination of peptidergic sensory neurons in the SC

Analysis of laminar termination of DRG sensory afferents at cervical levels of the SC **A-D:** Dorso-ventral extent of laminar terminations of heterozygous controls was revealed by immunocytochemistry to CGRP, Lbx1 and TrkA. **E-H:** In *Pkr2* mutant mice, CGRP sensory afferents do not exhibit significant changes in their central termination pattern relative to TrkA and Lbx1.

Taken together these results provide strong evidence that the suggested peripheral Pk2/Pkr2 interactions are neither necessary for skin innervation nor for appropriate central termination and it is therefore unlikely that changes in sensory afferent innervation patterns contribute to pain perception defects in *Pkr2* mutants (Negri et al.; 2007). Instead, the documented perturbations of pain perception and tactile sensitization in *Pkr2* mutants are probably solely generated by the deregulation of members of the family of transient receptor potential channels in DRG as has been described for Pkr1 (Negri et al., 2006) and suggested for Pkr2 signaling (Negri et al., 2007).

4.2.4.6 Pkr2 expression in the gustatory system

While a number of studies have contributed to significant insights about the role of Pkr1 and Pkr2 in nociception (Negri et al., 2002; Hu et al., 2006; Negri et al., 2006; Vellani et al., 2006), no studies have explored expression and functional relevance of Pkr2 in primary gustatory afferents of taste neurons, which directly contact taste buds in the tongue. Taste signals from the tongue are conducted centrally by neurons located in two different ganglia. When taste stimuli are presented to fungiform type papillae on the anterior two thirds of the tongue, the signal is propagated through the chorda tympani nerve to the NTS by taste neurons of the geniculate ganglion. Similarly, if taste stimuli are presented to circumvallate papillae on the posterior third of the tongue, the signal is propagated by taste neurons of petrosal ganglia which project through the glossopharyngeal nerve (branch of cranial nerve IX) and also terminates in the NTS. Since previous studies have only addressed the roles of prokineticin signaling on appetite by investigating distinct nuclei in the CNS using adult mice (Negri et al., 2004), we sought to explore if loss of Pkr2 from developing primary gustatory afferents could possibly cause defects in the developmental innervation of taste buds.

First evidence for Pkr2 expression in taste neurons came from examinations of embryonic brainstems sections that included adjacent facial nerve ganglia in $Pkr2^{Cre}Tau^{mGFP}$ mice where we observed ganglionic sensory neurons to express reporter GFP (not shown). Moreover, *Pkr2* BAC transgenic mice have most recently become available by GENSAT and the sample of online published Pkr2-mGFP bright field images (www.gensat.org) provided additional evidence that Pkr2-GFP could be expressed in taste buds themselves or, if not, at least in axons innervating taste buds (Figure 30, G, H).

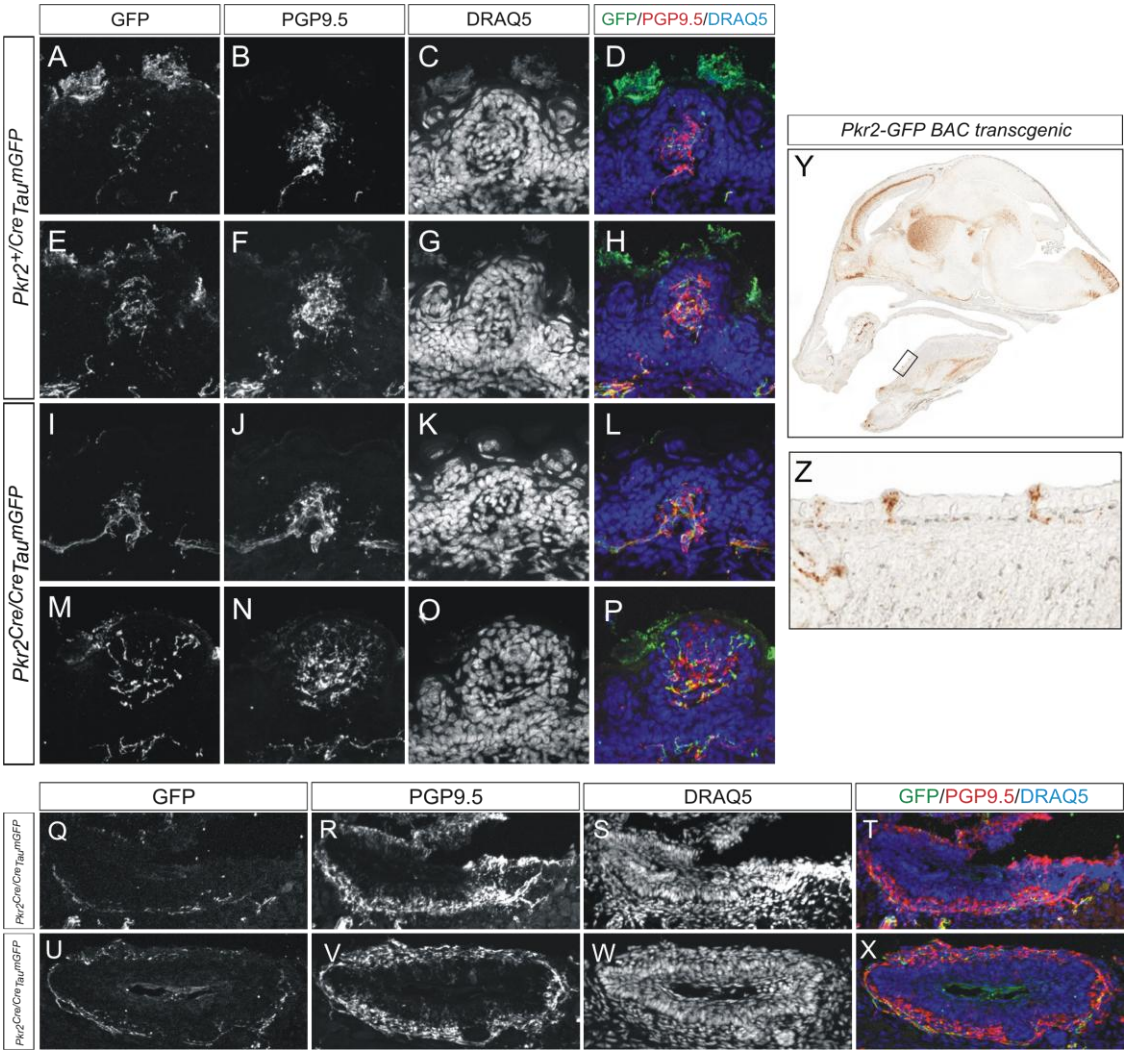

Figure 30: Analysis of Pkr2 expression in the gustatory system

Analysis of primary gustatory nerve terminals in fungiform and circumvallate taste buds. The ensemble of neuronal terminals was revealed by immunocytochemistry to the pan-neuronal marker PGP9.5; Pkr2-Cre induced Tau-mGFP signal was amplified by anti GFP antibodies. DRAQ5 was used to label the nuclei of all cell bodies. **A-D, E-H, Q-T:** Examples of fungiform (A-H) and circumvallate (Q-T) papillae innervated by *Pkr2*$^{+/Cre}$*Tau*^{mGFP} taste neurons. Comparison of GFP with PGP9.5 immunoreactivity indicates that only a subpopulation of taste neurons express Pkr2. **I-L, M-P, U-X:** Despite individual variations, the overall innervation pattern of taste buds in *Pkr2* mutant mice appeared indistinguishable from heterozygous littermates. **Y:** Bright-field GFP signal from *Pkr2*^{GFP} transgenic mice at E15.5 (adapted from www.gensat.org) reveals Pkr2-GFP signal in fungiform taste buds and a number of unidentified cells (or nerve bundles) at the base of the tongue. **Z:** A higher magnification of the inset indicated in G showing fungiform taste buds labeled by Pkr2-GFP.

We attempted to first establish if Pkr2 is actually expressed in taste receptor cells themselves or in gustatory afferents conveying the gustatory signals centrally. We focused our examination on two types of prominent and easily accessible types of papillae: fungiform taste papillae and circumvallate taste papillae. Pkr2 expression was tested by *in situ* hybridization and immunohistochemistry using *Pkr2* antisense probes and Pkr2-NLZ antibody stainings, respectively. Two embryonic (E12.5, E15.5) and two

postnatal developmental time points (P14, adult) were tested but *Pkr2* signal was not detected in any type of taste papillae (data not shown).

In a next step, we investigated the occurrence of primary gustatory nerve terminals in fungiform and circumvallate taste buds in *Pkr2* mutant and control, using genetic crosses with the conditional $Tau^{mGFP.IRES.NLZ}$ reporter strain. The ensemble of neuronal terminals, including somatosensory (through facial nerve V), was revealed by antibody stainings to the pan-neuronal marker PGP9.5. Despite documented discrepancies between *Pkr2 in situ* patterns and LacZ/GFP reporter signals in DRG sensory neurons of $Pkr2^{+/Cre}Tau^{mGFP.IRES.NLZ}$ mice (Figure 22), we still made use of these constructs to investigate possible defects in taste bud innervations by tracing GFP^+ axons. Lastly, in order to visualize the morphology of the tongue endothelium we used DRAQ5, labeling the nuclei of all cells. Despite individual variations, the overall innervation pattern of fungiform and circumvallate taste buds in *Pkr2* mutant mice appeared indistinguishable from heterozygous littermates (Figure 30, A-F). Interestingly, comparison of GFP and PGP9.5 patterns indicated that only a subpopulation of all taste neurons express Pkr2.

4.2.5 Pkr2 is expressed in ischiocavernousus MNs controlling erection

In situ hybridization experiments using embryonic and early postnatal SC revealed virtually complete overlap between *Pkr2* and *Pea3* not only at cervical but also at lumbosacral segmental levels (not shown). Previous investigations in our laboratory (Eline Vrieseling et al., unpublished observations), identified these $Pea3^+$ MNs to project to the sexually dimorphic ischiocavernousus (IC) muscle which supports penile erection (Wagner and Clemens, 1989; Tang et al., 1998).

While at cervical levels GFP/LacZ signals from $Pkr2^{+/Cre}Tau^{mGFP.IRES.NLZ}$ mice only incompletely reflect Pea3 expression (not shown), immunocytochemistry on lumbar SC

sections demonstrate a virtually complete overlap between Pea3 and LacZ (Figure 31, B-E). Retrograde labeling from the IC muscle nerve labels MNs at strikingly similar positions in the SC, emphasizing the selective expression of Pea3 and Pkr2 expression in IC MNs (Figure 31, A). Potential implications of these findings, especially with respect to a potential function of Pkr2 in the regulation of cellular excitability, will be discussed below.

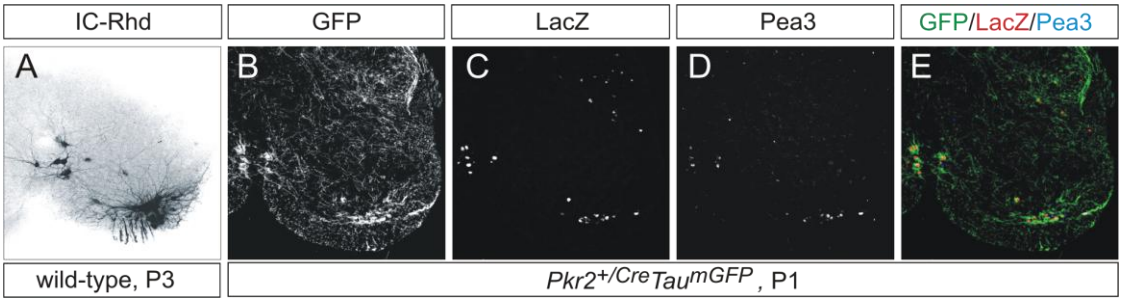

Figure 31: Pkr2 expression in sexually dimorphic MNs

A: Retrograde labeling from the Ischiocavernousus muscle (IC) nerve reveals the position of its MNs in the lumbosacral SC. Note the typical separation of the MN pool into two separate groups: a smaller cluster is located at the ventral midline while a larger cohort is found at the ventral border of the grey matter. This image is a courtesy of Eline Pecho-Vrieseling who performed the backfill. **B-E:** In P1 *Pkr2*^{Cre}*Tau*$^{mGFP.IRES.NLZ}$ pups combination of immunocytochemistry directed at LacZ/GFP and Pea3 revealed colocalization of Pea3 expressing MNs with Pkr2 driven reporters. The distribution of Pea3/LacZ double positive MNs was strikingly similar to the pattern observed by retrograde labeling from the IC nerve (A).

4.2.6 Additional sites of Pkr2 expression

Extensive literature has documented prokineticin signaling to be involved in a number of processes outside the nervous system, including angiogenesis (LeCouter et al., 2003), cell proliferation (Koyama et al., 2006) and hematopoetic cell mobilization in inflammation (LeCouter et al., 2004; Martucci et al., 2006; Shojaei et al., 2007). Pk2 and Pk1 have both been described to act as a tissue specific angiogenic factor in endocrine organs, ovaries and testis, where Pkr2 is expressed in endothelial cells, but not muscle or skin (Ferrara et al., 2004).

Here, we report the developmental expression of Pkr2 by X-Gal stainings in tissue where it had previously not been described. First, β-galactosidase activity from the *Pkr2*^{NLZ} locus was detected in hair follicles around the snout and nose (Figure 32, C, D) and the skin covering the skull (not shown). Second, β-galactosidase expression was

detected in developing forepaws (Figure 32, A, B) and hindpaws (data not shown), where at the same developmental stage Pk2 was expressed in a similar patterns (data not shown). Our preliminary gross examinations on the extent of the expression and overall morphological appearance of paws and follicles were not indicative for any anatomical defects caused by the lack of Pkr2. The increased X-Gal signal intensity in *Pkr2*^{NLZ} homozygous mice is attributed to the fact that they carry two copies of LacZ.

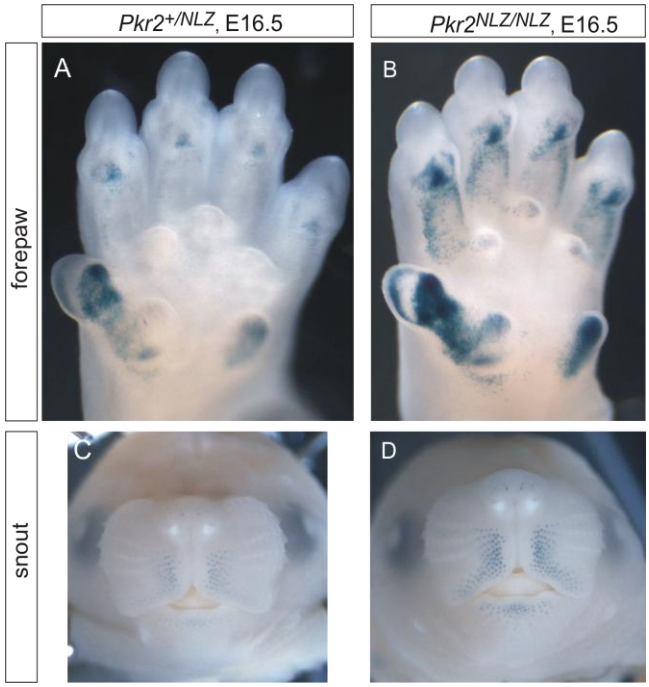

Figure 33: Pkr2 β-galactosidase activity is detected in digits and in hair follicles around the snout and nose

X-Gal/β-galactosidase stainings were performed on E16.5 *Pkr2*^{NLZ} homozygous and heterozygous embryos to investigate additional sites of Pkr2 expression. **A-B:** Pkr2-β-galactosidase activity was detected in developing digits of the forepaw. Although expression was stronger in homozygous mutants, the relative distribution of blue reaction precipitate and the general morphology of the paws did not appear significantly different between the two genotypes. **C-D:** β-galactosidase activity was also detected in subpopulations of hair follicles around the snout and the nose.

4.3 Discussion

4.3.1 Pkr2 does not play an apparent role in motor circuit assembly

Given the broad spectrum of biological processes essentially depending on Pkr2 signaling in the CNS and the occurrence of pronounced phenotypes in almost all neuronal systems where loss of function phenotypes have been investigated, we were

confident to unravel a functional importance of Pkr2 in spinal MNs. As a downstream target of Pea3, we sought to establish if loss of Pkr2 is sufficient to reproduce distinct aspects of phenotypes observed in *Pea3* mutant mice or causes new, yet undescribed phenotypes. Indications suggesting a role of Pkr2 in axon guidance arose from the detection of Pk2 in the axonal target area of both, Pkr2 expressing CM MNs and peptidergic sensory neurons and these findings additionally encouraged us to explore peripheral innervation patterns.

A critical point for the investigation of potential *Pkr2* mutant phenotypes is the time point of induction in the SC. If Pkr2 is not induced immediately after the onset of Pea3, it is actually unlikely to play important roles in MN migration or pool assembly which are processes that by E14, when *Pkr2 in situ* signals were first detected, have virtually reached completion. Similarly, motor axons begin to penetrate the CM muscle by E12-E13 and by E14 CM axons reach down to the caudal most muscle fibers and begin to ramify laterally (data not shown). Pea3 dependent processes of primary axon pathfinding and initial muscle penetration are therefore unlikely to be controlled by Pkr2. Peripheral Pk2/Pkr2 interactions could, however, control later aspects such as axonal fine-branching or the integrity and completeness of muscle innervation.

Considering Pkr2's published range of biological functions, a role of Pkr2 in Ia proprioceptive afferent connectivity with CM MNs would have required the existence of Pkr2 mediated modes of actions beyond chemoattraction or modulation of cellular excitability. For this reason the lack of detectable group Ia afferent ingrowth abnormalities in this system was not unexpected. However, since in other developing neuronal systems activity is a crucial factor contributing to pruning and refinement of synaptic connectivity, it remains a possibility that loss of Pkr2 affects other components of spinal motor circuitry. Particularly, virtually nothing is known about the molecular

mechanisms establishing the highly specific neuronal network enabling CM MN to control local skin withdrawal reflexes (Theriault and Diamond, 1988; Blight et al., 1990) or higher brain centers (Holstege and Blok, 1989; Gerrits et al., 2000). Possible changes in these nociceptive withdrawal reflex pathways in *Pea3* and *Pkr2* mutant mice could in the future be investigated.

4.3.2 A potential link between prokineticin signaling in immunoinflammatory response and CM MN excitability

In adult mice, Pk2 expression in the SC is equally sparse as during embryonic development. This raises the question about other possible sources of Pk2 for both, Pkr2 expressing nociceptors and CM MNs, in the periphery. Although, at first these two classes of Pkr2 expressing neurons appear functionally unrelated, there are commonalties in terms of their biological purpose and their axonal target areas, making it possible that sensory neurons and CM MNs exploit the same source of Pk2.

The CM muscle is special in that it lies directly underneath the skin spanning from the humerus bone all the way down to the hindlimbs the entire trunk of the mouse (Theriault and Diamond, 1988). Although CM MNs are not monosynaptically connected with any type of somatosensory neuron they are part of polysynaptic tactile and nociceptive reflex circuits of the skin (Theriault and Diamond, 1988; Blight et al., 1990). Experiments in rats have demonstrated that a local stimulus applied to the skin can elicit a CM muscle contraction restricted to the receptive field of the sensory neurons that conveyed the signal (Theriault and Diamond, 1988). Thus, noxious stimuli can be propagated by prokineticin receptor expressing sensory neurons, relayed through propriospinal ascending pathways and eventually converge back to Pkr2 expressing CM MNs. Propriospinal interneurons of this reflex circuit (reflex encoders) occur in

relatively high numbers and, at least in guinea pigs, are dispersed along the rostrocaudal extent of the thoracic SC (Borgens et al., 1987; Blight et al., 1990).

Since inflammation is often caused by skin damage and because Pk2 is strongly secreted by immune cells at sites of inflammation, its suggested persistence (Negri et al., 2002) could permit diffusion into adjacent tissue layers such as the CM muscle. Therefore, it is possible that Pkr2 expressing CM axons perceive local Pk2 gradients as would their sensory neuron counterparts. This hypothesis makes it possible that Pk2/Pkr2 signaling is not only exploited to modulate the immunoinflammatory response and sensitization of nociceptors, but that the same local Pk2 cues could signal on distinct populations of CM motor axons supply muscle fibers underlying the inflamed patch (Blight et al., 1990). If so, what could be the functional purpose of Pk2 signaling on distinct subpopulations of CM MNs? If Pk2 also exerts positive neuromodulatory effects on CM MNs, selective increase of MN excitability could ease the mouse's withdrawal reflexes specifically at sites of inflammation. According to this hypothesis, local expression of Pk2 would therefore at the same time increase the sensitivity of two components of the same reflex circuit by means of the same mechanism. Thus, the same factor could facilitate perception of noxious stimuli as well as avoidance.

4.3.3 A potential role for Pkr2 in mating behavior

Pkr2 mutant mice display virtually all symptoms for human Kallmann disease, an essential manifestation of which is pronounced hypogonadotrophic-hypogonadism resulting in impotence (Matsumoto et al., 2006; Monnier et al., 2009). Thus, the strikingly underdeveloped reproductive organs of both sexes in *Pkr2* mutant mice readily accounts for their infertility (Matsumoto et al., 2006) but might at the same time mask potential neuronal components of impotency. In mice loss of Pea3 does not cause

Kallmann Syndrome, but males are also sterile (Laing et al., 2000), and theirs IC MNs display migration defects and presumably slight abnormalities in neuromuscular endplate patterns (n=1, Eline Vrieseling et al., unpublished observations). Whether there is indeed a neuronal component underlying the loss of fertility in *Pea3* mutant males has however not been satisfactorily resolved (Laing et al., 2000).

In *Pkr2* mutant mice, preliminary examination revealed bulbocavernousus (BC) and IC muscle innervation and neuromuscular endplate patterns to be unchanged compared to controls (n=1, data not shown), which adds to mounting data arguing against a function of Pkr2 in axon pathfinding in the SC.

However, recent findings on the gastrin-releasing peptide (GRP) system in the lumbar SC provided indications that Pkr2's role in the regulation of neuronal excitation could be of particular interest in the context of IC expressing MNs (Sakamoto et al., 2008). This study identified a population of interneurons in the upper lumbar SC that project their axons containing GRP to lower lumbar regions known to control erection and ejaculation. GRP-receptor expressing targets in this region included somatic MNs supplying BC and possibly IC muscles (Sakamoto et al., 2008). Pharmacological short-circuiting of this neuronal system by directly activating GRP receptors restores penile reflexes and ejaculation in castrated mice (Sakamoto et al., 2008).

In the light of these findings we are presently exploring if the lumbar SC harbors a population of Pk2 expressing interneurons that could exert a similar effect on Pkr2 expressing IC MNs as in the GRP-system. If so, regulation of MN excitability through Pkr2 could constitute the functional mechanism underlying male infertility in Pea3 mutants.

In order to address this hypothesis experimentally, the use of *Pkr2* null mutants exhibiting Kallmann Syndrome is impossible. Not only does the lack of gonadotrophin

inhibit the development of sexual organs in both sex but the resulting reduction of sexual hormone such as testosterone or estrogen can directly impair the morphology and excitability of sexually dimorphic MNs in rats (Fargo et al., 2003; Fargo and Sengelaub, 2004). Our recently cloned *Pkr2* conditional mutants (Figure 21, B) which allow selective elimination of Pkr2 in MNs using $Olig2^{Cre}$ mice will allow us to circumvent these confounds. Matings of these mice are ongoing. In a first experiment, we will test the functionality of the sexually dimorphic neuromuscular system by mating $Pkr2^{F/F}Olig2^{Cre}$ males with wild-type females. If activation of Pkr2 in IC MNs indeed plays an important role in the excitability of spinal MNs, it is possible that MN specific elimination of Pkr2 is sufficient to cause erection deficiencies or infertility. In addition, Pk2 expression at lumbosacral levels including segments harboring sexually dimorphic MN pools must be investigated using sexually mature *Pk2-BAC* transgenics. It is also of outmost importance to establish expression pattern of Pkr2 at adult stages. As so far our research was primarily focused on the developmental role of Pkr2, we have not yet performed these important experiments.

Interestingly, the CM muscle has recently been proposed to play a role in female mating behavior. Upon stimulation estrous female hamsters take in a lordosis posture which is, among other, characterized by straightening of the back, tensing up the skin and elevation of the pelvis, movements which are controlled by the CM muscle (Gerrits et al., 2000). Anterograde tracing experiments in female hamster have demonstrated that projection neurons form the nucleus retroambiguus (NRA) specifically terminate on CM MNs (Gerrits et al., 2000) and this specific connectivity between NRA and CM MNs, including its role in mating posture, appears to be conserved in cats (Holstege and Blok, 1989; Vanderhorst and Holstege, 1995; Gerrits et al., 2000). These supraspinal projections are so far the only identified direct input to CM MNs from the

higher brain areas, but neither Pk1 nor Pk2 have been shown to be expressed in the NRA. Nonetheless, these findings raise the possibility that not only in male but also in female mice *Olig2^{Cre}Pkr2$^{F/F}$* could exhibit mating deficiencies. This hypothesis could be addressed by analysis of the mating efficiency between *Olig2^{Cre}Pkr2$^{F/F}$* females and wild-type males. However, since female *Pea3* mutant mice displaying severe CM muscle innervation defects are still fertile, these mating efficiency phenotypes are expected to be subtle.

4.3.4 A role for prokineticin signaling in taste perception

Ignoring concerns about the reliability of the Pkr2-Cre induced Tau-mGFP as an informative reporter for Pkr2 expression, the fact that Pkr2-GFP only marks a subpopulation of gustatory afferents, raises the intriguing possibility these taste neurons selectively convey information about distinct taste modalities. Although there is mounting data that the timing of neural events may also contribute to its representation in the CNS, significant evidence support models in which different taste modalities are encoded by discrete "labeled-lines (Lemon and Katz, 2007). However, similar to our findings in MNs and DRG sensory neurons, there were no indications of axon guidance abnormalities in *Pkr2* mutants. In the gustatory system, Pkr2 could in principle play an analogous role to its function in DRG sensory neurons, as number of transient receptor potential type channels, including Trpv1, have been shown to be expressed in subpopulations of geniculate ganglion neurons, too (Katsura et al., 2006).

Interestingly, the central termination zone of gustatory afferents, the NTS, has been shown to express Pk2 (Negri et al., 2004) and high levels of Pk1 which is almost equally potent to induce Pkr2 (Cheng et al., 2006; Negri et al., 2007). Immediately adjacent to the NTS, two additional structures express prokineticin receptors: the area postrema expresses Pkr2 (Figure 34, A, C) and nucleus 10N has been shown to express

Pkr1 (Cheng et al., 2006) (Figure 34, E). Since anatomical connectivity has been demonstrated in mammals (Strominger et al., 1994), it is plausible that Pk1/Pk2 expressing neurons of the NTS can integrate and relay gustatory information from the tongue to the adjacent area postrema, which among other acts as a vomiting inducing center (Price et al., 2008). Moreover, microinjection of Bv8, into ARC and SFO, which both express Pkr2 and reciprocally connect with the NTS, strongly affected drinking and food uptake behavior, respectively (Negri et al., 2004). Two of the involved nuclei, the SFO and the area postrema are circumventricular organs, capable of directly sensing concentrations of various compounds, particularly peptide hormones, in the bloodstream. In this context it should be noted, that activity of the NRA is not only important for female mating posture, but has also been correlated with (forced) expiration (Bainton and Kirkwood, 1979) and vomiting (Miller et al., 1995), both of which are behavioral outputs controlled by CM muscle contraction (Holstege and Blok, 1989).

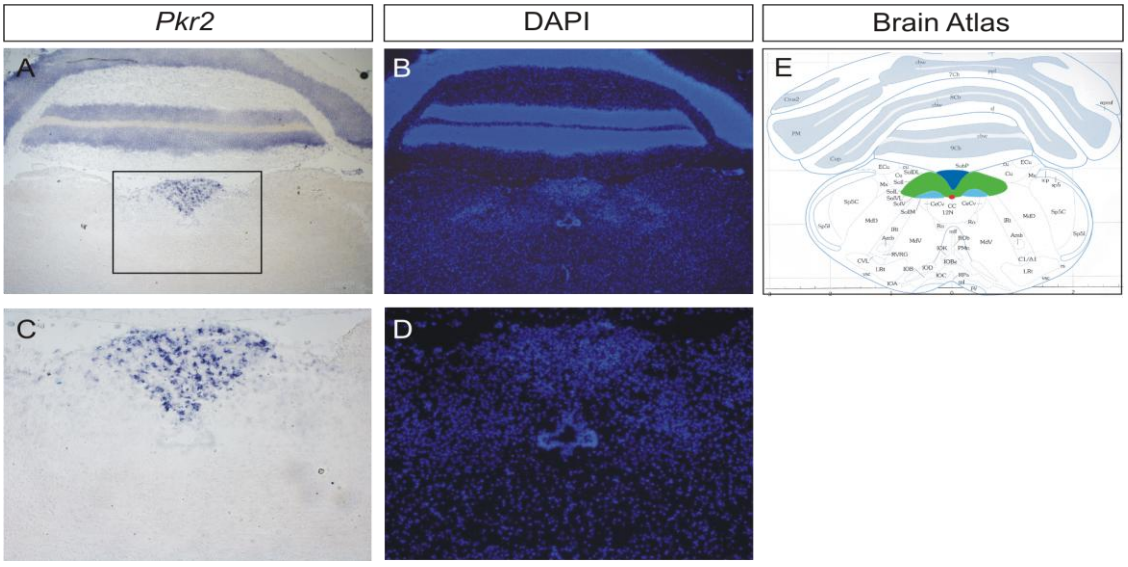

Figure 34: Pkr2 is expressed in the area postrema but not in the NTS

Pkr2 in situ hybridization and DAPI staining on hindbrain at P14. **A-D:** *Pkr2* is expressed in the area postrema, a circumventricular structure which measures blood toxins and acts as a vomiting inducing center. Adjacent structures of the NTS appear devoid of *Pkr2* signal. A magnified view of the area indicated in (A) is shown in (C) an (D). DAPI stainings reveal areas with increased cell density which allows distinguishing the outlines of the area postrema and the NTS (D). **E:** Relative positions of hindbrain nuclei expressing prokineticins and their cognate receptors Pkr1 and Pkr2. The area postrema (dark blue) expresses Pkr2, the nucleus 10N (light blue) expresses Pkr1 (Cheng et al., 2006) and NTS (green) have been shown to express Pk1 and Pk2 (Negri et al., 2004; Cheng et al., 2006; Negri et al., 2007). The central canal is marked in red.

Collectively, the emerging concept raises the possibility that prokineticins and its receptors also impact on the excitability status of an interconnected neuronal network controlling taste perception, appetite and ingestive behavior. For the elucidation of the individual contributions of these brain areas expressing Pkr2 or one of its cognate ligands to distinct behavioral outputs, Pkr2 conditional mutants should be employed in the future.

4.4 Materials and Methods

4.4.1 Generation of *Pkr2* mutant mice

4.4.1.1 *Pkr2* null alleles

PCR primers were designed using sequences retrieved from the UCSC Genome Bioinformatics platform (http://genome.ucsc.edu/). Annealing temperatures and PCR primer positions were adjusted with Primer3 (v. 0.4.0) bioinformatics' software tools (http://frodo.wi.mit.edu/). In order to disrupt the *Pkr2* locus, a Cre-IRES-NLS-LacZ-pA-TK-Neo targeting cassette was integrated into an artificially introduced NcoI site at the ATG start codon (Exon 2), and an artificially introduced PacI site ~100bps downstream of the end of Exon 2. A 6.5 kb 5' region (SacI–NcoI) and a 2.4 kb 3' region (PacI–StuI) were used to generate the targeting construct into which the reporter and (TK)-neomycin resistance cassettes were introduced. The Southern probe used to screen for homologous recombination in ES cells consisted of a 270bp PCR fragment (Fwd: 5'-caggcacacagccgtaatctagac-3' Rev: 5'-ggtaggatgtctgacccatcttc-3') located 3' to the region used for the generation of the targeting construct (Figure 16). Homologous integration at the targeted locus of homozygous and heterozygous $Pkr2^{NLZ}$ mutant mice was tested by Southern blotting using ERV restriction enzyme. Mutant ERV genomic

DNA digests yielded 12.9 kb, wild-type 19 kb bands. The target frequency of homologous recombination at the Pkr2 locus was about 1:30.

4.4.1.2 *Pkr2* conditional alleles

To generate a conditional *Pkr2* mutant allele, a floxP-site-flanked TK-Neo targeting cassette was integrated into the HpaI site located 3' of exon 2, and a floxP-site, containing an additional SpeI restriction site, into the HpaI site 5' of Exon 2. The same stretch of genomic locus as employed in null mutants was used to achieve homologous recombination at the *Pkr2* locus. Correct integration of 5' loxP sites was challenged by SpeI digests (wt: 15.2 vs. KO 9.5 kb) and by ERV digests for 3' floxed TK-Neo cassettes with (wt: 19 vs. KO 12.4 kb) using the same Southern probes as for *Pkr2* null mutants. The targeting frequency of homologous recombination at the *Pkr2* locus was about 1:100.

4.4.2 Immunohistochemistry

Cryostat sections were processed for immunohistochemistry as previously described (Arber et al., 1999). In this chapter the following antibodies were used: rabbit anti-Pea3 (c-term) (Arber et al., 2000); guinea pig-anti-Scip (kindly provided by Jeremy Dasen); rabbit anti-GFP (Molecular Probes); rabbit anti-rhodamine (Molecular Probes); goat anti-LacZ (Biogenesis Ltd); guinea pig anti-Isl1 (Arber et al., 2000); goat anit-Isl1 (Neuromics); mouse α-sarcomeric actin (Sigma); mouse anti-NeuN (Chemicon); rabbit anti-TrkA (Upstate); goat anti TrkA (Neuromics); goat anti-TrkB (Neuromics); goat anti-TrkB (R&D Systems), goat anti-mTrkC (R&D Systems); guinea pig anti-CGRP (Penlabs/Bachem); rabbit anti CRGP (Chemicon); goat anti-ChAT (Chemicon); chick anti-Neurofilament H (Neuromics); guinea pigs anti-Lbx1 (kindly provided by Carmen Birchmeier). Moreover DRAQ5 (Biostatus Limited) and DAPI (Boehringer) were used

to reveal cell bodies on tissue sections, which could be imaged in the Cy5 and UV channel, respectively.

Whole-mount dissected muscles were dissected in ice-cold oxygenated ACSF and immediately incubated with tetramethylrhodamine-conjugated α-bungarotoxin (Molecular Probes) to reveal NM. Subsequently, muscles were washed in PBS, fixed in 4% paraformaldehyd for 30 min and incubated with primary antibodies over night. Secondary antibodies were applied for 3-4 hours at room temperature. In all experiments we used Alexa488-, Cy3- and C5- conjugated fluorophores (Molecular Probes, Eugene, OR) as secondary antibodies.

Fluorescently labeled tissue sections and whole-mount muscles were imaged using an Olympus BX61 scanning microscope (Olympus).

4.4.3 Quantification of Ia afferent ingrowth in *Pkr2* mutant mice

Quantification of the MN pool areas covered by vGlut1 in *Pkr2* mutant and wild-type mice was performed by dividing the measured area of ChAT labeled MNs covered by vGlut1 terminals by the measured total area of ChAT labeled MNs using ImageJ software version 1.35i. Means and standard deviations were calculated using Microsoft Office Excel functions.

5 Assessment of Del1 Function in Motor and Sensory Systems

5.1 Introduction

5.1.1 Del1 function in angiogenesis

Del1 emerged as one of the top hits of genes enriched in wild-type CM but downregulated in *Pea3* mutant CM MNs. It encodes a secreted, extracellular matrix (ECM)-associated protein and was originally identified in a screen for genes stimulating embryonic vasculogenesis (Hidai et al., 1998). Del1 protein comprises five defined structural features: three epidermal growth factor (EGF)-like repeats and two discoidin-like domains. While the second EGF-like repeat contains an arginine-glycine-aspartic acid (RGD) motif mediating the binding to integrins, discoidin domains are responsible for the deposition of Del1 in the ECM (Hidai et al., 2007).

Del1 is expressed in vascular endothelial cells during embryonic vascular development and has been shown to elicit a strong angiogenic response by binding to αvβ5 integrin complexes on resting endothelial cells (Penta et al., 1999; Rezaee et al., 2002). Upon stimulation of this receptor complex, intracellular signaling events lead to the activation HoxD3 which initiates expression of an array of proangiogenic molecules, including avβ3 integrins. As a result, resting endothelium converts to angiogenic endothelium. αvβ3 integrin complexes also display high affinity for Del1 and signaling through these receptors is well known for its stimulatory effect on angiogenesis (Zhong et al., 2003). Taken together, Del1 signaling through different αβ integrin receptors subtypes engages downstream pathways, including Hox transcription factors, which activate angiogenesis programs promoting adherence and migration of endothelial cells.

With the exception of the brain and lung endothelial cells, Del1 expression is downregulated at the time of birth. However, adeno-associated virus mediated delivery of Del1 to mouse brains has been shown to significantly increase vascular densities for up to 6 weeks after gene delivery (Fan et al., 2008). Similarly, expression of Del1 has been shown to be sufficient to neovascularize ischemic hindlimb muscles (Zhong et al., 2003) and for accelerating the growth of tumor (Aoka et al., 2002). Together, these data suggest that Del1 normally governs embryonic vasculogenesis, but retains the potential to augment vasculogenesis in adult tissue, if expressed.

Recently, first results from phenotypical analysis of *Del1* mutant mice have been reported and revealed a role for Del1 in the inhibition of leukocyte-endothelial cell interactions, which is a pivotal triggering event in the recruitment of inflammatory cells to sites of infection (Choi et al., 2008). The authors of this study also demonstrated that Del1 is upregulated upon hypoxia and vascular injury, suggesting new pathway of induction in adult tissue.

5.1.2 A potential role for Del1 in neurogenic processes

Although expression of Del1 in the CNS has been detected by RT-PCR (Choi et al., 2008), expression patterns and their biological relevance, such as the potential role in neovascularization of injured brain, have not been addressed yet. Interestingly, mutual interactions between the developing nervous system and the vascular system have been described by a number of studies (Palmer et al., 2000; Sondell et al., 2000; Mukouyama et al., 2002; Zhang et al., 2003; Mukouyama et al., 2005). It has, for instance, been demonstrated that vascular endothelial growth factor A (Vegfa) derived from sensory neurons, MNs or Schwann cells is required for arteriogenesis *in vivo*, and that mutations leading to misrouting of axons concurrently lead to paralleled misrouting of the vascular system (Mukouyama et al., 2005). Similarly, examples of chemotactic

guidance molecules classically involved in angiogenesis and vasculogenesis influence migration of neuronal progenitors. Vegfa, for instance, is not only essential for embryonic vascularization but also stimulates axonal outgrowth of cultured DRG sensory neurons expressing the cognate Vegfa receptor Flk1 (Sondell et al., 2000).

In summary, nerves and blood vessels often form tightly interweaved networks among tissues and the mechanistic interdependences in their developmental processes raise the question of whether Del1 secreted from sensory neurons and CM MNs primarily impacts on the development of the vascular system or whether its expression and function in the nervous system is independent of vasculogenic processes.

5.1.3 Members of the semaphorin 3 class counteract pro-angiogenic processes induced by Del1

Members of the semaphorin family of cell surface and secreted proteins are known for their chemotactic roles in neuronal cell migration and axon pathfinding, dendritic guidance and target selection (He et al., 2002; Chauvet et al., 2007).

During physiological vascular development and angiogenesis, the activity of endogenous proangiogenic factors such as Vegf or Del1 is counterbalanced by endogenous anti-angiogenic factors such as members of the class of secreted semaphorin3s (Sema3s). Mechanistically, Sema3s indirectly reduce the affinity of integrin receptors towards ECM ligands by inhibiting two key integrin activators: the small GTPase R-Ras and the focal adhesion protein talin (Gu et al., 2005; Bussolino et al., 2006).

Recently, Sema3e and its receptor PlexinD1 (Plxnd1) have been shown to control distinct processes of blood vessel development. Sema3e is highly expressed in developing somites, where it acts as a repulsive guidance cue for Plxnd1 expressing endothelial cells of adjacent intersomitic blood vessels and loss of either Sema3e or

Plxnd1 results in disruption of vascular patterning, *in vivo* (Gu et al., 2005). Intriguingly, neuropilin 1, which can form a receptor complex with Plxnd1 (Chauvet et al., 2007), also functions as a receptor for isoforms of the Vegf family.

Del1 and Sema3e are the only two Pea3 dependent proteins which are specifically expressed in CM MNs. Moreover, our *in situ* data demonstrated Del1 expression in virtually all DRG sensory neurons. Taken together, these considerations implicate a potential role for Del1 in intersomitic vascular patterning and for axon pathfinding of sensory neurons and CM motor neurons. We were, therefore, interested to explore the functionality of Del1 through analysis of *Del1* loss of function mutant mice (Choi et al., 2008).

5.2 Results

5.2.1 Del1 expression in two cervical clusters of MNs

To recapitulate, Del1 was found 6.5-fold enriched in CM MNs compared to other MN pools (Table 2) and *Pea3* mutant chip data indicated it to be 6.3-fold positively regulated by Pea3 (Table 6).

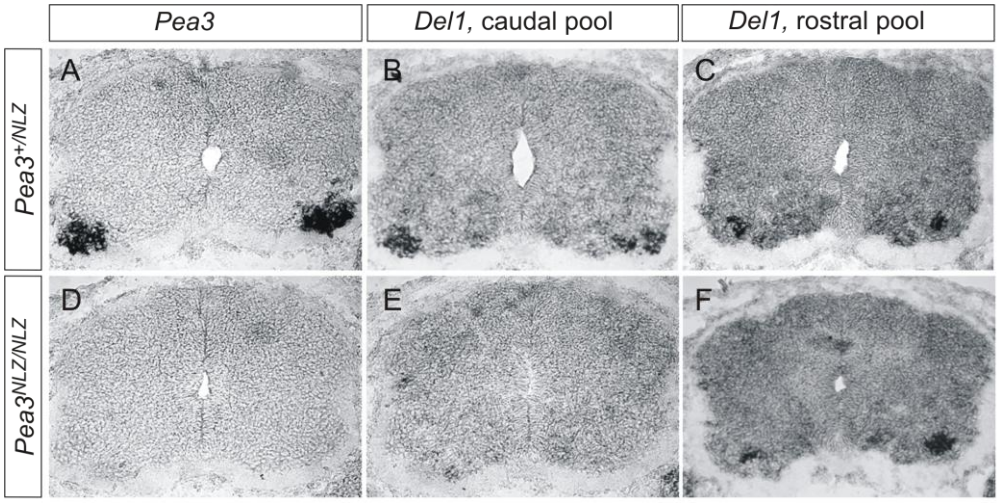

Figure 35: Del1 expression in cervical MN pools of *Pea3* mutant mice
In situ hybridization were performed on $Pea3^{+/NLZ}$ and $Pea3^{NLZ/NLZ}$ P1 pups to verify the dependence of *Del1* on *Pea3* **A,D:** *Pea3 in situ* signals were used as positional landmarks and for confirmation of genotype identities. **B, E:** Consecutive sections of (A) and (D), respectively. In *Pea3* expressing MN pools, induction of *Del1* is clearly dependent on *Pea3*: no signal could be detected in $Pea3^{NLZ/NLZ}$ (E). **C, F:** In more rostral *Pea3*-negative *Del1* expressing MNs, induction of Del1 appears independent of Pea3.

At cervical levels of the SC, *Del1* signal was detected in two discrete clusters of MNs located at different rostrocaudal levels (Figure 35). As established by the validation of our Affymetrix screen, the caudally positioned cluster of $Del1^{+}$ MNs colocalizes with CM MNs (Figure 35), whereas the more rostral $Del1^{+}$ cluster was located at segmental levels completely devoid of Pea3 expressing MNs (data not shown). *Del1 in situ* hybridization results100

clearly indicate that in MNs usually expressing Pea3, induction of Del1 is dependent on Pea3 (Figure 35, B and E). In contrast, expression of *Del1* in the rostral cluster of MNs remains completely unaffected by loss of Pea3. These findings suggests that induction of Del1 in MNs cannot solely depend on Pea3, but that there must also be other, Pea3-independent, parallel pathways leading to the induction of Del1 in these rostral MNs.

5.2.2 Characterization of Del1-LacZ expression patterns in rostral and lumbar SC

In a first step, we sought to demonstrate that Del1-LacZ immunoreactivity faithfully reflects *Del1 in situ* hybridization patterns in cervical MN pools. To this end, we performed whole-mount X-Gal stainings using $Del1^{+/NLZ}$ mouse embryos at E13.5 (Figure 36; A). In these experiments Del1 was also detected at segmental levels of the thoracic and lumbar SC. The medial position of these MNs, in conjunction with Scip immunoreactivity, suggests that Del1 is also a marker of MMC_l MNs (Rousso et al., 2008) (Figure 36, F,G).

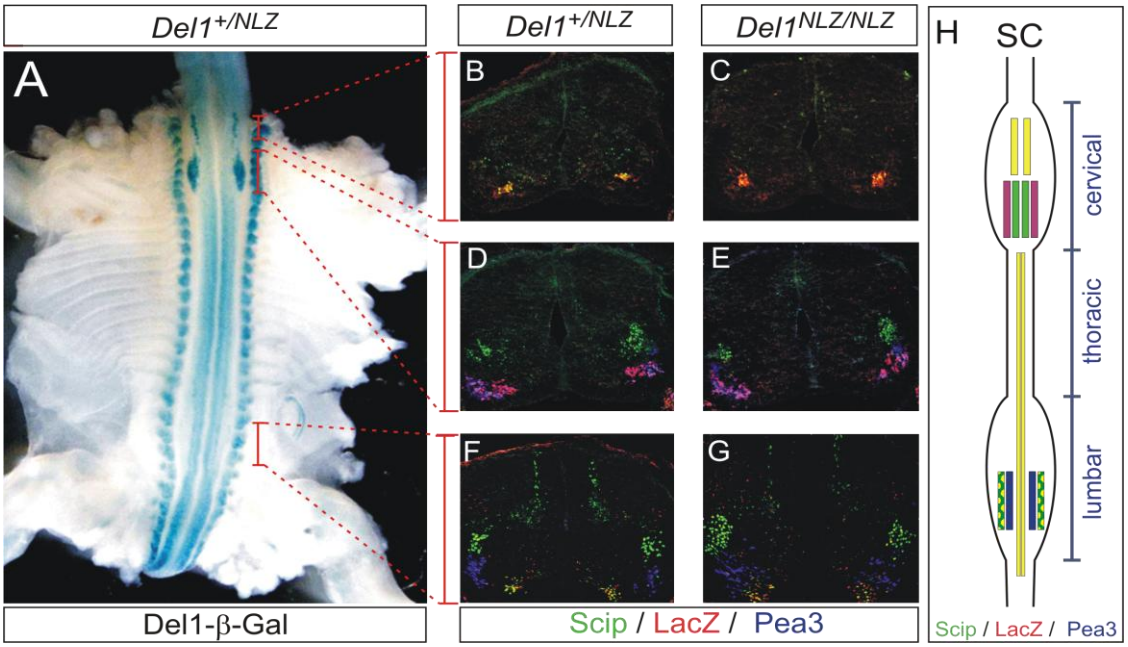

Figure 36: Assessment of MN pool position and marker gene expression in *Del1* mutant mice

Whole-mount X-Gal stainings in *Del1*^{NLZ} mice and immunocytochemical detection of Del1-LacZ, Pea3 and Scip on transverse sections of E13.5 *Del1*$^{+/NLZ}$ and *Del1*$^{NLZ/NLZ}$ SCs. **A** Del1 expression patterns were established by whole mount β-Gal staining of E13.5 *Del1*$^{+/NLZ}$ embryos. Del1-β-Gal activity was detected in DRG and, prominently, in two cervical MN pools. At thoracic and lumbar levels β-Gal signals were weaker and exhibited an apparent medial to lateral gradient. **B-G:** MN pool organization appears unaffected by the loss of Del1 at all examined levels. Rostral Del1-LacZ expressing MNs faithfully colocalize with Scip immunoreactivity, which we have established to mark MNs supplying the diaphragm. At segmental levels of the CM MN pool (D, E) Del1-LacZ colocalizes with ventrally located Pea3 expressing MNs. More dorso-laterally located Pea3 expressing MNs are often devoid of Del1-LacZ signal (D, E). At lumbar levels, Pea3 expressing MNs do not coexpress Del1-LacZ (F, G). Del1-LacZ signals are detected in medial Scip^{+} MNs of the MMC_l and, in a salt and pepper pattern, in a dorsal Scip expressing population of the LMC_m (F, G). **H:** Schematic illustration of Pea3, Del1-LacZ and Scip expression patterns at E13.5.

In the LMC, strong Del1 β-galactosidase signal appears to be restricted to cervical levels (Figure 36, A). In order to characterize Del1 expressing MNs pools, we combined immunocytochemical stainings for Del1-LacZ, Pea3 and Scip on *Del1*^{LacZ} heterozygous E13.5 tissue (Figure 36; B, D, F). Interestingly, at cervical levels we identified Pea3-negative, Del1-expressing MNs to perfectly match immunoreactivity of Scip which is a marker for MNs innervating the diaphragm (Figure 36, B). Because of its atypical transcriptional profile and functionally distinct target muscle, the phrenic MN pool has recently been suggested to appertain not to the LMC, but to the MMC_l, a motor column which was previously considered absent from limb innervating levels (Rousso et al., 2008). Thus, the specific expression pattern of Del1 in both the phrenic MN pool and MNs of the MMC_l further strengthens this notion.

Taken together, the similarities in the relative distribution of β-galactosidase signals and LacZ immunocytochemistry with the previously established *in situ* patterns makes us confident that the observed X-Gal signals faithfully recapitulate *Del1* expression.

5.2.3 Assessment of Del1 function in motor pool assembly and motor axon guidance

Similar to our experimental approach directed at the elucidation of Pkr2 function in CM MNs we also examined Del1 for its potential contributions to phenotypes described in *Pea3* mutant mice (Livet et al., 2002; Vrieseling and Arber, 2006).

As a first step we compared immunocytochemical stainings for LacZ, Pea3 and Scip of E13.5 $Del1^{LacZ}$ heterozygous embryos with homozygous littermates (Figure 36; C, E, G). We detected no apparent difference in cervical or lumbar MN pool organization between the two genotypes insofar as all tested markers of neuronal subpopulations exhibited similar expression patterns and the relative positions of identified MNs pools appeared unaffected. We therefore conclude that Del1 does not influence the terminal migration of Pea3 expressing MNs.

We have also begun to examine *Del1* mutants for gross defects in CM muscle innervation. Until now, only a preliminary visual inspection of CM muscle innervation patterns at E16.5 and P1 could be performed but no defects were identified (n=2, data not shown). A more thorough examination of Del1 potential in motor axon pathfinding is in progress. We presently plan to map the innervations patterns of the diaphragm and the CM muscle using genetic intercrosses with $Hb9^{mGFP}$ transgenic mice in conjunction with markers for the vascular system.

5.2.4 Del1 is expressed throughout all subpopulations of DRG sensory neurons

Our developmental analysis of the Del1 expression patterns in the SC also revealed strong Del1 expression DRG sensory neurons (Figure 36.A). The proportion of sensory neurons expressing *Del1* appeared to increase from E13.5 until P1 (Figure 7). Therefore, we analyzed the distribution of Del1 expression in subpopulations of DRG sensory neurons conveying different somatosensory modalities by combining immunocytochemical stainings for Del1-LacZ with TrkA, TrkB and TrkC, known to mediated nociceptive, mechanical and proprioceptive stimuli, respectively (Bibel and Barde, 2000), on transverse sections of E13.5 and P1 $Del1^{LacZ/+}$ DRG (Figure 37).

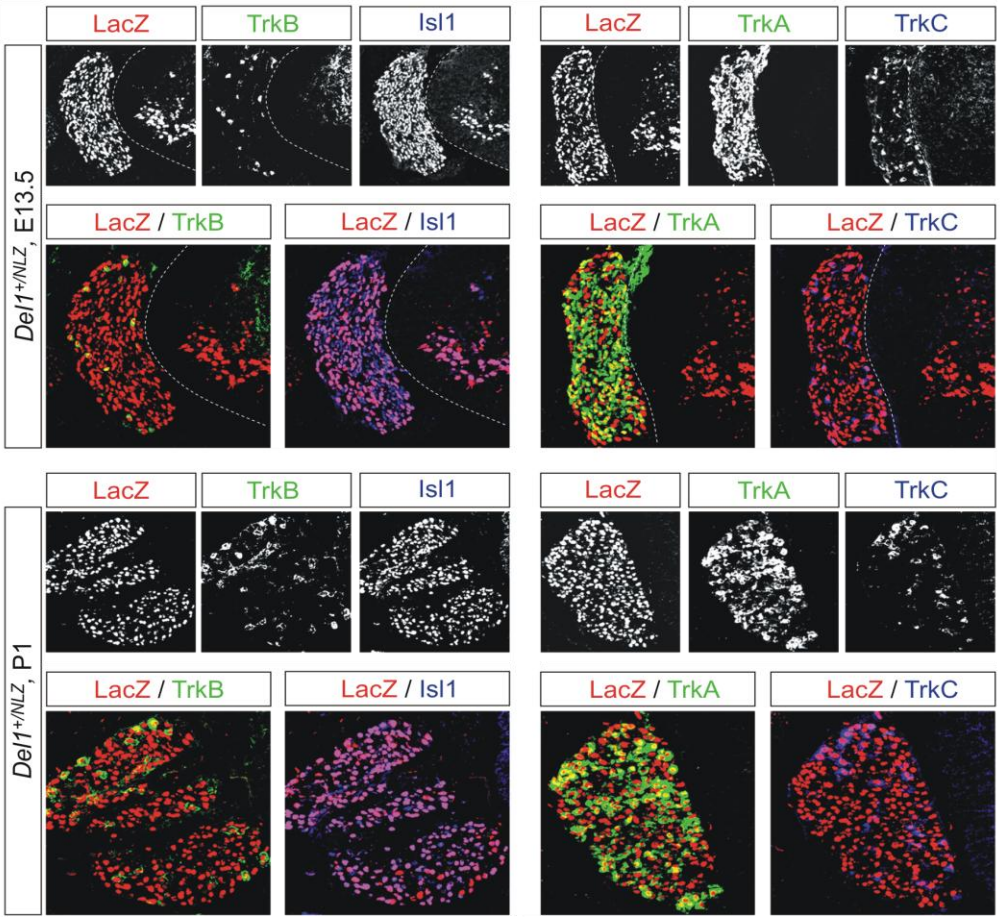

Figure 37: Developmental upregulation of Del1 in DRG sensory neurons

Immunocytochemical expression patterns of Del1-LacZ, TrkA, TrkB, TrkC and Isl1 in DRG at E13.5 and P1 in heterozygous $Del1^{NLZ}$ mice. At P1, Del1-LacZ is expressed in virtually all DRG sensory neurons, whereas at E13.5, a subgroup of $TrkA^{+}$ nociceptive neurons still lacks the expression of Del1-LacZ, suggesting a sequential acquisition of Del1-LacZ expression in distinct subclasses of sensory neurons in the DRG. White dashed lines in top panel mark outline of the SC, where Del1 immunoreactivity is detected in CM MNs.

At E13.5, we observed Del1-LacZ expression in about two thirds of all DRG sensory neurons marked by Isl1 (Pfaff et al., 1996). Virtually all $TrkB^+$ and $TrkC^+$ neurons but only about two thirds of $TrkA^+$ neurons colocalized with Del1-LacZ at E13.5 (Figure 37) while by P1, all DRG sensory neurons equally expressed LacZ reporter protein.

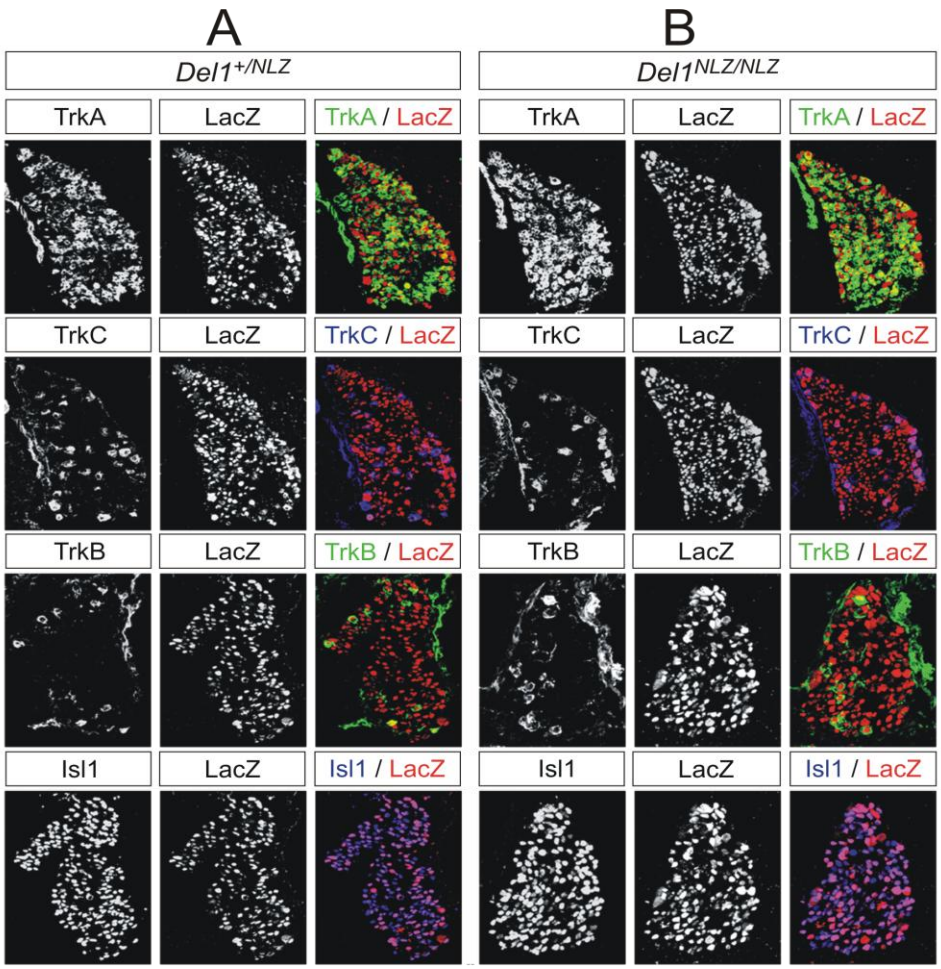

Figure 38: Integrity of DRG sensory modalities appear unaffected in *Del1* mutant mice

DRG sensory neurons were labeled with Del1-LacZ in combination with Isl1 and Trk receptors to reveal colocalization with subpopulations of sensory neurons conveying different sensory modalities. **A:** In *Del1*$^{+/NLZ}$ E13.5 embryos, Del1-LacZ immunoreactivity colocalized with all TrkB and TrkC but only a subpopulation of TrkA sensory neurons. **B:** In *Del1*$^{NLZ/NLZ}$ E13.5 embryos, Del1-LacZ also colocalized with all TrkB and TrkC but only a subpopulation of TrkA sensory neurons and the relative distributions of Del1-LacZ expression did not appear significantly different form heterozygous littermates.

In order to establish if Del1 signaling is required for the specification or maintenance of their sensory modalities, we also examined the Del1-LacZ and neurotrophin receptor status (Trk) in *Del1* mutant mice. The combinatorial expression of DRG subclass markers TrkA, TrkB and TrkC and Del1-LacZ remained, however, unaffected. The fact that the transcriptional control of Del1 remained intact (as assessed by LacZ

expression) also suggested that in sensory neurons Del1 is not involved in the regulation of its own expression (Figure 38, B).

Notably, large-diameter $TrkC^+$ and $TrkB^+$ sensory neurons are born before a second wave of neurogenesis gives rise to small-diameter TrkA+ neurons (Ma et al., 1999). This creates the possibility that, since Del1 is progressively upregulated in all sensory neurons, induction of Del1 in TrkA+ population is solely lagging behind because these neurons are born slightly later in time. However, there is not experimental data supporting these speculations and they were not further investigated.

5.2.5 Preliminary experiments addressing a potential role for Del1 in axon pathfinding

We sought to investigate if secretion of Del1 into the ECM could (in an autocrine mode of action) be involved in the guidance of sprouting sensory neuron axons or (in a paracrine mode of action) impact on the development of intersomitic blood vessels. For this purpose, we first investigated the relative distribution of *Del1, Sema3e* and *Plxnd1* in intersomitic space by *in situ* hybridization experiments at E11.5 (Figure 39). As previously described by others (Gu et al., 2005), we detected *Sema3*e transcript in the caudal compartment of developing somites (Figure 39, B), *Plxnd1* in developing vascular endothelial cells and in DRG (Figure 39, D) and *Del1* in DRG. In addition, at E13.5, Del1-LacZ signal was also detected in developing chondrocytes (Figure 39 E), which confirms previous observations (Hidai et al., 1998). Together, our data suggest that sensory neurons and CM MNs expressing Del1 (and to some extent Plxnd1) in conjunction with vascular endothelial cells expressing Plxnd1, pervade the rostral intersomitic space under the local repulsive influence of Sema3e (Figure 39, F).

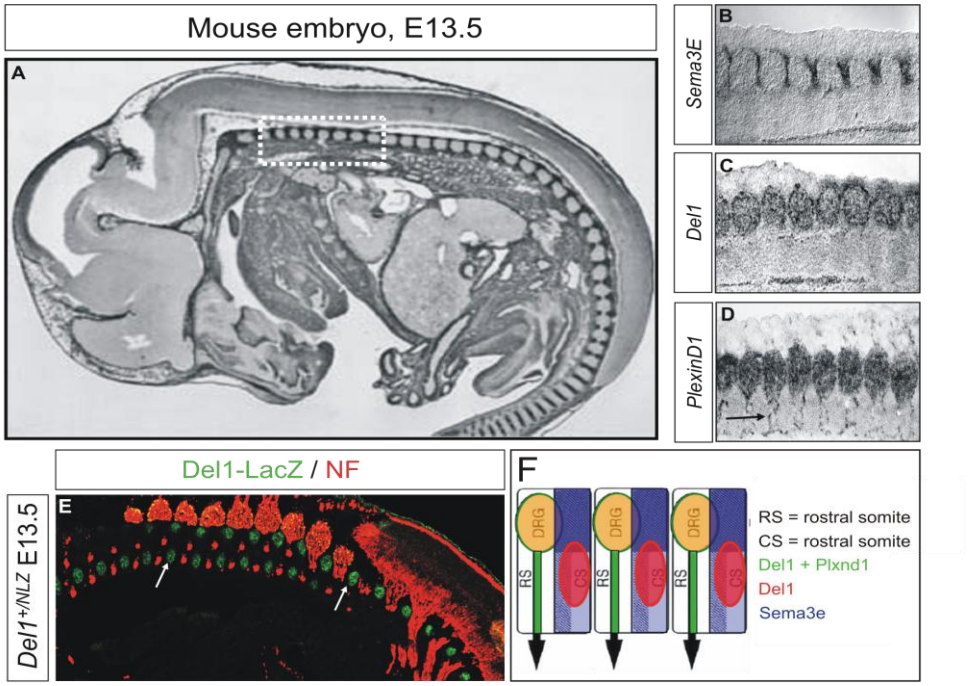

Figure 39: Expression of *Sema3e* and *Del1* in the intersomitic space

In situ hybridization and immunocytochemistry were performed to reveal expression of *Sema3e, Del1*, and *Plxnd1* at E11.5 and E13.5 mouse embryos to reveal the relative distribution of proteins controlling intersomitic angiogenesis. **A:** Parasagittal view of a mouse embryo at E13.5. White dotted box marks a region were somites are aligned. **B**: A close up view of a similar region as boxed in (A). *Sema3e* signal is detected in the caudal compartment of each somite (CS) and exhibits a faint dorsoventral gradient of expression (Gu et al. 2005). **C:** *Del1* mRNA was detected in DRG but not in chondrocytes, where it peaks at E13.5 (Hidai et al., 1998). **D:** Strong Plxnd1 signal was found in DRG sensory neurons and ventro-laterally directed vascular endothelial cells (black arrow). **E:** Immunocytochemical staining of Del1-LacZ and NF on parasagittal section of E13.5 *Del1*$^{+/NLZ}$ embryos indicated the positions of DRG and display axon bundles growing through the rostral compartments of somites (RS) towards peripheral targets, respectively. Additional Del1-LacZ expression was detected in developing chondrocytes located in the CS (white arrows). **F:** Schematic illustration of alternating Del1-LacZ, Sema3e and Plxnd1 expression patterns in somites.

We have now begun to explore whether the loss of Del signaling affects the propagation of sprouting sensory neurons (and blood vessels) through developing RS. To this end we have performed parasagittal sections on E13.5 *Del1*^{NLZ} heterozygous and homozygous mutants which allowed us to monitor DRG and outgrowing axon within the same cutting plane. Sensory axons were marked with antibodies directed at neurofilament H (NF), vascular endothelial cells and developing chondrocytes with Plxnd1 and Del1-LacZ immunoreactivity, respectively (Figure 40). Although expression of Plxnd1 was not readily attributable to blood vessel or axons, the overall pattern of at least sensory axons passing through the RS compartment in *Del1* mutants does not appear significantly different from heterozygous littermates. Our preliminary experiments are, therefore, not indicative for an essential role of Del1 in the earliest

events of sensory axon guidance towards peripheral targets. Similarly, our experiments do not reveal defects in the vascularization pattern, but potential deficiency should be addressed by other experimental methods in the future (Gu et al., 2005).

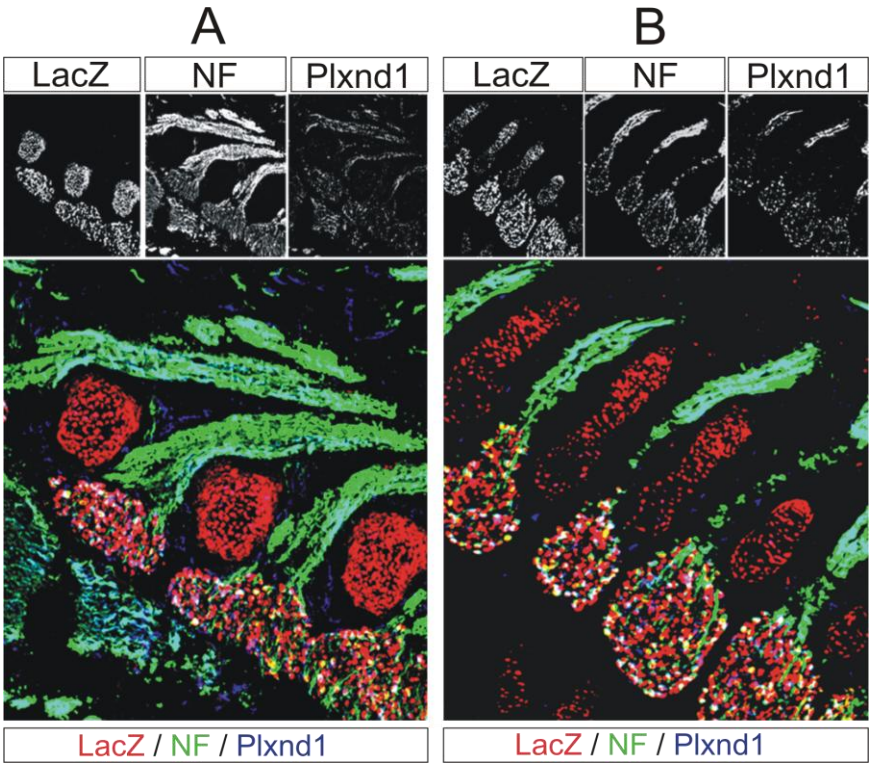

Figure 40: Assessment of sensory axon guidance defects in *Del1* mutant mice.
Immunocytochemical detection of Del1-LacZ, NF and Plxnd1 on parasagittal sections of E13.5 *Del1*$^{+/NLZ}$ (A) and *Del1*$^{NLZ/LNLZ}$ (B) embryos. **A:** While most somas of DRG sensory neurons express Del1-LacZ, only a subpopulation is marked by Plxnd1. NF/Plxnd1 double positive axons pervade the rostral intersomitic space in conjunction with Plxnd1 expressing blood vessels. **B:** No significant differences in marker gene expression or the morphological appearance of nerve bundles and blood vessels were detected in *Del1*$^{NLZ/LNLZ}$.

5.3 Discussion

5.3.1 Del1 expression in DRG sensory neurons

Experimental work on the functionality of Del1 in the nervous system has only just begun and no published information is available on the subject. In the past the Del1 has mostly been described in the context of immune cells migration, angiogenesis, and remodeling of the vascular system in ischemic tissue. Considering the spatial and temporal interdependences in the development of the vascular and nervous system, and with respect to the fact that these systems share sets of chemotactic guidance

molecules, we have begun to explore potential functions of Del1 in aspects of sensory-motor circuit formation.

The broad expression of Del1 in DRG sensory neurons suggests a biological function, equally important to all sensory modalities. Del1 could, for instance, be involved in the guidance of sensory axons through the rostral somite compartment, which is one of the earliest chemotactic pathfinding events equally important to all sprouting sensory neurons. Similarly, it is possible that Del1 acts in paracrine fashion and primarily impacts on sprouting intersomitic blood vessels. Either way, preliminary results were not indicative of any structural abnormalities in the trajectories of sensory afferents or blood vessels in the intersomitic space. It must, however, be considered that our experimental approach was not ideal to detect subtle defects. Notably, even the loss of Sema3e, providing a main repulsive cue to funnel Plxnd1 expressing blood vessels through the intersomitic cleft causes only slight phenotypes in the fasciculation and branching of intersomitic vessels (Gu et al., 2005). It is therefore possible that development and remodeling of the neurovascular system are under the control of partially redundant genetic systems which can, if necessary, to some extent compensate for loss of a single factor. Our experiments have by no means exhaustively elucidated the role of Del1 in sensory neurons and future experiments should explore potential axon guidance abnormalities in more detail.

5.3.2 Del1 expression in CM MNs

We have established that in CM MNs Del1 expression is dependent on Pea3, genetic elimination of which causes severe muscle innervation defects (Livet et al., 2002). However, preliminary visual inspections of CM muscle in *Del1* mutant mice are not indicative for at least gross abnormalities in axonal branching patterns but more detailed aspects of neuromuscular innervation patterns remain unexplored. Previous

work on CM muscle and the overlying skin led to the observation that the vascular system supplying the CM muscle is interweaved with the axonal branching pattern of CM motor axons and the same blood vessels appear to supply both, muscle and skin. It is therefore plausible that vascularization and innervation of skin and CM muscles are not independent developmental events, but might be guided by intersecting molecular mechanisms of superordinate neurovascular programs. For these reasons, we presently plan to investigate the neurovascular patterns of the CM muscle in parallel with the overlaying skin at high resolution.

Lastly, MNs of the $MMC_{l,}$ including the phrenic MN pool all express both, Del1 and Scip. In principle Scip is expressed in all Del1 expressing MNs, unless they also express Pea3. These observations further strengthen the notion of Scip being negatively regulated by Pea3 and might in the future contribute to our understanding of the role of Del1 in the CNS as well.

5.4 Materials and Methods

5.4.1 Immunohistochemistry

Cryostat sections were processed for immunohistochemistry as previously described (Arber et al., 1999). In this chapter the following antibodies were used: rabbit anti-Pea3 (c-term) (Arber et al., 2000); goat anti-Plxnd1 (R&D Systems), guinea pig anti-Scip (kindly provided by Jeremy Dasen); goat anti-LacZ (Biogenesis Ltd), guinea pig anti-Isl1 (Arber et al., 2000); goat anit-Isl1 (Neuromics); rabbit anti-TrkA (Upstate); goat anti TrkA (Neuromics); goat anti-TrkB (Neuromics); goat anti-TrkB (R&D Systems); goat anti-mTrkC (R&D Systems); chick anti-Neurofilament H (Neuromics). Alexa488-, Cy3- and C5-conjugated fluorophores (Molecular Probes, Eugene, OR) were used as secondary antibodies.

Fluorescently labeled tissue sections and whole-mount muscles were imaged using an Olympus BX61 scanning microscope (Olympus).

5.4.2 *In Situ* hybridization

In situ hybridization using digoxigenin-labeled probes was performed on unfixed tissue according to previously described protocols (Schaeren-Wiemers and Gerfin-Moser, 1993; Wright and Snider, 1995). Antisense riboprobes used in this chapter were produced from plasmids harboring the following cDNAs: *mPea3* and *Sema3e* (Livet et al., 2002), *Del1* (Genebank accession number BC056386); *Tacr3* (BC066845) and *Plxnd1* (BC19530). Images from *in situ* hybridization experiments were recorded using a mountable Leica DFC480 digital camera.

References

Andrew BL, Part NJ (1972) Properties of fast and slow motor units in hind limb and tail muscles of the rat. Q J Exp Physiol Cogn Med Sci 57:213-225.

Aoka Y, Johnson FL, Penta K, Hirata Ki K, Hidai C, Schatzman R, Varner JA, Quertermous T (2002) The embryonic angiogenic factor Del1 accelerates tumor growth by enhancing vascular formation. Microvasc Res 64:148-161.

Arber S, Ladle DR, Lin JH, Frank E, Jessell TM (2000) ETS gene Er81 controls the formation of functional connections between group Ia sensory afferents and motor neurons. Cell 101:485-498.

Arber S, Han B, Mendelsohn M, Smith M, Jessell TM, Sockanathan S (1999) Requirement for the homeobox gene Hb9 in the consolidation of motor neuron identity. Neuron 23:659-674.

Bainton CR, Kirkwood PA (1979) The effect of carbon dioxide on the tonic and the rhythmic discharges of expiratory bulbospinal neurones. J Physiol 296:291-314.

Bermingham JR, Jr., Scherer SS, O'Connell S, Arroyo E, Kalla KA, Powell FL, Rosenfeld MG (1996) Tst-1/Oct-6/SCIP regulates a unique step in peripheral myelination and is required for normal respiration. Genes Dev 10:1751-1762.

Bibel M, Barde YA (2000) Neurotrophins: key regulators of cell fate and cell shape in the vertebrate nervous system. Genes Dev 14:2919-2937.

Blight AR, McGinnis ME, Borgens RB (1990) Cutaneus trunci muscle reflex of the guinea pig. J Comp Neurol 296:614-633.

Borgens RB, Blight AR, McGinnis ME (1987) Behavioral recovery induced by applied electric fields after spinal cord hemisection in guinea pig. Science 238:366-369.

Boyd IA (1986) Two types of static gamma-axon in cat muscle spindles. Q J Exp Physiol 71:307-327.

Briscoe J, Pierani A, Jessell TM, Ericson J (2000) A homeodomain protein code specifies progenitor cell identity and neuronal fate in the ventral neural tube. Cell 101:435-445.

Brumovsky P, Shi TS, Landry M, Villar MJ, Hokfelt T (2007) Neuropeptide tyrosine and pain. Trends Pharmacol Sci 28:93-102.

Bullock CM, Li JD, Zhou QY (2004) Structural determinants required for the bioactivities of prokineticins and identification of prokineticin receptor antagonists. Mol Pharmacol 65:582-588.

Burke RE, Glenn LL (1996) Horseradish peroxidase study of the spatial and electrotonic distribution of group Ia synapses on type-identified ankle extensor motoneurons in the cat. J Comp Neurol 372:465-485.

Bussolino F, Valdembri D, Caccavari F, Serini G (2006) Semaphoring vascular morphogenesis. Endothelium 13:81-91.

Butt SJ, Lebret JM, Kiehn O (2002) Organization of left-right coordination in the mammalian locomotor network. Brain Res Brain Res Rev 40:107-117.

Carpenter EM (2002) Hox genes and spinal cord development. Dev Neurosci 24:24-34.

Chauvet S, Cohen S, Yoshida Y, Fekrane L, Livet J, Gayet O, Segu L, Buhot MC, Jessell TM, Henderson CE, Mann F (2007) Gating of Sema3E/PlexinD1 signaling by neuropilin-1 switches axonal repulsion to attraction during brain development. Neuron 56:807-822.

Chen AI, de Nooij JC, Jessell TM (2006) Graded activity of transcription factor Runx3 specifies the laminar termination pattern of sensory axons in the developing spinal cord. Neuron 49:395-408.

Chen CL, Broom DC, Liu Y, de Nooij JC, Li Z, Cen C, Samad OA, Jessell TM, Woolf CJ, Ma Q (2006) Runx1 determines nociceptive sensory neuron phenotype and is required for thermal and neuropathic pain. Neuron 49:365-377.

Chen HH, Hippenmeyer S, Arber S, Frank E (2003) Development of the monosynaptic stretch reflex circuit. Curr Opin Neurobiol 13:96-102.

Cheng MY, Leslie FM, Zhou QY (2006) Expression of prokineticins and their receptors in the adult mouse brain. J Comp Neurol 498:796-809.

Cheng MY, Bullock CM, Li C, Lee AG, Bermak JC, Belluzzi J, Weaver DR, Leslie FM, Zhou QY (2002) Prokineticin 2 transmits the behavioural circadian rhythm of the suprachiasmatic nucleus. Nature 417:405-410.

Choe A, Phun HQ, Tieu DD, Hu YH, Carpenter EM (2006) Expression patterns of Hox10 paralogous genes during lumbar spinal cord development. Gene Expr Patterns 6:730-737.

Choi EY, Chavakis E, Czabanka MA, Langer HF, Fraemohs L, Economopoulou M, Kundu RK, Orlandi A, Zheng YY, Prieto DA, Ballantyne CM, Constant SL, Aird WC, Papayannopoulou T, Gahmberg CG, Udey MC, Vajkoczy P, Quertermous T, Dimmeler S, Weber C, Chavakis T (2008) Del-1, an endogenous leukocyte-endothelial adhesion inhibitor, limits inflammatory cell recruitment. Science 322:1101-1104.

Dasen JS, Liu JP, Jessell TM (2003) Motor neuron columnar fate imposed by sequential phases of Hox-c activity. Nature 425:926-933.

Dasen JS, Tice BC, Brenner-Morton S, Jessell TM (2005) A Hox regulatory network establishes motor neuron pool identity and target-muscle connectivity. Cell 123:477-491.

Dickson BJ (2002) Molecular mechanisms of axon guidance. Science 298:1959-1964.

Eccles JC, Eccles RM, Lundberg A (1957) The convergence of monosynaptic excitatory afferents on to many different species of alpha motoneurones. J Physiol 137:22-50.

Fry M, Cottrell GT, Ferguson AV (2008) Prokineticin 2 influences subfornical organ neurons through regulation of MAP kinase and the modulation of sodium channels. Am J Physiol Regul Integr Comp Physiol 295:R848-856.

Garcia NV, Jessell TM (2008) Early Motor Neuron Pool Identity and Muscle Nerve Trajectory Defined by Postmitotic Restrictions in Nkx6.1 Activity. Neuron 57:217-231.

Gerrits PO, Vodde C, Holstege G (2000) Retroambiguus projections to the cutaneus trunci motoneurons may form a pathway in the central control of mating. J Neurophysiol 83:3076-3083.

Gomez-Skarmeta JL, Modolell J (2002) Iroquois genes: genomic organization and function in vertebrate neural development. Curr Opin Genet Dev 12:403-408.

Gonzalez-Martinez D, Hu Y, Bouloux PM (2004) Ontogeny of GnRH and olfactory neuronal systems in man: novel insights from the investigation of inherited forms of Kallmann's syndrome. Front Neuroendocrinol 25:108-130.

Grunwald IC, Klein R (2002) Axon guidance: receptor complexes and signaling mechanisms. Curr Opin Neurobiol 12:250-259.

Gu C, Yoshida Y, Livet J, Reimert DV, Mann F, Merte J, Henderson CE, Jessell TM, Kolodkin AL, Ginty DD (2005) Semaphorin 3E and plexin-D1 control vascular pattern independently of neuropilins. Science 307:265-268.

Haase G, Dessaud E, Garces A, de Bovis B, Birling M, Filippi P, Schmalbruch H, Arber S, deLapeyriere O (2002) GDNF acts through PEA3 to regulate cell body

positioning and muscle innervation of specific motor neuron pools. Neuron 35:893-905.
Hanson MG, Milner LD, Landmesser LT (2008) Spontaneous rhythmic activity in early chick spinal cord influences distinct motor axon pathfinding decisions. Brain Res Rev 57:77-85.
Hatten ME (2002) New directions in neuronal migration. Science 297:1660-1663.
He Z, Wang KC, Koprivica V, Ming G, Song HJ (2002) Knowing how to navigate: mechanisms of semaphorin signaling in the nervous system. Sci STKE 2002:RE1.
Helmbacher F, Dessaud E, Arber S, deLapeyriere O, Henderson CE, Klein R, Maina F (2003) Met signaling is required for recruitment of motor neurons to PEA3-positive motor pools. Neuron 39:767-777.
Hidai C, Kawana M, Kitano H, Kokubun S (2007) Discoidin domain of Del1 protein contributes to its deposition in the extracellular matrix. Cell Tissue Res 330:83-95.
Hidai C, Zupancic T, Penta K, Mikhail A, Kawana M, Quertermous EE, Aoka Y, Fukagawa M, Matsui Y, Platika D, Auerbach R, Hogan BL, Snodgrass R, Quertermous T (1998) Cloning and characterization of developmental endothelial locus-1: an embryonic endothelial cell protein that binds the alphavbeta3 integrin receptor. Genes Dev 12:21-33.
Hippenmeyer S, Vrieseling E, Sigrist M, Portmann T, Laengle C, Ladle DR, Arber S (2005) A developmental switch in the response of DRG neurons to ETS transcription factor signaling. PLoS Biol 3:e159.
Hobert O (2005) Specification of the nervous system. WormBook:1-19.
Hokfelt T, Stanic D, Sanford SD, Gatlin JC, Nilsson I, Paratcha G, Ledda F, Fetissov S, Lindfors C, Herzog H, Johansen JE, Ubink R, Pfenninger KH (2008) NPY and its involvement in axon guidance, neurogenesis, and feeding. Nutrition 24:860-868.
Hollyday M, Jacobson RD (1990) Location of motor pools innervating chick wing. J Comp Neurol 302:575-588.
Holstege G, Blok BF (1989) Descending pathways to the cutaneous trunci muscle motoneuronal cell group in the cat. J Neurophysiol 62:1260-1269.
Houghton AK, Ogilvie J, Clarke RW (2000) The involvement of tachykinin NK2 and NK3 receptors in central sensitization of a spinal withdrawal reflex in the decerebrated, spinalized rabbit. Neuropharmacology 39:133-140.
Hu WP, Zhang C, Li JD, Luo ZD, Amadesi S, Bunnett N, Zhou QY (2006) Impaired pain sensation in mice lacking prokineticin 2. Mol Pain 2:35.
Jami L (1992) Golgi tendon organs in mammalian skeletal muscle: functional properties and central actions. Physiol Rev 72:623-666.
Jessell TM (2000) Neuronal specification in the spinal cord: inductive signals and transcriptional codes. Nat Rev Genet 1:20-29.
Johnson AW, Crombag HS, Takamiya K, Baraban JM, Holland PC, Huganir RL, Reti IM (2007) A selective role for neuronal activity regulated pentraxin in the processing of sensory-specific incentive value. J Neurosci 27:13430-13435.
Kandel ER, Schwartz JH, Jessell TM (2000) Principles of neural science, 4 Edition.
Kania A, Jessell TM (2003) Topographic motor projections in the limb imposed by LIM homeodomain protein regulation of ephrin-A:EphA interactions. Neuron 38:581-596.

Kania A, Johnson RL, Jessell TM (2000) Coordinate roles for LIM homeobox genes in directing the dorsoventral trajectory of motor axons in the vertebrate limb. Cell 102:161-173.

Kaser A, Winklmayr M, Lepperdinger G, Kreil G (2003) The AVIT protein family. Secreted cysteine-rich vertebrate proteins with diverse functions. EMBO Rep 4:469-473.

Katsura H, Tsuzuki K, Noguchi K, Sakagami M (2006) Differential expression of capsaicin-, menthol-, and mustard oil-sensitive receptors in naive rat geniculate ganglion neurons. Chem Senses 31:681-688.

Kernell D (2006) The motoneurone and its muscle fibres: Oxford University Press.

Kiehn O (2006) Locomotor circuits in the mammalian spinal cord. Annu Rev Neurosci 29:279-306.

Klur S, Toy K, Williams MP, Certa U (2004) Evaluation of procedures for amplification of small-size samples for hybridization on microarrays. Genomics 83:508-517.

Kmita M, Duboule D (2003) Organizing axes in time and space; 25 years of colinear tinkering. Science 301:331-333.

Kramer I, Sigrist M, de Nooij JC, Taniuchi I, Jessell TM, Arber S (2006) A role for Runx transcription factor signaling in dorsal root ganglion sensory neuron diversification. Neuron 49:379-393.

Ladle DR, Pecho-Vrieseling E, Arber S (2007) Assembly of motor circuits in the spinal cord: driven to function by genetic and experience-dependent mechanisms. Neuron 56:270-283.

Lance-Jones C, Omelchenko N, Bailis A, Lynch S, Sharma K (2001) Hoxd10 induction and regionalization in the developing lumbosacral spinal cord. Development (Cambridge, England) 128:2255-2268.

Landmesser L (1978) The development of motor projection patterns in the chick hind limb. J Physiol 284:391-414.

Landmesser L (1978) The distribution of motoneurones supplying chick hind limb muscles. J Physiol 284:371-389.

Landmesser LT (2001) The acquisition of motoneuron subtype identity and motor circuit formation. Int J Dev Neurosci 19:175-182.

LeCouter J, Lin R, Tejada M, Frantz G, Peale F, Hillan KJ, Ferrara N (2003) The endocrine-gland-derived VEGF homologue Bv8 promotes angiogenesis in the testis: Localization of Bv8 receptors to endothelial cells. Proc Natl Acad Sci U S A 100:2685-2690.

Lemon CH, Katz DB (2007) The neural processing of taste. BMC Neurosci 8 Suppl 3:S5.

Li M, Bullock CM, Knauer DJ, Ehlert FJ, Zhou QY (2001) Identification of two prokineticin cDNAs: recombinant proteins potently contract gastrointestinal smooth muscle. Mol Pharmacol 59:692-698.

Liddell EGT, Sherrington CT (1925) Recruitment and some other factors of reflex inhibition. ProcRSocLond B Biol Sci:488-518.

Lin AW, Carpenter EM (2003) Hoxa10 and Hoxd10 coordinately regulate lumbar motor neuron patterning. Journal of neurobiology 56:328-337.

Lin DC, Bullock CM, Ehlert FJ, Chen JL, Tian H, Zhou QY (2002) Identification and molecular characterization of two closely related G protein-coupled receptors activated by prokineticins/endocrine gland vascular endothelial growth factor. J Biol Chem 277:19276-19280.

Lin JH, Saito T, Anderson DJ, Lance-Jones C, Jessell TM, Arber S (1998) Functionally related motor neuron pool and muscle sensory afferent subtypes defined by coordinate ETS gene expression. Cell 95:393-407.

Livet J, Sigrist M, Stroebel S, De Paola V, Price SR, Henderson CE, Jessell TM, Arber S (2002) ETS gene Pea3 controls the central position and terminal arborization of specific motor neuron pools. Neuron 35:877-892.

Ma Q, Fode C, Guillemot F, Anderson DJ (1999) Neurogenin1 and neurogenin2 control two distinct waves of neurogenesis in developing dorsal root ganglia. Genes Dev 13:1717-1728.

Ma QP, Woolf CJ (1995) Involvement of neurokinin receptors in the induction but not the maintenance of mechanical allodynia in rat flexor motoneurones. J Physiol 486 (Pt 3):769-777.

Madhavan R, Peng HB (2005) Molecular regulation of postsynaptic differentiation at the neuromuscular junction. IUBMB Life 57:719-730.

Maher PA, Schubert D (1995) Schwannoma-derived growth factor interacts with the epidermal growth factor receptor. J Neurochem 65:1895-1898.

Masuda Y, Takatsu Y, Terao Y, Kumano S, Ishibashi Y, Suenaga M, Abe M, Fukusumi S, Watanabe T, Shintani Y, Yamada T, Hinuma S, Inatomi N, Ohtaki T, Onda H, Fujino M (2002) Isolation and identification of EG-VEGF/prokineticins as cognate ligands for two orphan G-protein-coupled receptors. Biochem Biophys Res Commun 293:396-402.

McGinnis W, Krumlauf R (1992) Homeobox genes and axial patterning. Cell 68:283-302.

Mears SC, Frank E (1997) Formation of specific monosynaptic connections between muscle spindle afferents and motoneurons in the mouse. J Neurosci 17:3128-3135.

Melchiorri D, Bruno V, Besong G, Ngomba RT, Cuomo L, De Blasi A, Copani A, Moschella C, Storto M, Nicoletti F, Lepperdinger G, Passarelli F (2001) The mammalian homologue of the novel peptide Bv8 is expressed in the central nervous system and supports neuronal survival by activating the MAP kinase/PI-3-kinase pathways. Eur J Neurosci 13:1694-1702.

Mendelson B, Frank E (1991) Specific monosynaptic sensory-motor connections form in the absence of patterned neural activity and motoneuronal cell death. J Neurosci 11:1390-1403.

Miller AD, Nonaka S, Siniaia MS, Jakus J (1995) Multifunctional ventral respiratory group: bulbospinal expiratory neurons play a role in pudendal discharge during vomiting. J Auton Nerv Syst 54:253-260.

Moens CB, Selleri L (2006) Hox cofactors in vertebrate development. Developmental biology 291:193-206.

Monnier C, Dode C, Fabre L, Teixeira L, Labesse G, Pin JP, Hardelin JP, Rondard P (2009) PROKR2 missense mutations associated with Kallmann syndrome impair receptor signalling activity. Hum Mol Genet 18:75-81.

Monuki ES, Kuhn R, Lemke G (1993) Repression of the myelin P0 gene by the POU transcription factor SCIP. Mech Dev 42:15-32.

Monuki ES, Weinmaster G, Kuhn R, Lemke G (1989) SCIP: a glial POU domain gene regulated by cyclic AMP. Neuron 3:783-793.

Muhr J, Andersson E, Persson M, Jessell TM, Ericson J (2001) Groucho-mediated transcriptional repression establishes progenitor cell pattern and neuronal fate in the ventral neural tube. Cell 104:861-873.

Mukouyama YS, Shin D, Britsch S, Taniguchi M, Anderson DJ (2002) Sensory nerves determine the pattern of arterial differentiation and blood vessel branching in the skin. Cell 109:693-705.

Mukouyama YS, Gerber HP, Ferrara N, Gu C, Anderson DJ (2005) Peripheral nerve-derived VEGF promotes arterial differentiation via neuropilin 1-mediated positive feedback. Development 132:941-952.

Muller T, Brohmann H, Pierani A, Heppenstall PA, Lewin GR, Jessell TM, Birchmeier C (2002) The homeodomain factor lbx1 distinguishes two major programs of neuronal differentiation in the dorsal spinal cord. Neuron 34:551-562.

Mummenhoff J, Houweling AC, Peters T, Christoffels VM, Ruther U (2001) Expression of Irx6 during mouse morphogenesis. Mech Dev 103:193-195.

Negri L, Lattanzi R, Giannini E, Metere A, Colucci M, Barra D, Kreil G, Melchiorri P (2002) Nociceptive sensitization by the secretory protein Bv8. Br J Pharmacol 137:1147-1154.

Negri L, Lattanzi R, Giannini E, Colucci M, Margheriti F, Melchiorri P, Vellani V, Tian H, De Felice M, Porreca F (2006) Impaired nociception and inflammatory pain sensation in mice lacking the prokineticin receptor PKR1: focus on interaction between PKR1 and the capsaicin receptor TRPV1 in pain behavior. J Neurosci 26:6716-6727.

Ng KL, Li JD, Cheng MY, Leslie FM, Lee AG, Zhou QY (2005) Dependence of olfactory bulb neurogenesis on prokineticin 2 signaling. Science 308:1923-1927.

Nguyen-Ba-Charvet KT, Chedotal A (2002) Role of Slit proteins in the vertebrate brain. J Physiol Paris 96:91-98.

Nilsson A, Kanje M (2005) Amphiregulin acts as an autocrine survival factor for adult sensory neurons. Neuroreport 16:213-218.

Palmer TD, Willhoite AR, Gage FH (2000) Vascular niche for adult hippocampal neurogenesis. J Comp Neurol 425:479-494.

Park HT, Wu J, Rao Y (2002) Molecular control of neuronal migration. Bioessays 24:821-827.

Patel TD, Kramer I, Kucera J, Niederkofler V, Jessell TM, Arber S, Snider WD (2003) Peripheral NT3 signaling is required for ETS protein expression and central patterning of proprioceptive sensory afferents. Neuron 38:403-416.

Penta K, Varner JA, Liaw L, Hidai C, Schatzman R, Quertermous T (1999) Del1 induces integrin signaling and angiogenesis by ligation of alphaVbeta3. J Biol Chem 274:11101-11109.

Peters T, Dildrop R, Ausmeier K, Ruther U (2000) Organization of mouse Iroquois homeobox genes in two clusters suggests a conserved regulation and function in vertebrate development. Genome Res 10:1453-1462.

Pfaff SL, Mendelsohn M, Stewart CL, Edlund T, Jessell TM (1996) Requirement for LIM homeobox gene Isl1 in motor neuron generation reveals a motor neuron-dependent step in interneuron differentiation. Cell 84:309-320.

Powers RK, Binder MD (2001) Input-output functions of mammalian motoneurons. Rev Physiol Biochem Pharmacol 143:137-263.

Price CJ, Hoyda TD, Ferguson AV (2008) The area postrema: a brain monitor and integrator of systemic autonomic state. Neuroscientist 14:182-194.

Rezaee M, Penta K, Quertermous T (2002) Del1 mediates VSMC adhesion, migration, and proliferation through interaction with integrin alpha(v)beta(3). Am J Physiol Heart Circ Physiol 282:H1924-1932.

Romanes GJ (1942) The development and significance of the cell columns in the ventral horn of the cervical und upper thoracic spinal cord of the rabbit. J Anat 76:112-130.
Romanes GJ (1951) The motor cell columns of the lumbo-sacral spinal cord of the cat. J Comp Neurol 94:313-363.
Rottkamp CA, Lobur KJ, Wladyka CL, Lucky AK, O'Gorman S (2008) Pbx3 is required for normal locomotion and dorsal horn development. Developmental biology 314:23-39.
Rousso DL, Gaber ZB, Wellik D, Morrisey EE, Novitch BG (2008) Coordinated actions of the forkhead protein Foxp1 and Hox proteins in the columnar organization of spinal motor neurons. Neuron 59:226-240.
Ryan JM, Cushman J, Jordan B, Samuels A, Frazer H, Baier C (1998) Topographic position of forelimb motoneuron pools is conserved in vertebrate evolution. Brain Behav Evol 51:90-99.
Ryu EJ, Wang JY, Le N, Baloh RH, Gustin JA, Schmidt RE, Milbrandt J (2007) Misexpression of Pou3f1 results in peripheral nerve hypomyelination and axonal loss. J Neurosci 27:11552-11559.
Salinas PC (2003) The morphogen sonic hedgehog collaborates with netrin-1 to guide axons in the spinal cord. Trends Neurosci 26:641-643.
Sanes JR, Lichtman JW (1999) Development of the vertebrate neuromuscular junction. Annu Rev Neurosci 22:389-442.
Schouenborg J (2008) Action-based sensory encoding in spinal sensorimotor circuits. Brain Res Rev 57:111-117.
Schouenborg J, Weng HR, Kalliomaki J, Holmberg H (1995) A survey of spinal dorsal horn neurones encoding the spatial organization of withdrawal reflexes in the rat. Exp Brain Res 106:19-27.
Shepherd G (2004) The Synapitc Organization of the Brain, 5 Edition: Oxford University Press.
Shirasaki R, Pfaff SL (2002) Transcriptional codes and the control of neuronal identity. Annu Rev Neurosci 25:251-281.
Shirasaki R, Lewcock JW, Lettieri K, Pfaff SL (2006) FGF as a target-derived chemoattractant for developing motor axons genetically programmed by the LIM code. Neuron 50:841-853.
Smith PA, Moran TD, Abdulla F, Tumber KK, Taylor BK (2007) Spinal mechanisms of NPY analgesia. Peptides 28:464-474.
Snider WD, McMahon SB (1998) Tackling pain at the source: new ideas about nociceptors. Neuron 20:629-632.
Sondell M, Sundler F, Kanje M (2000) Vascular endothelial growth factor is a neurotrophic factor which stimulates axonal outgrowth through the flk-1 receptor. Eur J Neurosci 12:4243-4254.
Soshnikova N, Duboule D (2008) Epigenetic regulation of Hox gene activation: the waltz of methyls. BioEssays 30:199-202.
Starr KA, Wolpaw JR (1994) Synaptic terminal coverage of primate triceps surae motoneurons. J Comp Neurol 345:345-358.
Strominger NL, Knox AP, Carpenter DO (1994) The connectivity of the area postrema in the ferret. Brain Res Bull 33:33-47.
Tarchini B, Huynh TH, Cox GA, Duboule D (2005) HoxD cluster scanning deletions identify multiple defects leading to paralysis in the mouse mutant Ironside. Genes Dev 19:2862-2876.

Tatemoto K, Carlquist M, Mutt V (1982) Neuropeptide Y--a novel brain peptide with structural similarities to peptide YY and pancreatic polypeptide. Nature 296:659-660.

Terashima T (1995) Anatomy, development and lesion-induced plasticity of rodent corticospinal tract. Neurosci Res 22:139-161.

Thaler J, Harrison K, Sharma K, Lettieri K, Kehrl J, Pfaff SL (1999) Active suppression of interneuron programs within developing motor neurons revealed by analysis of homeodomain factor HB9. Neuron 23:675-687.

Thaler JP, Koo SJ, Kania A, Lettieri K, Andrews S, Cox C, Jessell TM, Pfaff SL (2004) A postmitotic role for Isl-class LIM homeodomain proteins in the assignment of visceral spinal motor neuron identity. Neuron 41:337-350.

Theokli C, Morsi El-Kadi AS, Morgan R (2003) TALE class homeodomain gene Irx5 is an immediate downstream target for Hoxb4 transcriptional regulation. Dev Dyn 227:48-55.

Theriault E, Diamond J (1988) Nociceptive cutaneous stimuli evoke localized contractions in a skeletal muscle. J Neurophysiol 60:446-462.

Tiret L, Le Mouellic H, Maury M, Brulet P (1998) Increased apoptosis of motoneurons and altered somatotopic maps in the brachial spinal cord of Hoxc-8-deficient mice. Development 125:279-291.

Tsuchida T, Ensini M, Morton SB, Baldassare M, Edlund T, Jessell TM, Pfaff SL (1994) Topographic organization of embryonic motor neurons defined by expression of LIM homeobox genes. Cell 79:957-970.

Tsui CC, Copeland NG, Gilbert DJ, Jenkins NA, Barnes C, Worley PF (1996) Narp, a novel member of the pentraxin family, promotes neurite outgrowth and is dynamically regulated by neuronal activity. J Neurosci 16:2463-2478.

Vanderhorst VG, Holstege G (1995) Caudal medullary pathways to lumbosacral motoneuronal cell groups in the cat: evidence for direct projections possibly representing the final common pathway for lordosis. J Comp Neurol 359:457-475.

Vellani V, Colucci M, Lattanzi R, Giannini E, Negri L, Melchiorri P, McNaughton PA (2006) Sensitization of transient receptor potential vanilloid 1 by the prokineticin receptor agonist Bv8. J Neurosci 26:5109-5116.

Vermot J, Schuhbaur B, Le Mouellic H, McCaffery P, Garnier JM, Hentsch D, Brulet P, Niederreither K, Chambon P, Dolle P, Le Roux I (2005) Retinaldehyde dehydrogenase 2 and Hoxc8 are required in the murine brachial spinal cord for the specification of Lim1+ motoneurons and the correct distribution of Islet1+ motoneurons. Development 132:1611-1621.

Vrieseling E, Arber S (2006) Target-induced transcriptional control of dendritic patterning and connectivity in motor neurons by the ETS gene Pea3. Cell 127:1439-1452.

Wang G, Scott SA (2007) Onset of ETS expression is not accelerated by premature exposure to signals from limb mesenchyme. Dev Dyn 236:2109-2117.

Wu Y, Wang G, Scott SA, Capecchi MR (2008) Hoxc10 and Hoxd10 regulate mouse columnar, divisional and motor pool identity of lumbar motoneurons. Development (Cambridge, England) 135:171-182.

Xu XJ, Maggi CA, Wiesenfeld-Hallin Z (1991) On the role of NK-2 tachykinin receptors in the mediation of spinal reflex excitability in the rat. Neuroscience 44:483-490.

Yashpal K, Dam TV, Quirion R (1990) Quantitative autoradiographic distribution of multiple neurokinin binding sites in rat spinal cord. Brain Res 506:259-266.

Yoshihara S, Omichi K, Yanazawa M, Kitamura K, Yoshihara Y (2005) Arx homeobox gene is essential for development of mouse olfactory system. Development 132:751-762.

Yu TW, Bargmann CI (2001) Dynamic regulation of axon guidance. Nat Neurosci 4 Suppl:1169-1176.

Yuill EA, Hoyda TD, Ferri CC, Zhou QY, Ferguson AV (2007) Prokineticin 2 depolarizes paraventricular nucleus magnocellular and parvocellular neurons. Eur J Neurosci 25:425-434.

Zhang H, Vutskits L, Pepper MS, Kiss JZ (2003) VEGF is a chemoattractant for FGF-2-stimulated neural progenitors. J Cell Biol 163:1375-1384.

Zhong J, Eliceiri B, Stupack D, Penta K, Sakamoto G, Quertermous T, Coleman M, Boudreau N, Varner JA (2003) Neovascularization of ischemic tissues by gene delivery of the extracellular matrix protein Del-1. J Clin Invest 112:30-41.

Appendix

Acknowledgements

Foremost, I am grateful to Prof. Dr. Silvia Arber for giving me the opportunity to do my Ph.D. in her laboratory and for providing the best possible working conditions one could wish for.

I would especially like to thank David Ladle for his friendship, unbreakable good spirits and inspiring scientific and non-scientific discussions. I am also grateful to Alison Macintyre, Joachim Luginbühl, Anna Stepien, Jun Lee and Roland Huber for their help and sense of humor in good and bad times.

My warmest thanks go to my family who has continuously supported and encouraged me.

Many thanks also go to my dear friends in Bern, Basel and elsewhere who have made sure that my mind stays diverted in leisure time.